Renormalization-group approach to the Anderson model of dilute magnetic alloys. II. Static properties for the asymmetric case

H. R. Krishna-murthy*
Department of Physics, University of Illinois, Urbana Illinois 61801

J. W. Wilkins and K. G. Wilson
Physics Department, Cornell University, Ithaca, New York 14853

(Received 10 September 1979)

The temperature-dependent impurity susceptibility for the asymmetric Anderson model is calculated over a broad, physically relevant range of its parameters ϵ_d (the energy of impurity orbital), U (the Coulomb correlation energy), and Γ (the impurity-level width). Within the context of renormalization-group theory four fixed points and their associated regimes are identified: (i) the free-orbital regime which is unstable and flows into (ii) or (iv); (ii) the valence-fluctuation regime which is characteristic of the asymmetric Anderson model. Properties are dominated by a temperature-dependent impurity-orbital energy $E_d(T) \cong \epsilon_d + (\Gamma/\pi)\ln(U/T)$. If $E_d(T)$ is negative and large compared to Γ as T decreases, the system is unstable with respect to (iii), otherwise it flows to (iv); (iii) the local-moment regime is similar to that in the symmetric Anderson model except that it has potential scattering. That is, this regime maps onto the Kondo model with potential scattering, the latter having little effect on the susceptibility; (iv) the frozen-impurity regime, into which all the regimes above flow, is stable, having only irrelevant operators. Furthermore, in the valence-fluctuation regime nonuniversal properties are observed for $-E_d(T) < \Gamma$. These conclusions are supported with extensive analytic and numerical calculations, the latter based on the numerical renormalization-group approach. Analytic formulas for the impurity susceptibility and free energy in all four regimes are presented, together with the impurity-specific heat in the frozen-impurity regime.

I. INTRODUCTION

In this paper, we continue the discussion started in the previous paper,[1] hereafter referred to as I, of the application of Wilson's numerical renormalization-group techniques[2] to the Anderson model[3] of dilute magnetic alloys.[4,5] In I we summarized the basic techniques and discussed in detail their application to the calculation of the static properties of the symmetric Anderson model. In this paper we discuss in detail the static properties of the asymmetric Anderson model.

The plan of this paper is as follows. In Sec. I A, we recapitulate the basic results of I. In Sec. I B we give a survey of the susceptibility results of the asymmetric model, and discuss a simple picture of the manifold of the states of the model in terms of which roughly to understand these results. The discussion is quite qualitative, and essentially serves as a summary of the results of the present investigation, and should be intelligibile even to a reader unfamiliar with the details of I.

The rest of the paper, namely Secs. II and III and the appendices, contain the quantitative details. This material depends heavily on the material presented in I, and is likely to be hard to understand without an understanding of the details of I. In Sec. II we identify the fixed points of the asymmetric Anderson model, and set up the formal renormalization-group apparatus which is used to analyze the numerical results. The detailed analysis of the numerical results and the detailed analytical descriptions of the various regimes of behavior of the susceptibility are presented in Sec. III. Section III is hence the core of the paper. The appendices mostly contain technical details concerning the derivation of some results used in the body of the paper.

A. Recapitulation of the basic results of I

The model Hamiltonian we use throughout the present investigation is a simplified version of the Anderson model[3] and can be written [cf. Paper I Eq. (2.4)]

$$\frac{\mathcal{H}_A}{D} = \int_{-1}^{1} k a_{k\mu}^{\dagger} a_{k\mu}\, dk + \frac{\epsilon_d}{D}(c_{d\mu}^{\dagger} c_{d\mu} - 1) + \frac{U}{D}(c_{d\uparrow}^{\dagger} c_{d\uparrow})(c_{d\mu}^{\dagger} c_{d\mu})(c_{d\downarrow}^{\dagger} c_{d\downarrow}) + \left(\frac{\Gamma}{\pi D}\right)^{1/2} \int_{-1}^{1} dk\, (a_{k\mu}^{\dagger} c_{d\mu} + c_{d\mu}^{\dagger} a_{k\mu}) \quad . \tag{1.1}$$

The nature of the simplifications has been discussed in Sec. II A of I. In Eq. (1.1), $a^{\dagger}_{k\mu}$ refers to a conduction-electron s-wave state (about the impurity) of energy k (all energies are in units of the bandwidth D unless otherwise specified); $c^{\dagger}_{d\mu}$ refers to a nondegenerate impurity orbital. ϵ_d is the energy of the impurity orbital, U is the Coulomb energy for putting two electrons into the impurity orbital, and $\Gamma \equiv \pi\rho|V|^2$ is the level width of the impurity orbital arising from its mixing with the conduction band (V is the mixing matrix element). In the symmetric case $\epsilon_d = -\frac{1}{2}U$.

The logarithmic discretization in terms of the parameter Λ (>1), etc., as discussed in Secs. II B–II D of I leads us to the sequence of Hamiltonians [cf. Paper Eq. (2.18)]

$$H_N \equiv \Lambda^{(N-1)/2}\left[\sum_{n=0}^{N-1}\Lambda^{-n/2}\,\xi_n(f^{\dagger}_{n\mu}f_{n+1\,\mu}+f^{\dagger}_{n+1\,\mu}f_{n\mu}) + \tilde{\epsilon}_d c^{\dagger}_{d\mu}c_{d\mu}+\tilde{\Gamma}^{1/2}(c^{\dagger}_{d\mu}f_{0\mu}+f^{\dagger}_{0\mu}c_{d\mu}) + 2\tilde{U}n_{d\uparrow}n_{d\downarrow}\right], \tag{1.2}$$

where f_n refers to a conduction-electron-shell state, centered at the impurity and of extent $\sim\Lambda^{n/2}/k_F$; and

$$2\tilde{U} \equiv \left(\frac{2}{1+\Lambda^{-1}}\right)\frac{U}{D}, \tag{1.3a}$$

$$\tilde{\Gamma} \equiv \left(\frac{2}{1+\Lambda^{-1}}\right)^2\frac{2\Gamma}{\pi D}, \tag{1.3b}$$

$$\tilde{\epsilon}_d \equiv \left(\frac{2}{1+\Lambda^{-1}}\right)\frac{\epsilon_d}{D} = \tilde{\delta}_d - \tilde{U}. \tag{1.3c}$$

The notation used above is consistent with I. [See Eqs. (2.18)–(2.20) in I.]

The important point (for a detailed discussion of this refer to Sec. II E of I) is that the energy levels of H_N can be used to calculate the impurity susceptibility and the impurity free energy at a sequence of temperatures [cf. Eq. (2.39) in I]

$$k_B T_N/D = \tfrac{1}{2}(1+\Lambda^{-1})\Lambda^{-(N-1)/2}/\bar{\beta}. \tag{1.4}$$

This is done using the formulas

$$k_B T_N \chi(T_N) \cong \frac{\mathrm{Tr}\,S^2_{Nz}\exp-\bar{\beta}H_N}{\mathrm{Tr}\exp-\bar{\beta}H_N} - \frac{\mathrm{Tr}\,S^{0\,2}_{Nz}\exp-\bar{\beta}H^0_N}{\mathrm{Tr}\exp-\bar{\beta}H^0_N}, \tag{1.5}$$

$$F(T_N) \cong -k_B T_N(\ln\mathrm{Tr}\exp-\bar{\beta}H_N - \ln\mathrm{Tr}\exp-\bar{\beta}H^0_N) \tag{1.6}$$

Here $\bar{\beta}$ is a small parameter. In practice, for a given value of N, several values of $\bar{\beta}$ are used, resulting in fine mesh of temperatures in which the susceptibility and free energy are calculated. In all the calculations described in this paper, $\Lambda = 3$ has been used and the following values of $\bar{\beta}$ were used: 0.400, 0.459, 0.526, 0.604, and 0.692. (See also the discussion in Sec. II E of I.) H^0_N refers to the conduction-electron part of H_N, namely

$$H^0_N = \Lambda^{(N-1)/2}\left[\sum_{n=0}^{N-1}\Lambda^{-n/2}\xi_n(f^{\dagger}_{n+1\,\mu}f_{n\mu}+f^{\dagger}_{n\mu}f_{n+1\,\mu})\right], \tag{1.7}$$

and $\vec{S}_{Nz}$ and $\vec{S}^0_{Nz}$ are the spin operators appropriate to H_N and H^0_N.

All the special features of the present calculation stem from the fact that $\{H_N\}$ obey the following renormalization-group recursion relation [which follows from Eq. (1.2)]

$$H_{N+1} \equiv \mathcal{T}[H_N] = \Lambda^{1/2}H_N + \xi_N(f^{\dagger}_{N\mu}f_{N+1\,\mu}+f^{\dagger}_{N+1\,\mu}f_{N\mu}) \tag{1.8}$$

First, this recursion relation enables us to set up a numerical iterative diagonalization scheme to calculate the energy levels of H_N, and hence to calculate numerically $\chi(T_N)$ and $F(T_N)$. Second, it enables us to use the machinery of fixed points, linearized behavior near fixed points etc.,[2,6] in order to understand the flow (with N) of H_N and hence the temperature dependence of $\chi(T_N)$ and $F(T_N)$. In particular, for those ranges of T_N where the corresponding H_N are near the fixed points of $\mathcal{T}^2$ [where $\mathcal{T}$ denotes the transformation Eq. (1.8)], we can write down effective Hamiltonians in terms of which we can calculate the temperature dependence of $\chi(T_N)$ and $F(T_N)$ analytically using perturbation theory.

The basic picture in terms of which we can qualitatively understand the results of the present calculation is the picture of the manifold of the states of $\mathcal{H}_A$ with Γ set to zero, when the states of $\mathcal{H}_A$ are just direct products of the states of the impurity orbital and of the conduction band. Figure 1 is an attempt to draw this picture for the symmetric case. With the conduction band in its ground state (i.e., a filled Fermi sea), the impurity orbital can be empty ($n_d = 0$), occupied by one electron ($n_d = 1$) or completely filled ($n_d = 2$). These states are represented by the thick lines in Fig. 1. For each of these configurations of the impurity orbital, the conduction band can also be in any of its continuum of many-body excited states. These states are represented by the thin lines in Fig. 1. Turning on Γ causes these states to be mixed up as indicated in Fig. 1, and the resulting spectrum of states is very complicated. But when Γ is small compared to the separators between the various subspaces (i.e., to $|\epsilon_d|$ and $\epsilon_d + U$), Fig. 1 still retains some meaning; and in general helps greatly in understanding the properties of $\mathcal{H}_A$.

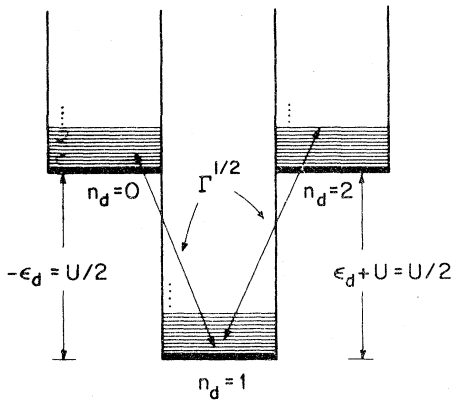

FIG. 1. Manifold of states of the symmetric Anderson model when the impurity level width Γ is zero. The thick lines represent states in which the conduction band is in its ground state, but the impurity orbital configuration corresponds to occupancy $n_d=0$, 1, or 2. By reference to Eq. (1.1), we see that the orbital energy ϵ_d represents the difference of the many-body ground states $n_d=1$ and 0. For each impurity configuration, the conduction band can also be a continuum of many-body excited states, indicated by the light lines lying at higher energy. The three sets of states overlap in energy. The inclusion of Γ causes transitions between the states as indicated by the diagonal arrows.

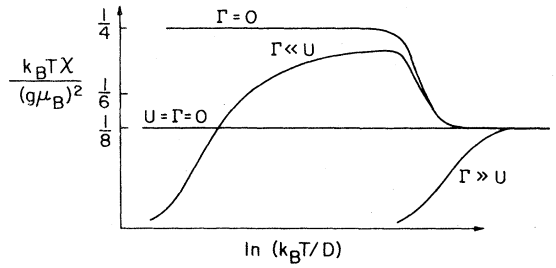

FIG. 2. Schematic sketch of $k_BT\chi(T)/(g\mu_B)^2$ vs $\ln(k_BT/D)$ for the symmetric Anderson model. At sufficiently high temperatures ($T>>U$) all four configurations $n_d=0$, $n_d=2$, and $n_d=1$ (spin up or spin down) are equally occupied resulting in the free-orbital susceptibility ($T\chi=\frac{1}{8}$) which will persist for all temperatures only if $\Gamma=U=0$. Otherwise, as the temperature is lowered the $n_d=0$ and $n_d=2$ configurations will tend to be depopulated. For $\Gamma<<U$, $T\chi$ rises toward the local-moment value of $\frac{1}{4}$. At still lower temperatures ($T\lesssim T_K$), the conduction electrons "freeze out" the local moment so that $T\chi$ drops to zero. If $\Gamma>>U$, this freezing process (the strong-coupling regime) proceeds directly from the free-orbital regime.

In I we discussed the symmetric case which occurs when $\epsilon_d=-\frac{1}{2}U$ so that the $n_d=0$ and $n_d=2$ subspaces are both $\frac{1}{2}U$ above the $n_d=1$ subspace as in Fig. 1, and $\mathcal{H}_A$ is invariant under particle $\leftrightarrow$ hole transformation (which corresponds to $a_k\leftrightarrow a^\dagger_{-k}$, $c_d\leftrightarrow -c_d^\dagger$ so that $n_d\leftrightarrow 2-n_d$, i.e., the $n_d=0$ and $n_d=2$ subspaces in Fig. 1 are interchanged). Figure 2 shows schematic plots of $k_BT\chi$ for the symmetric Anderson model. When $T>>\max(U,\Gamma)$, all the impurity configurations are equally populated and the splittings and the couplings between them are irrelevant. The situation is as if U and Γ are both zero, so that $T\chi$ is close to $\frac{1}{8}$, and this is referred to as the free-orbital regime. Next suppose $\Gamma<<U$. Then as T drops well below U, to a first approximation one can ignore the subspaces for which $n_d=0$ or 2 and set $\Gamma=0$. Within the subspace in which $n_d=1$, the impurity degree of freedom looks like a spin-$\frac{1}{2}$ object, so that we expect $T\chi=\frac{1}{4}$. The next level of approximation is to permit virtual transitions induced by Γ, which results in effective interactions between the impurity spin and the conduction electrons. The most dominant of such interactions turns out to be[1] a spin-spin interaction of the form

$$\mathcal{H}_{\rm int}=-J_{\rm eff}\vec{s}(0)\cdot\vec{S}_i;\quad \rho J_{\rm eff}=-\frac{8\Gamma}{\pi U}\ , \tag{1.9}$$

where $\vec{S}_i$ is the impurity spin operator and $\vec{s}(0)$ the conduction-electron spin density at the impurity site. This interaction leads to the Kondo effect[1,4,5] as a consequence of which $T\chi$ gradually decreases and vanishes as $T\to 0$. Furthermore χ obeys a scaling law, namely that $T\chi$ is a universal function[1] of $T/T_K(J_{\rm eff})$ where the scaling temperature, called the

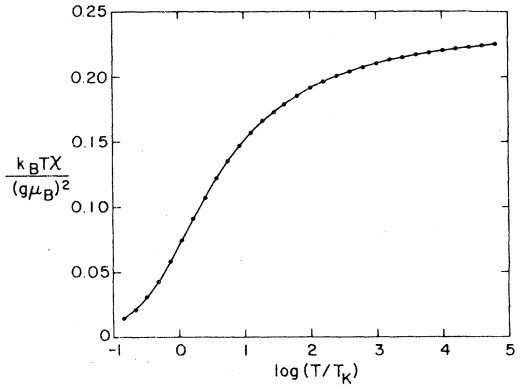

FIG. 3. Universal plot of $k_BT\chi(T)/(g\mu_B)^2$ vs $\ln(T/T_K)$ where $\chi(T)$ is the impurity susceptibility for the spin-$\frac{1}{2}$ Kondo Hamiltonian and T_K is the Kondo temperature, the only quantity depending on the details of the model. For $T<<T_K$ the local moment is frozen out by the conduction electrons. The residual interactions between the electrons in this so-called strong-coupling regime results in a zero-temperature susceptibility $0.1\ (g\mu_B)^2/k_BT_K$.

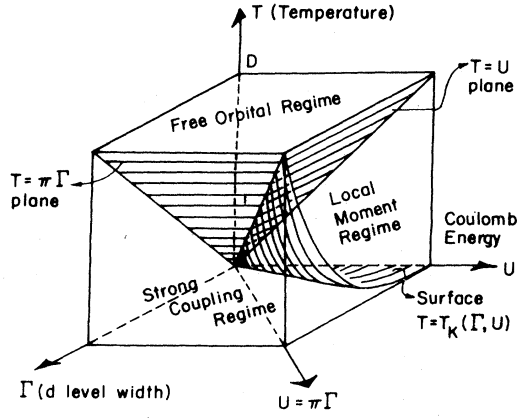

FIG. 4. Schematic sketch of the various regimes for the symmetric Anderson model. The separations between the various regimes, in contrast to the drawing, are actually quite fuzzy.

Kondo temperature, is given by

$$T_K \sim U|\rho J_{\rm eff}|^{1/2}\exp\left(-\frac{1}{|\rho J_{\rm eff}|}\right) \sim (\Gamma U)^{1/2}\exp\left(-\frac{\pi U}{8\Gamma}\right) . \quad (1.10)$$

See Fig. 3. The zero-temperature behavior corresponds to the situation in which the impurity degree of freedom is frozen out, leaving behind only residual interactions between renormalized conduction-electron degrees of freedom. This leads to a constant χ and a linear specific heat, and is referred to as the strong-coupling regime. The regime above T_K is referred to as the local-moment regime, in which χ is approximately Curie-Weiss-like but with a diminished effective moment. The various regimes are illustrated in Fig. 4.

Next consider what happens when Γ is increased keeping U fixed. The basic effect is that $|J_{\rm eff}|$ (and hence T_K) increases, the local-moment regime shrinks and the strong-coupling regime grows, until when $\Gamma \sim U$ the two transitions merge. When $\Gamma >> U$, there is a direct transition from the free-orbital regime for $T >> \Gamma$ to the strong-coupling regime for $T << \Gamma$.

B. Survey of susceptibility results for the asymmetric case

In this section, we present a qualitative survey of the susceptibility results for the asymmetric case. Quantitative details and proofs of assertions are presented in the following sections. When $\epsilon_d \neq -\frac{1}{2}U$, we have a four-parameter (ϵ_d, U, Γ, and T) space which to survey for regimes; we first note that the particle-hole transformation takes $\mathcal{H}_A$ to itself with ϵ_d replaced by $-(\epsilon_d + U)$, as a consequence of which we have

$$\chi[U,\Gamma,\epsilon_d,T] = \chi[U,\Gamma,-(\epsilon_d+U),T] . \quad (1.11)$$

It is therefore sufficient for us to discuss the region of the parameter space for which $\epsilon_d > -\frac{1}{2}U$. We will organize this discussion as follows. For each of the characteristic cases $\Gamma = 0$, $\Gamma << U$, and $\Gamma >> U$, we will consider how the $T\chi$ vs T curve changes as we sweep ϵ_d from $-\frac{1}{2}U$ through zero to a positive value, and try to connect this to the picture of states such as in Fig. 1.

1. *Case when* $\Gamma = 0$

First consider the case when $\Gamma = 0$. Then the impurity degree of freedom is decoupled from the conduction-electron degrees of freedom. The susceptibility is just that of the impurity orbital, and it is easy to verify that

$$\frac{k_B T\chi}{(g\mu_B)^2} = \tfrac{1}{2}(2 + e^{\epsilon_d/T} + e^{-(\epsilon_d+U)/T})^{-1} . \quad (1.12)$$

For the symmetric ($\epsilon_d = -\frac{1}{2}U$) case, as we discussed earlier, we have a transition from the free-orbital regime (in which $T\chi = \frac{1}{8}$) for $T >> U$ to the local-moment regime (in which $T\chi = \frac{1}{4}$) for $T << U$, as indicated by curve A of Fig. 5.

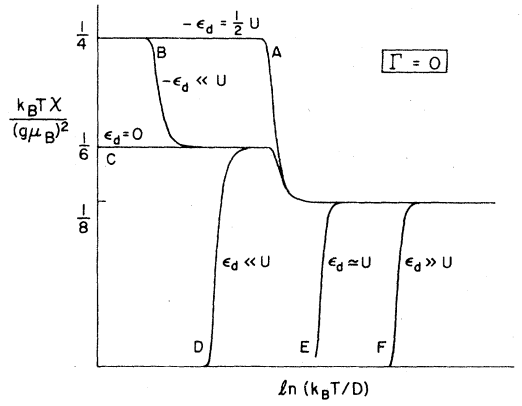

FIG. 5. Plots of $k_B T\chi(T)/(g\mu_B)^2$ vs $\ln(k_B T/D)$ for the asymmetric Anderson model in which the d-level width Γ is zero. The labeled curves A through F correspond to the orbital energy ϵ_d being increased from $-\frac{1}{2}U$ to $>>U$. In the valence-fluctuation regime, defined by $-\epsilon_d << T << U$, the $n_d = 0$ and $n_d = 1$ configurations are essentially equally populated resulting in a $T\chi$ value of $\frac{1}{6}$ (cf. curves B, C, and D). Note that for positive ϵ_d there is always a temperature below which the $n_d = 0$ configuration dominates, resulting in a zero susceptibility (cf. curves D, E, and F). For comparison with the symmetric case note that curve A is identical to the curve labeled $\Gamma = 0$ in Fig. 2.

Consider what happens as we steadily decrease $-\epsilon_d$ from $\frac{1}{2}U$. The manifold of the states of $\mathcal{H}_1$ for the case when $-\epsilon_d \ll U$ is depicted in Fig. 6. From this figure we see that for $T \gg U$, the impurity states will still be effectively degenerate, so that we still get the free-orbital regime in which $T\chi = \frac{1}{8}$. But now, as T drops below U, and for temperatures such that $-\epsilon_d \ll T \ll U$, we get a whole new regime, in which the $n_d = 0$ and the $n_d = 1$ subspaces are equally thermally populated and can be regarded as degenerate, whereas the $n_d = 2$ subspace is thermally depopulated and can be ignored. This regime, in which $T\chi$ has the characteristic value $\frac{1}{6}$, will be referred to as the valence-fluctuation regime, and turns out to play an extremely important role in determining the properties of the asymmetric Anderson model, as we will see later. Finally, as T drops well below $-\epsilon_d$, all the subspaces except the $n_d = 1$ subspace get thermally depopulated. Hence, we get the local-moment regime in which the impurity degree of freedom is effectively a spin $\frac{1}{2}$, and $T\chi = \frac{1}{4}$. When $\Gamma = 0$, the local-moment regime is stable as $T \to 0$. All this is indicated by curve B of Fig. 5.

Clearly, if $-\epsilon_d$ is decreased to be equal to zero exactly, then $n_d = 1$ and $n_d = 0$ subspaces are exactly degenerate, and hence the valence fluctuation regime will be stable all the way to $T = 0$, as indicated by curve C of Fig. 5.

Now consider what happens as ϵ_d is driven positive

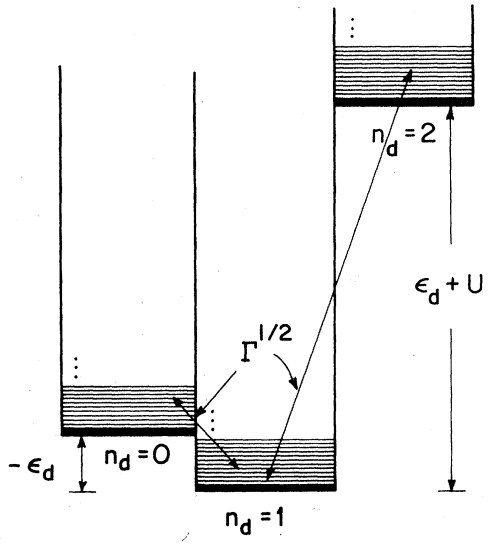

FIG. 6. Manifold of states of the asymmetric Anderson model when the impurity level width Γ is zero and $-\epsilon_d \ll U$. Compare with the symmetric case shown in Fig. 2. For finite Γ this figure can be used to understand the results of the valence-fluctuation regime ($-\epsilon_d \ll T \ll U$) if we replace the relative energy of the $n_d = 0$ configuration $-\epsilon_d$ by $-E_d(T) = -\epsilon_d - (\Gamma/\pi)\ln(U/T)$.

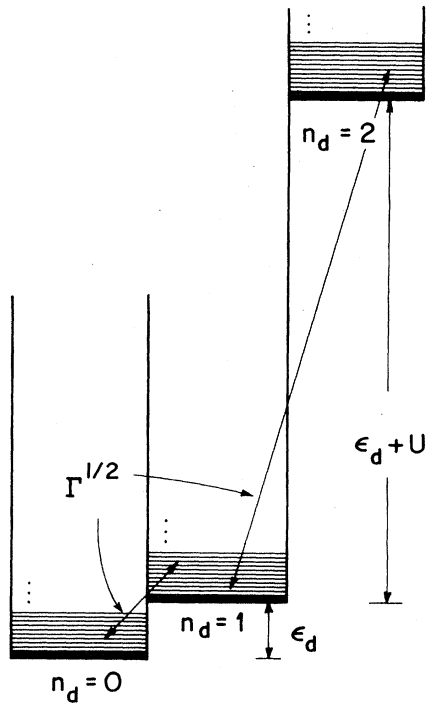

FIG. 7. Manifold of states of the asymmetric Anderson model when the impurity level width Γ is zero *and* $0 < \epsilon_d \ll U$.

but $|\epsilon_d| \ll U$ still. The picture of the manifold of the states of H_A for this case is drawn in Fig. 7. Clearly for $T \gg U$, we still have the free-orbital regime, and for $\epsilon_d \ll T \ll U$, we once again have the valence-fluctuation regime. But now the ground-state subspace is the one for which $n_d = 0$, which carries no moment. As T drops below ϵ_d, all subspaces except $n_d = 0$ get thermally depopulated, and as a result $T\chi$ drops sharply to zero, as indicated by curve D of Fig. 5. We will refer to the low-temperature regime in which $T\chi$ is zero as the frozen-impurity regime, thereby meaning only that effectively the impurity degree of freedom is frozen out.

For ϵ_d values other than the characteristic values considered above, the behavior of $T\chi$ can be understood by considering how the transition temperatures of Fig. 5 move around. For example, if ϵ_d is increased to become of order U, the two transitions of curve D in Fig. 5 merge to give curve E. For $\epsilon_d \gg U$ we get curve F.

2. *Case when* $\Gamma \ll U$

Next we discuss the case when Γ is nonzero, but $\Gamma \ll U$. This is the most interesting of the asymmetric cases and, as we will see below, *exhibits characteristic new features.* The schematic $T\chi$ plots

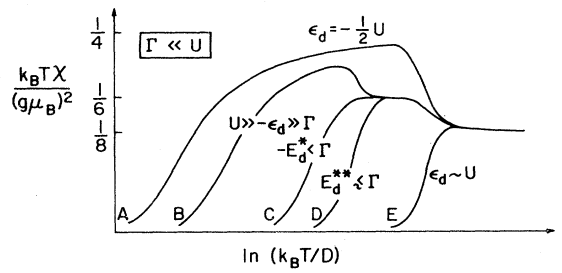

FIG. 8. Schematic plots of $k_B T\chi(T)/(g\mu_B)^2$ vs $\ln(k_B T/D)$ for the case $\Gamma << U$ of the asymmetric Anderson model. The extreme curves are easy to understand: *A* is the symmetric Anderson model result shown in Fig. 2 ($\Gamma << U$ curves) while *E* correspond to such a large, positive ϵ_d that the susceptibility drops directly from the free-orbital to the frozen-impurity regime (see $\epsilon_d \simeq U$ curve in Fig. 5). The remaining three curves illustrate possible transitions from the valence-fluctuation regime ($T\chi = \frac{1}{6}$) as ϵ_d is increased. In *B*, since $\epsilon_d >> \Gamma$, a local-moment develops before the frozen-impurity regime takes over. Note that the low-temperature shapes of *A* and *B* have the universal shape of the Kondo susceptibility. This is no longer true for curve *C* where $-\epsilon_d << \Gamma$. Now the $n_d = 0$ and $n_d = 1$ configurations are so strongly hybridized that not only is there no local moment but the transition to the frozen-impurity regime is steeper than the universal curve. Finally, in *D*, where ϵ_d is positive and $<<\Gamma$, the transition is even steeper. See the discussion in Sec. I B 2 for a definition of E_d^* and E_d^{**}.

for this case are shown in Fig. 8, where curve *A* represents the symmetric case which has already been discussed briefly in Sec. I A.

As we decrease $-\epsilon_d$ from $\frac{1}{2}U$, the first characteristic case for us to consider is that for which $\Gamma << -\epsilon_d << U$. Then at first glance we expect Fig. 6 to remain a good picture, since Γ is small compared to the splittings between the subspaces which it connects. So (as for $\Gamma = 0$) we expect to get the free-orbital regime (in which $T\chi = \frac{1}{8}$) for $T >> U$, and a transition to the valence-fluctuation regime (in which $T\chi = \frac{1}{6}$) as T drops below U. This much indeed turns out to be true; see curve *B* of Fig. 8.

But now, within the valence fluctuation regime (i.e., for $T << U$) a crucial, new feature appears which is characteristic of the asymmetric case. This new feature is that now we can continue to think in terms of Fig. 6 for $T << U$ only if we are prepared to *replace ϵ_d by an effective, temperature-dependent, impurity orbital energy* $E_d(T)$ given by

$$-E_d(T) \simeq -\epsilon_d - \frac{\Gamma}{\pi}\ln\left(\frac{U}{T}\right) . \tag{1.13}$$

This feature, which is demonstrated in Sec. III C, arises due to the virtual transitions induced by Γ from the $n_d = 1$ subspace to the $n_d = 2$ subspace. We note that as T decreases, $-E_d(T)$ decreases slowly, so that depending on the parameter values, $-E_d(T)$ can become comparable to or less than Γ, or $E_d(T)$ can go positive. So, what transitions we get from the valence-fluctuation regime depends very much on the relative values of $E_d(T)$ and Γ.

To start with, suppose that $-\epsilon_d$ is sufficiently large compared to Γ that as we decrease T, $-E_d(T)$ still remains much larger than Γ. In this case we will eventually hit a temperature T_2^* where

$$T_2^* \simeq -E_d(T_2^*) \equiv -E_d^* . \tag{1.14}$$

Then as T drops below T_2^*, we once again see the local moment developing due to the thermal depopulation of the $n_d = 0$ subspace. As in the symmetric case, the virtual transitions induced by Γ from the $n_d = 1$ subspace to the $n_d = 0$ subspace give rise to effective interactions between the impurity and the conduction-electron degrees of freedom, but now these interactions include potential scattering in addition to spin-spin scattering. As is demonstrated in Sec. III D, we can write

$$\mathcal{H}_{\rm int} = -J_{\rm eff}\vec{s}(0)\cdot\vec{S}_i + K_{\rm eff}n(0) , \tag{1.15}$$

where $n(0)$ is the conduction-electron density at the impurity site, and $\rho J_{\rm eff}$ and $\rho K_{\rm eff}$ are given by

$$\rho J_{\rm eff} \simeq -\frac{2\Gamma}{\pi|E_d^*|} ,$$

$$\rho K_{\rm eff} = \frac{\Gamma}{2\pi|E_d^*|} = \frac{1}{4}|\rho J_{\rm eff}| . \tag{1.16}$$

[These results are basically obtained by considering the transitions induced by Γ from the $n_d = 1$ subspace to the $n_d = 0$ subspace (which is essentially $-E_d^*$ above) in second-order perturbation theory.] It is also demonstrated in Sec. III D that potential scattering has little effect on the temperature dependence of the susceptibility, in the sense that the $T\chi$ curve for this case can be mapped to the same universal Kondo $T\chi$ curve as in the symmetric case, as indicated by curve *B* of Fig. 8. So we get a gradual transition to the frozen-impurity regime in which $T\chi = 0$, with the Kondo temperature being given by

$$T_K \sim T_2^*|\rho J_{\rm eff}|^{1/2}\left(\exp -\frac{1}{|\rho J_{\rm eff}|}\right)$$

$$\sim (\Gamma U)^{1/2}\exp\left(-\frac{2\Gamma}{\pi|\epsilon_d|}\right) . \tag{1.17}$$

Now consider what happens as we decrease $-\epsilon_d$. As $-\epsilon_d$ decreases, so does $-E_d^*$, and eventually we reach the situation when $-E_d^* \lesssim \Gamma$, as happens once $-\epsilon_d \lesssim (\Gamma/\pi)\ln(U/\Gamma)$. Now the $n_d = 0$ and $n_d = 1$ subspaces get hybridized, which hybridization is hard to treat analytically. Another way to think about this situation is to note that as $-E_d^*$ decreases to become

of order Γ, $|\rho J_{\text{eff}}|$ increases to become of order unity and T_K rises to become of order T_2^*. So we get a direct transition from the valence fluctuation to the frozen-impurity regime, as indicated by curve C of Fig. 8.

If $-\epsilon_d$ is made sufficiently small compared to Γ or is driven positive (when $\Gamma \neq 0$, there is nothing special about $\epsilon_d = 0$), we have the situation that $E_d(T)$ can be positive and increasing as T decreases within the valence-fluctuation regime. In this case the picture to think in terms of is Fig. 7 with ϵ_d replaced by $E_d(T)$. Now we expect a transition to the frozen-impurity regime as we hit a temperature T_3^* such that

$$T_3^* \simeq E_d(T_3^*) = E_d^{**} \quad . \tag{1.18}$$

We note that when $E_d^{**} \gtrsim \Gamma$, the numerical results for $T\chi$ display sharp drops in $T\chi$ as T drops below T_3^*, reminiscent of the sharp drops in $T\chi$ for $\Gamma = 0$ and $\epsilon_d > 0$ (cf. curve D of Fig. 5), as indicated by curve D of Fig. 8. These sharp drops in the $T\chi$ vs $\ln T$ curves give rise to broad maxima when we plot χ vs T. For more discussion see Sec. III E.

When ϵ_d is positive and increasing, so is E_d^{**}. Eventually when ϵ_d gets to be of order U, so does E_d^{**}, and the two transitions of curve D in Fig. 8 merge, and we get a direct transition from the free orbital to the frozen-impurity regime, as indicated by curve E of Fig. 8. The temperature scale determining this transition is basically set by ϵ_d.

3. *Case when* $\Gamma >> U$

Finally, we consider the case when $\Gamma >> U$. Now, as long as $|\epsilon_d| << \Gamma$ (recall $\epsilon_d \geq -\frac{1}{2}U$), Γ dominates the show. We have the free-orbital regime as before for $T >> \Gamma$. But for $T << \Gamma$, the impurity degree of freedom dissolves into the conduction-electron continuum and $T\chi$ goes to zero. (The ϵ_d and U terms only consitute interactions between the new effective conduction-electron degrees of freedom and lead to a constant susceptibility for $T << \Gamma$.) See curve A of Fig. 9. On the other hand, if $\epsilon_d >> \Gamma$, we have a transition from the free orbital to the frozen-impurity regime at $T \sim \epsilon_d$, as in curve B of Fig. 9.

We note that the zero-temperature regime has been referred to as the frozen-impurity regime in all the cases, which is to indicate only that, effectively, the impurity degree of freedom is always frozen out, leaving behind only residual interactions between renormalized conduction-electron degrees of freedom. In the asymmetric case, since particle-hole symmetry is no longer valid, these residual interactions include potential scattering. The information as to which parameter values we are considering is contained in the relation between the renormalized conduction-electron degrees of freedom and the original conduction-electron degrees of freedom (i.e., in questions as to whether a conduction-electron degree of freedom is frozen out in addition to the impurity degree of freedom being frozen out, etc.) and in the strengths of the residual interactions among the conduction electrons. In Sec. III F we show that the most dominant of these interactions lead to a constant susceptibility and to a linear specific heat (as $T \to 0$).

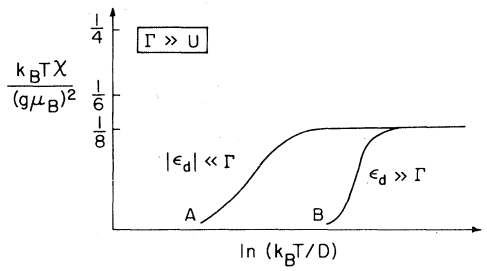

FIG. 9. Plots of $k_B T\chi(T)/(g\mu_B)^2$ vs $\ln(k_B T/D)$ for the case $\Gamma >> U$ of the asymmetric Anderson model. For all values of ϵ_d there is a direct transition, as the temperature is lowered, from the free-orbital regime to the frozen-impurity one. The case $|\epsilon_d| << \Gamma$, curve A, is indistinguishable from the symmetric Anderson model for $\Gamma >> U$ (cf. the $\Gamma >> U$ curve of Fig. 2). For $\epsilon_d >> \Gamma$, curve B, the transition occurs at $T \sim \epsilon_d$.

This completes our survey of the susceptibility results for the asymmetric case. The rest of the sections of the paper will deal with the detailed quantitative discussion of the basic features presented above. Some of our results, such as Eqs. (1.13) and (1.17), were first derived by Haldane[7] using perturbative scaling techniques.

II. FIXED POINTS AND EFFECTIVE HAMILTONIANS FOR THE ASYMMETRIC ANDERSON MODEL

In this section we set up the formal machinery of fixed points, eigenoperators, and effective Hamiltonians that are associated with the renormalization-group transformation T^2 and are of interest in the case of the asymmetric Anderson model. It is only with the help of this machinery that the results of the numerical calculations can be understood. In Sec. II A we identify the basic fixed points for the asymmetric Anderson model. In Sec. II B we discuss a complication that can arise due to the presence of asymmetry—namely, the possibility of potential scattering and lines of fixed points. In Sec. II C we identify the eigenoperators, eigenvalues, and effective Hamiltonians around each of the fixed points for the asymmetric case.

A. Basic fixed points for the asymmetric Anderson model

To start with we want to identify the basic fixed points of $\mathcal{T}^2$ that are of interest for the asymmetric Anderson model. These fixed points are important because each of the various regimes we discussed in Sec. I B is associated with one of these fixed points. Three of the basic fixed points that we will encounter, namely the free-orbital, the local-moment, and the strong-coupling fixed points, are the same as in the symmetric case. The major new fixed point that is characteristic of the asymmetric case is the valence-fluctuation fixed point (associated with the valuence-fluctuation regime discussed in Sec. I A). Another fixed point, the frozen-impurity fixed point, is related to the strong-coupling fixed point via potential scattering (as discussed in Sec. II B).

The method we follow in order to identify the fixed points for the asymmetric case will be the same as for the symmetric case: namely, we consider special values (basically 0 or ∞) for the parameters Γ, U, and ϵ_d and compare the resulting H_N [cf. Eq. (1.2)], in the limit $N \to \infty$, with the free-electron Hamiltonian. For details, see Secs. III A and III B of I. In accordance with the restriction $\epsilon_d \geq -\frac{1}{2}U$, we need only consider $\tilde{\epsilon}_d \geq -\tilde{U}$ *Furthermore we will only describe the odd-N case throughout the rest of this paper.*

1. *Free-orbital fixed point:* $H^*_{\rm FO}$

This is the same fixed point as discussed in Sec. III B 1 of I, and can be obtained by setting Γ, U, and ϵ_d to zero in Eq. (1.2). The resulting generating Hamiltonian, denoted by $H^*_{N,\rm FO}$, is just the free-electron Hamiltonian H^0_N plus a free-impurity orbital of zero energy. As (odd) $N \to \infty$, $H^*_{N,\rm FO}$ goes rapidly to the fixed point $H^*_{\rm FO}$, which is just the even free-electron fixed point H^* plus a zero-energy impurity orbital. For details see Secs. III A and III B of I.

2. *Valence-fluctuation fixed point:* $H^*_{\rm VF}$

This is the characteristic new fixed point associated with the asymmetric case, and corresponds to the situation in which only the $n_d=0$ and $n_d=1$ configurations of the impurity are present, are degenerate, and are decoupled from the conduction electrons. It can be obtained by setting Γ and ϵ_d to zero in Eq. (1.2) while letting $U \to \infty$, as a result of which the subspace of states in which $n_d=2$ gets removed from consideration. The resulting generating Hamiltonian, to be denoted $H^*_{N,\rm VF}$, is just H^0_N plus a new effective impurity degree of freedom corresponding to the $n_d=(0,1)$ configurations only. Clearly, for (odd) $N \to \infty$, $H^*_{N,\rm VF}$ goes to a new fixed point to be denoted $H^*_{\rm VF}$, which is just the even free-electron fixed point H^* plus the new impurity degree of freedom.

In order to make this more explicit, as well as to derive some results that we will need later, we now consider a situation in which Γ and ϵ_d are small but U is much larger than the energies of interest. In particular, consider how this affects the energy levels and states of the initial Hamiltonian H_0 (H_N for $N=0$). From Eq. (1.2) we get

$$H_0 = \tilde{\Lambda}^{-1/2}[\tilde{\epsilon}_d(c^\dagger_{d\mu}c_{d\mu}-1) + \tilde{\Gamma}^{1/2}(f^\dagger_{0\mu}c_{d\mu}+c^\dagger_{d\mu}f_{0\mu}) + 2\tilde{U}n_{d\uparrow}n_{d\downarrow}] \ . \tag{2.1}$$

If we neglect states which have energies $\tilde{U}$ above the ground state, we get rid of the subspace in which $n_d=2$. By calculating the remaining energies and states up to $O(\tilde{\Gamma}/\tilde{U})$, it is straightforward to show that H_0 is equivalent to

$$H_0 \simeq \Lambda^{-1/2}\left[\tilde{\epsilon}_d(b^\dagger_{d\mu}b_{d\mu}-1) + \tilde{\Gamma}^{1/2}(f^\dagger_{0\mu}b_{d\mu}+b^\dagger_{d\mu}f_{0\mu}) + \frac{\tilde{\Gamma}}{2(\tilde{\epsilon}_d+2\tilde{U})}(b^\dagger_{d\mu}\vec{\sigma}_{\mu\nu}b_{d\nu})(f^\dagger_{0\mu'}\vec{\sigma}_{\mu'\nu'}f_{0\nu'}) - \frac{\tilde{\Gamma}}{2(\tilde{\epsilon}_d+2\tilde{U})}(b^\dagger_{d\mu}b_{d\mu})(f^\dagger_{0\nu}f_{0\nu})\right] \ ; \tag{2.2}$$

where the operator $b_{d\mu}$ acts on the remaining ($n_d=0$ and $n_d=1$) impurity states only, and is defined by

$$b^\dagger_{d\mu}|\Omega\rangle = |\mu\rangle, \quad b^\dagger_{d\mu}|\nu\rangle = 0 \ , \tag{2.3}$$

$$b_{d\mu}|\Omega\rangle = 0, \quad b_{d\mu}|\nu\rangle = \delta_{\mu\nu}|\Omega\rangle \ . \tag{2.4}$$

Here $|\Omega\rangle$ represents the state in which the impurity orbital is empty, and $|\mu\rangle$ the state in which it is occupied by one electron of spin μ ($\uparrow$ or $\downarrow$). It is easy to verify that

$$b^\dagger_{d\mu} = c^\dagger_{d\mu}(1-n_d), \quad b_{d\mu} = (1-n_d)c_{d\mu} \ ,$$
$$b^\dagger_{d\mu}b_{d\mu} = n_d \ . \tag{2.5}$$

Therefore, for any N, if one can neglect states that have energies $\sim \tilde{U}\Lambda^{(N-1)/2}$, then to $O(\tilde{\Gamma}/\tilde{U})$ one is considering, in effect, a Hamiltonian

$$H_N = \Lambda^{(N-1)/2}\left[\sum_{n=0}^{N-1}\Lambda^{-n/2}\xi_n(f^\dagger_{n\mu}f_{n+1\,\mu}+f^\dagger_{n+1\,\mu}f_{n\mu}) + \tilde{\epsilon}_d(b^\dagger_{d\mu}b_{d\mu}-1) + \tilde{\Gamma}^{1/2}(f^\dagger_{0\mu}b_{d\mu}+b^\dagger_{d\mu}f_{0\mu}) + \frac{\tilde{\Gamma}}{2(\tilde{\epsilon}_d+2\tilde{U})}(b^\dagger_{d\mu}\vec{\sigma}_{\mu\nu}b_{d\nu})(f^\dagger_{0\mu'}\vec{\sigma}_{\mu'\nu'}f_{0\nu'}) - \frac{\tilde{\Gamma}}{2(\tilde{\epsilon}_d+2\tilde{U})}(b^\dagger_{d\mu}b_{d\mu})(f^\dagger_{0\nu}f_{0\nu})\right] \ . \tag{2.6}$$

If in addition we consider the case when $\epsilon_d = \Gamma = 0$), the impurity degree of freedom b_d gets decoupled from the conduction electrons, and we get the generating Hamiltonian $H^*_{N,\mathrm{VF}}$. As (odd) $N \to \infty$, $H^*_{N,\mathrm{VF}}$ goes to the valence-fluctuation fixed point H^*_{VF}, which is just the free-electron fixed point H^* plus the free-impurity degree of freedom b_d; i.e., from every state of H^* we can construct three degenerate states of H^*_{VF} corresponding to each of the three impurity states ($|\Omega\rangle$, $|\uparrow\rangle$, $|\downarrow\rangle$).

3. Local-moment fixed point: H^*_{LM}

This is the same fixed point as in the symmetric case, and corresponds to the situation in which only the $n_d = 1$ configuration of the impurity is present and is decoupled from the conduction electrons. It can be obtained by setting $\Gamma = 0$ and $\epsilon_d = -\infty$ in Eq. (2.6), which removes the $n_d = 0$ subspace of states from consideration as well [$n_d = 2$ states are already removed in Eq. (2.6)].

In order to make this more explicit, consider what happens to the Hamiltonian H_0 of Eq. (2.2) when $-\epsilon_d$ is much larger than the energies of interest (i.e., $\epsilon_d < 0$ and large in magnitude). Then the subspace in which $n_d = 0$ can be ignored, and within the remaining ($n_d = 1$) subspace, H_0 can be shown to be equivalent to [up to $O(\Gamma/|\epsilon_d|)$]

$$H_0 = \Lambda^{-1/2}[\tilde{J}(f^\dagger_{0\mu}\,\vec{\sigma}_{\mu\nu} f_{0\nu})\cdot\vec{\tau} + \tilde{K}(f^\dagger_{0\mu} f_{0\mu} - 1)] \ ; \tag{2.7}$$

$$\tilde{J} = -\frac{\tilde{\Gamma}}{2\tilde{\epsilon}_d} + \frac{\tilde{\Gamma}}{4\tilde{U} + 2\tilde{\epsilon}_d} \ , \qquad \tilde{K} = -\frac{\tilde{\Gamma}}{2\tilde{\epsilon}_d} - \frac{\tilde{\Gamma}}{4\tilde{U} + 2\tilde{\epsilon}_d} \ . \tag{2.8}$$

Here $\vec{\tau}$ is a spin-$\frac{1}{2}$ operator associated with the impurity states. Hence, for any N, if one can neglect both the states of energy $\sim U\Lambda^{(N-1)/2}$ and $-\epsilon_d\Lambda^{(N-1)/2}$, then to $O(\Gamma/|\epsilon_d|, \Gamma/U)$ one is in effect considering a Hamiltonian[8]

$$H_N = \Lambda^{(N-1)/2}\left[\sum_{n=0}^{N-1}\Lambda^{-n/2}\xi_n(f^\dagger_{n\mu} f_{n+1\,\mu} + f^\dagger_{n+1\,\mu} f_{n\mu}) + \tilde{J} f^\dagger_{0\mu}\,\vec{\sigma}_{\mu\nu} f_{0\nu}\cdot\vec{\tau} + \tilde{K}(f^\dagger_{0\mu} f_{0\mu} - 1)\right] \tag{2.9}$$

If in addition we consider the case when $\Gamma = 0$, then $\tilde{J} = \tilde{K} = 0$, and H_N is just the Hamiltonian $H^*_{N,\mathrm{LM}}$ discussed in Sec. III B 2 of I, and leads to the local-moment fixed point H^*_{LM} for (odd) $N \to \infty$. H^*_{LM} is just the even free-electron fixed point H^* plus the impurity spin $\vec{\tau}$.

4. Strong-coupling fixed point: H^*_{SC}

This fixed point is also the same as in the symmetric case, and can be obtained by letting $\Gamma \to \infty$ for fixed U and ϵ_d. It is easy to verify that this removes all the states of H_0 [cf. Eq. (2.1)] except its ground state, so that the effective Hamiltonian H_N for any N is Eq. (1.2) with all terms involving c_d and f_0 removed, and is denoted $H^*_{N,\mathrm{SC}}$

$$H^*_{N,\mathrm{SC}} = \Lambda^{(N-1)/2}\sum_{n=1}^{N-1}\Lambda^{-n/2}\xi_n(f^\dagger_{n\mu} f_{n+1\,\mu} + f^\dagger_{n+1\,\mu} f_{n\mu}) \ . \tag{2.10}$$

As discussed in Sec. III B of I, as (odd) $N \to \infty$, $H^*_{N,\mathrm{SC}}$ goes to the odd strong-coupling fixed point H^*_{SC}, with single-particle levels $\hat{\eta}^*_l$.

5. Frozen-impurity fixed point: H^*_{FI}

Finally consider the case in which we set Γ and $U = 0$ in Eq. (1.2) but let $\epsilon_d \to +\infty$. This removes all the states in which $n_d = 1$ or 2 from consideration. The resulting generating Hamiltonian, which we will denote as $H^*_{N,\mathrm{FI}}$, is essentially the free-electron Hamiltonian H^0_N *with the added proviso* that the ground state be assigned a charge of -1. {This is because the charge operator Q_N was defined so that [cf. Eq. (2.25) of I] $n_d = 1$ has zero charge.} As (odd) $N \to \infty$, $H^*_{N,\mathrm{FI}}$ goes to H^*_{FI} which is just the even fixed point H^* plus a ground state of charge -1.

B. Potential scattering and lines of fixed points

In Sec. II A, we identified the basic fixed points of the asymmetric Anderson model. All these were essentially simply related to the free-electron Hamiltonian H^0_N. However, since the Hamiltonians we are dealing with do not obey particle-hole symmetry, there is an added complication that we must consider, namely that the H^0_N associated with the fixed points can have potential scattering.

Consider the Hamiltonian

$$H^0_N(\tilde{K}) \equiv \Lambda^{(N-1)/2}\left[\sum_{n=0}^{N-1}\Lambda^{-n/2}\xi_n(f^\dagger_{n\mu} f_{(n+1)\mu} + f^\dagger_{(n+1)\mu} f_{n\mu}) + \tilde{K}(f^\dagger_{0\mu} f_{0\mu} - 1)\right] . \tag{2.11}$$

The $\tilde{K}$ term describes potential scattering of the conduction electrons at the impurity site. Since Eq. (2.11) is a quadratic Hamiltonian it can be diagonalized exactly (numerically) in terms of new electron

and hole operators and energies: for odd N,

$$H_N^0(\tilde{K}) = \sum_{j=1}^{(N+1)/2} [\eta_j^+(\tilde{K},N) g_{j\mu}^\dagger g_{j\mu} + \eta_j^-(\tilde{K},N) h_{j\mu}^\dagger h_{j\mu}] \ . \tag{2.12}$$

The properties of $H_N^0(\tilde{K})$ are investigated in detail in Appendix A. Here we just note down some results, the most important of which is that $\eta_j^+(\tilde{K},N)$ and $\eta_j^-(\tilde{K},N)$ for fixed j have well-defined limits $\eta_j^+(\tilde{K})$ and $\eta_j^-(\tilde{K})$ at $N \to \infty$. $\eta_j^+(\tilde{K})$ and $\eta_j^-(\tilde{K})$ vary with $\tilde{K}$ in a smooth monotonic fashion, as depicted in Fig. 16(b). Thus we have a whole line of fixed points of $\mathcal{T}^2$, one for each value of $\tilde{K}$, which we will denote (for odd $N \to \infty$) by $H^*(\tilde{K})$.

Clearly from each of the basic fixed points considered in Sec. II A, we can generate a whole line of fixed points simply by adding potential scattering. So at first sight, we can think of five lines of fixed points for the asymmetric Anderson model: namely, the lines of free-orbital, valence-fluctuation, local-moment, strong-coupling, and frozen-impurity fixed points, which we will denote by $H_{\rm FO}^*(\tilde{K})$, $H_{\rm VF}^*(\tilde{K})$, $H_{\rm LM}^*(\tilde{K})$, $\hat{H}_{\rm SC}^*(\tilde{K})$, and $H_{\rm FI}^*(\tilde{K})$.

However, we can show that the lines of strong-coupling and frozen-impurity fixed points are the same. For this purpose recall that [cf. Sec. III B 3 of I] $\hat{H}_{\rm SC}^*$ is the same as the odd fixed point $\hat{H}^*$; therefore $\hat{H}_{\rm SC}^*(\tilde{K})$ is the same as the line of odd fixed points $\hat{H}^*(\tilde{K})$ arising from $H_N^0(\tilde{K})$ for even N. But as proved in Appendix A, $\hat{H}^*(\tilde{K})$ can be mapped to $H^*(\tilde{K}')$ [where $\tilde{K}'$ is related to $\tilde{K}$ by Eq. (A64)] with the added proviso that the ground state of the latter be assigned a charge of -1. Hence $\hat{H}_{\rm SC}^*(\tilde{K})$ is the same as $H^*(\tilde{K}')$ plus a ground state of charge -1; i.e., it is the same as $H_{\rm FI}^*(\tilde{K}')$.

Thus we have identified four distinct lines of fixed points for the asymmetric Anderson model, namely the lines of free-orbital, valence-fluctuation, local-moment, and frozen-impurity fixed points, denoted by $H_{\rm FO}^*(\tilde{K})$, $H_{\rm VF}^*(\tilde{K})$, $H_{\rm LM}^*(\tilde{K})$, and $H_{\rm FI}^*(\tilde{K})$, respectively. The generating Hamiltonians for these fixed points will be denoted $H_{N,\rm FO}^*(\tilde{K})$, $H_{N,\rm VF}^*(\tilde{K})$, $H_{N,\rm LM}^*(\tilde{K})$, and $H_{N,\rm FI}^*(\tilde{K})$: $H_{N,\rm FO}^*(\tilde{K})$ is just $H_N^0(\tilde{K})$ plus the free-orbital states determined by c_d; $H_{N,\rm VF}^*(\tilde{K})$ is just $H_N^0(\tilde{K})$ plus the valence-fluctuation states determined by b_d; $H_{N,\rm LM}^*(\tilde{K})$ is just $H_N^0(\tilde{K})$ plus the local-moment states determined by $\vec{\tau}$; $H_{N,\rm FI}^*(\tilde{K})$ is just $H_N^0(\tilde{K})$ plus a ground state of charge -1. Table I lists the first few states of the four lines of fixed points, together with the energies and charge and spin quantum numbers associated with these states.

We recall that (cf., I Sec. III C) when H_N is near a fixed point, H_N hardly changes with N, so that for the corresponding temperature range, $T\chi$ is a constant. Each of the above fixed points is hence associated with a characteristic, constant $T\chi$ value. To identify these, we calculate $T\chi$ using Eq. (1.5) but using the generating Hamiltonians $H_{N,\rm FO}^*(\tilde{K})$, $H_{N,\rm VF}^*(\tilde{K})$, etc., for H_N. Since the impurity degree of freedom is decoupled from the conduction electrons the calculation is trivial, and we get

$$\begin{aligned} k_B T_N \chi(T_N) &= \langle S_{iz}^2 \rangle_i + (\langle S_{Nz}^{02} \rangle_{H_N^0(K)} - \langle S_{Nz}^{02} \rangle_{H_N^0}) \\ &= \langle S_{iz}^2 \rangle_i + k_B T_N \chi_0(T_N, \bar{\beta}, \Lambda, \tilde{K}) \ . \end{aligned} \tag{2.13}$$

Here S_{iz} is the impurity spin operator and $\langle\ \rangle_i$ denotes the expectation value evaluated using just the zero-energy impurity states; and $\langle S_{iz}^2 \rangle_i$ is trivially verified to be $\frac{1}{8}$, $\frac{1}{6}$, $\frac{1}{4}$, and 0 for the FO, VF, LM, and FI cases, respectively. χ_0 is obviously the change

TABLE I. First few states and energies of the various fixed-point Hamiltonians.

Charge Q	Spin S	Index r	$H_{\rm FO}^*(\tilde{K})$ state	$H_{\rm FO}^*(\tilde{K})$ energy	$H_{\rm VF}^*(\tilde{K})$ state	$H_{\rm VF}^*(\tilde{K})$ energy	$H_{\rm LM}^*(\tilde{K})$ state	$H_{\rm LM}^*(\tilde{K})$ energy	$H_{\rm FI}^*(\tilde{K}<0)$ state	$H_{\rm FI}^*(\tilde{K}<0)$ energy
0	$\frac{1}{2}$	1	c_d	0	b_d	0	τ	0	g_1	η_1^+
		2	g_1	η_1^+	g_1	η_1^+	$\tau+g_1+h_1$	$\eta_1^+ + \eta_1^-$	g_2	η_2^+
		3	$2c_d+h_1$	η_1^-	$b_d+g_1+h_1$	$\eta_1^+ + \eta_1^-$	$\tau+g_1+h_1$	$\eta_1^+ + \eta_1^-$	$2g_1+h_1$	$2\eta_1^+ + \eta_1^-$
-2	$\frac{1}{2}$	1	h_1	η_1^-	h_1	η_1^-	$\tau+2h_1$	$2\eta_1^-$	h_1	η_1^-
$+2$	$\frac{1}{2}$	1	$2c_d+g_1$	η_1^+	b_d+2g_1	$2\eta_1^+$	$\tau+2g_1$	$2\eta_1^+$	$2g_1+g_2$	$2\eta_1^+ + \eta_2^+$
-1	0	1	—	0	—	0	$\tau+h_1$	η_1^-	—	0
		2	c_d+h_1	η_1^-	b_d+h_1	η_1^-	$\tau+g_1+2h_1$	$\eta_1^+ + 2\eta_1^-$	g_1+h_1	$\eta_1^+ + \eta_1^-$
	1	1	c_d+h_1	η_1^-	b_d+h_1	η_1^-	$\tau+h_1$	η_1^-	g_1+h_1	$\eta_1^+ + \eta_1^-$
$+1$	0	1	$2c_d$	0	b_d+g_1	η_1^+	$\tau+g_1$	η_1^+	$2g_1$	$2\eta_1^+$
		2	c_d+g_1	η_1^+	$2g_1$	$2\eta_1^+$	$\tau+2g_1+h_1$	$2\eta_1^+ + \eta_1^-$	g_1+g_2	$\eta_1^+ + \eta_2^+$
	1	1	c_d+g_1	η_1^+	b_d+g_1	η_1^+	$\tau+g_1$	η_1^+	g_1+g_2	$\eta_1^+ + \eta_2^+$

in the susceptibility due to potential scattering, and is given by (N odd)

$$k_B T_N \chi_0(T_N) = \sum_{l=1}^{(N+1)/2} \left[\frac{e^{-\bar{\beta}\eta_l^{+(N)}}}{(1+e^{-\bar{\beta}\eta_l^{+(N)}})^2} + \frac{e^{-\bar{\beta}\eta_l^{-(N)}}}{(1+e^{-\bar{\beta}\eta_l^{-(N)}})^2} - \frac{2e^{-\bar{\beta}\eta_l^{*}}}{(1+e^{-\bar{\beta}\eta_l^{*}})^2} \right] . \tag{2.14}$$

In Appendix A we demonstrate that if we replace $\eta_l^{\pm}(N)$ above by their fixed-point values $\eta_l^{\pm}$, the resulting expression for $k_B T_N \chi_0(T_N)$ vanishes as $\exp(-\pi^2/\ln\Lambda)$ as $\Lambda \to 1$. The contribution to Eq. (2.14) hence comes from the deviations of $\eta_l^{\pm}(N)$ from their fixed-point values and can be shown to be of order $(k_B T_N/D)$. We can therefore neglect the second term in Eq. (2.13). Evaluating the first term for each of the lines of fixed points, we get for the characteristic $T\chi$ values,

$$\frac{k_B T \chi}{(g\mu_B)^2} = \begin{cases} \frac{1}{8} & \text{for } H_{\rm FO}^*(\tilde{K}) , \\ \frac{1}{6} & \text{for } H_{\rm VF}^*(\tilde{K}) , \\ \frac{1}{4} & \text{for } H_{\rm LM}^*(\tilde{K}) , \\ 0 & \text{for } H_{\rm FI}^*(\tilde{K}) . \end{cases} \tag{2.15}$$

From our discussion of the fixed points of the asymmetric Anderson model, it should be reasonably evident by now that each of the regimes that we discussed in Sec. 1 A is associated with the line of fixed points of the same name [i.e., the free-orbital regime is associated with $H_{\rm FO}^*(K)$, etc.]. This association becomes even more explicit when we consider the actual flow of H_N between the various fixed points, and the correspondence of such a flow to the temperature dependence of the susceptibility. This will be done in detail in Sec. III. But for this purpose, we need to identify the eigenoperators of $\mathcal{T}^2$ around each of the above fixed points, and construct effective Hamiltonians that approximately describe the flow of H_N when it is in the vicinity of these fixed points. This is done in Sec. II C. Once again we emphasize that the discussion in this section assumes familiarity with the discussion in Secs. IV A and IV B of I, which should be consulted for details.

C. Eigenoperators and effective Hamiltonians for the asymmetric Anderson model

The method we follow in order to identify the eigenoperators and construct the effective Hamiltonians for a fixed point of $\mathcal{T}^2$ in the asymmetric case is exactly the same as in the symmetric case, namely we examine the properties of $H_N^* + \Lambda^{(N-1)/2}\,\delta H$, where δH is small and depends only on the first few degrees of freedom consistent with the fixed point, and H_N^* is the generating Hamiltonian for the fixed point (cf. Secs. IV A and IV B of I). For this purpose we need expansions for f_0, f_1, etc., in terms of the electron and hole operators that diagonalize $H_N^0(\tilde{K})$. In Appendix A it is shown that

$$f_{0\mu} = \Lambda^{-(N-1)/4} \sum_j (\alpha_{0j}^{+} g_{j\mu} + \alpha_{0j}^{-} h_{j\mu}^{\dagger}) , \tag{2.16}$$

$$A_{1\mu} \equiv (\tilde{K} f_{0\mu} + \xi_0 f_{1\mu}) = \Lambda^{-3[(N-1)/4]} \sum_j (\alpha_{0j}^{+} \eta_j^{+} g_{j\mu} - \alpha_{0j}^{-} \eta_j^{-} h_j^{\dagger}) , \tag{2.17}$$

$$A_{2\mu} \equiv (\xi_0^2 f_{0\mu} + \tilde{K} A_{1\mu} + \Lambda^{-1/2} \xi_0 \xi_1 f_{2\mu}) = \Lambda^{-5[(N-1)/4]} \sum_j [\alpha_{0j}^{+} (\eta_j^{+})^2 g_{j\mu} + \alpha_{0j}^{-} (\eta_j^{-})^2 h_{j\mu}^{\dagger}] , \tag{2.18}$$

where $\alpha_{0j}^{\pm}$ are essentially independent of N, and $\eta_j^{\pm}$ are the fixed-point single-particle energies of $H^*(\tilde{K})$. Thus the roles played by f_0, A_1, etc., in the asymmetric case are analogous to the roles played by f_0, f_1, etc., in the symmetric case: namely using f_0 in δH gives rise to a factor of $\Lambda^{-N/4}$, use of $A_{1\mu}$ in δH gives rise to a factor $\Lambda^{-3N/4}$, etc. On this basis, using the methodology of Secs. IV A and IV B of I, we arrive at the results of Table II, which lists the dominant hierarchy of δH's near each of the fixed points discussed earlier, together with the eigenvalues of the eigenoperators that they generate. Then, for those values of N where H_N is close to a fixed point, for example to the free-orbital fixed point, its flow can be described in terms of the effective Hamiltonian

$$H_N^{\rm eff} = H_{N,\rm FO}^*(\tilde{K}) + \omega_1 \Lambda^{(N-1)/2} \delta H_{1,\rm FO} + \omega_2 \Lambda^{(N-1)/2} \delta H_{2,\rm FO} + \cdots . \tag{2.19}$$

For general values of $\tilde{\epsilon}_d$, $\tilde{U}$, and $\tilde{\Gamma}$, the parameters $\tilde{K}$, ω_1, ω_2, etc., can be determined by fitting the energy levels calculated using Eq. (2.19) to the numerical results from the iterative diagonalization. For limiting cases the dependence of $\tilde{K}$, ω_1, ω_2, etc., on $\tilde{\epsilon}_d$, $\tilde{U}$, and $\tilde{\Gamma}$ can be calculated analytically. Once ω_1, ω_2, etc., are determined, $H_N^{\rm eff}$ can also be used to calculate $k_B T_N \chi(TN)$ and $F(T_N)$ for the appropriate temperature ranges. Exactly similar procedures can be adopted when H_N is close to any of the other fixed points. The actual implementation of these procedures is carried out in Sec. III.

TABLE II. Hierarchy of generators of eigenoperators for the fixed points of the asymmetric Anderson model.

Fixed point	Label δH	Operator	Eigenvalue λ_l^*	Relevance character	Coefficient with which the eigenoperator appears in Sec. III
Free-	$\delta H_{1,\mathrm{FO}}$	$n_{d\uparrow}n_{d\downarrow}$	Λ	Relevant	$2\tilde{U}$
orbital	$\delta H_{2,\mathrm{FO}}$	$(c_{d\mu}^{\dagger}c_{d\mu}-1)$	Λ	Relevant	$\tilde{\epsilon}_d$
fixed	$\delta H_{3,\mathrm{FO}}$	$(c_{d\mu}^{\dagger}f_{0\mu}+f_{0\mu}^{\dagger}c_{d\mu})$	$\Lambda^{1/2}$	Relevant	$\tilde{\Gamma}^{1/2}$
point	$\delta H_{4,\mathrm{FO}}$	$(c_{d\mu}^{\dagger}c_{d\mu}-1)(c_{d\nu}^{\dagger}f_{0\nu}+f_{0\nu}^{\dagger}c_{d\nu})$	$\Lambda^{1/2}$	Relevant	$\cdots$
$H_{\mathrm{FO}}^*(K)$	$\delta H_{5,\mathrm{FO}}$	$c_{d\mu}^{\dagger}\vec{\sigma}_{\mu\nu}c_{d\nu}f_{0\mu'}^{\dagger}\vec{\sigma}_{\mu'\nu'}f_{0\nu'}$	1	Marginal	$\cdots$
	$\delta H_{6,\mathrm{FO}}$	$(c_{d\mu}^{\dagger}c_{d\mu}-1)(f_{0\nu}^{\dagger}f_{0\nu}-1)$	1	Marginal	$\cdots$
	$\delta H_{7,\mathrm{FO}}$	$(c_{d\mu}^{\dagger}f_{0\mu}+f_{0\mu}^{\dagger}c_{d\mu})^2$	1	Marginal	$\cdots$
	$\delta H_{8,\mathrm{FO}}$	$n_{d\uparrow}n_{d\downarrow}(f_{0\nu}^{\dagger}f_{0\nu}-1)$	1	Marginal	$\cdots$
	$\delta H_{9,\mathrm{FO}}$	$(f_{0\mu}^{\dagger}f_{0\mu}-1)$	1	Marginal	$\cdots$
Valence-	$\delta H_{1,\mathrm{VF}}$	$(b_{d\mu}^{\dagger}b_{d\mu}-1)$	Λ	Relevant	$\tilde{\epsilon}_d$
fluctuation	$\delta H_{2,\mathrm{VF}}$	$b_{d\mu}^{\dagger}f_{0\mu}+f_{0\mu}^{\dagger}b_{d\mu}$	$\Lambda^{1/2}$	Relevant	$\tilde{\Gamma}^{1/2}$
fixed point	$\delta H_{3,\mathrm{VF}}$	$b_{d\mu}^{\dagger}\vec{\sigma}_{\mu\nu}b_{d\nu}f_{0\mu'}^{\dagger}\vec{\sigma}_{\mu'\nu'}f_{0\nu'}$	1	Marginal	$\tilde{J}_1$
$H_{\mathrm{VF}}^*(K)$	$\delta H_{4,\mathrm{VF}}$	$b_{d\mu}^{\dagger}b_{\mu}f_{0\nu}^{\dagger}f_{0\nu}$	1	Marginal	$\tilde{K}_1$
	$\delta H_{5,\mathrm{VF}}$	$(f_{0\mu}^{\dagger}f_{0\mu}-1)$	1	Marginal	$\cdots$
Local-	$\delta H_{1,\mathrm{LM}}$	$\vec{\tau}\cdot f_{0\mu}^{\dagger}\vec{\sigma}_{\mu\nu}f_{0\nu}$	1	Marginal	$\tilde{J}$
moment	$\delta H_{2,\mathrm{LM}}$	$(f_{0\mu}^{\dagger}f_{0\mu}-1)$	1	Marginal	$\tilde{K}$
fixed point	$\delta H_{3,\mathrm{LM}}$	$f_{0\mu}^{\dagger}A_{1\mu}+A_{1\mu}^{\dagger}f_{0\mu}$	Λ^{-1}	Irrelevant	$\cdots$
$H_{\mathrm{LM}}^*(K)$	$\delta_{4,\mathrm{LM}}$	$(f_{0\mu}^{\dagger}f_{0\mu}-1)^2$	Λ^{-1}	Irrelevant	$\cdots$
Frozen-	$\delta H_{1,\mathrm{FI}}$	$(f_{0\mu}^{\dagger}A_{1\mu}+A_{1\mu}^{\dagger}f_{0\mu})$	Λ^{-1}	Irrelevant	ω_1
impurity	$\delta H_{2,\mathrm{FI}}$	$(f_{0\mu}^{\dagger}f_{0\mu}-1)^2$	Λ^{-1}	Irrelevant	ω_2
fixed point	$\delta H_{3,\mathrm{FI}}$	$A_{1\mu}^{\dagger}A_{1\mu}$	Λ^{-2}	Irrelevant	$\cdots$
$H_{\mathrm{FI}}^*(K)$	$\delta H_{4,\mathrm{FI}}$	$(f_{0\mu}^{\dagger}f_{0\mu}-1)(f_{0\nu}^{\dagger}A_{1\nu}+A_{1\nu}^{\dagger}f_{0\nu})$	Λ^{-2}	Irrelevant	$\cdots$
	$\delta H_{5,\mathrm{FI}}$	$f_{0\mu}^{\dagger}A_{2\mu}+A_{2\mu}^{\dagger}f_{0\mu}$	Λ^{-2}	Irrelevant	$\cdots$

III. DISCUSSION OF NUMERICAL RESULTS FOR THE ASYMMETRIC ANDERSON MODEL

In this section, we enter into the detailed discussion of the results of the renormalization-group calculations on the asymmetric Anderson model.

A. Preliminary look at the numerical results

To start with, we want to demonstrate that the fixed points identified in Sec. II are relevant to describe the numerical results. For this purpose, we have plotted in Fig. 10 the energies of the first few states of H_N as a function of N (for odd N) for the parameter values $U/D=10^{-3}$, $\epsilon_d/D=-10^{-5}$, and $\Gamma/D=1.571\times10^{-6}$. These states have been chosen to have the same charge and spin quantum numbers as the ones listed in Table I. Thus we can compare the energies of Fig. 10 with the values they would have in the fixed points (the latter are indicated in Fig. 10 for $\tilde{K}=0$). From this comparison it is quite clear that for $N\leq 9$ H_N can be said to be close to H_{FO}^* (with $\tilde{K}=0$), for $13<N<17$ H_N is close to H_{VF}^* (with $\tilde{K}=0$), $23<N<31$ H_N is close to $H_{\mathrm{LM}}^*(\tilde{K})$ and for $N>41$ H_N is close to $H_{\mathrm{FI}}^*(\tilde{K})$.

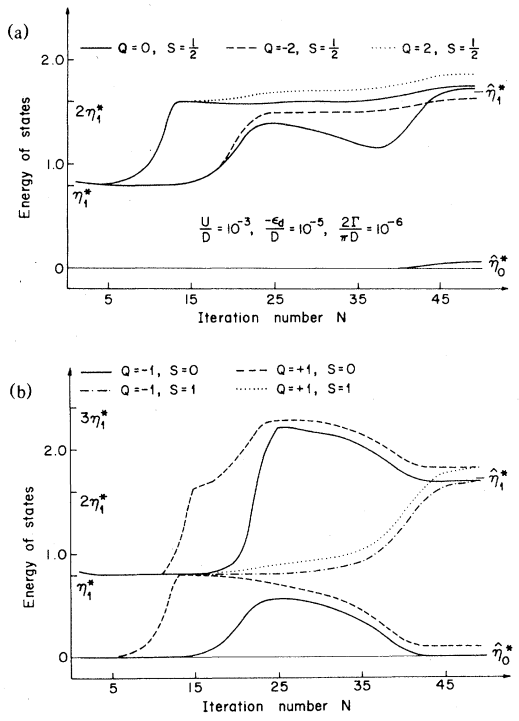

FIG. 10. Low-lying energy levels of H_N as a function of odd N for $\Lambda = 3$, and parameters indicated on the figure. On the left-hand vertical side are the lowest-lying free-electron fixed-point levels for N odd (0, η_1^*, $2\eta_1^*$, and $3\eta_1^*$), while on the right-hand side are the equivalent levels for N even ($\hat{\eta}_0^*$, $\hat{\eta}_1^*$). (a) Levels for even charge and half-integral spin. The following fixed points can be observed by comparing the curves with Table I: free orbital ($N < 9$), valence fluctuation ($13 < N < 17$), local moment ($23 < N < 31$), and frozen impurity ($N > 41$). In the case of the latter two fixed points, the value of impurity scattering is important (see Fig. 11, curve A, and Table VI). (b) Levels for odd charge and integral spin. Note how in the valence-fluctuation regime the $Q = 1$ and $Q = -1$ states (for $S = 0$) are split only to nearly merge again in the local-moment regime. See the discussion following Eq. (3.29).

Flows of H_N such as in Fig. 10 will be analyzed in detail in Secs. III B and III E. Here we just *note some results*. The crossover from $H_{\rm FO}^*$ and $H_{\rm VF}^*$ is due to the relevant variable $\tilde{U}$ and occurs when $\tilde{U}\Lambda^{(N-1)/2}$ grows to become of order 1. The crossover from $H_{\rm VF}^*$ to $H_{\rm LM}^*(\tilde{K})$ is due to the relevant variable $-\tilde{\epsilon}_d$ and occurs (*roughly*) when $-\tilde{\epsilon}_d\Lambda^{(N-1)/2}$ becomes of order 1. The crossover from $H_{\rm LM}^*(\tilde{K})$ to $\hat{H}_{\rm FI}^*(\tilde{K})$ is due to a marginal variable ($\sim\tilde{\Gamma}/-\tilde{\epsilon}_d$) and occurs (*roughly*) when $(\tilde{\Gamma}/-\tilde{\epsilon}_d)N\ln\Lambda$ gets to be of order 1.

Plot A of Fig. 11 shows the plot of $T\chi$ vs T for the same parameter values as above. As in the symmetric case, we can make a one-to-one correspondence between the susceptibility plot and the flow of H_N, with the temperature being related to N via Eq. (1.4). We recall that when H_N is near a fixed point, $T\chi$ is roughly constant as T changes. Figure 11 shows that for $T >> U$, $T\chi$ has the value $\frac{1}{8}$ characteristic of the free-orbital fixed point. As T drops below U, we have a transition to the value $T\chi \simeq \frac{1}{6}$, characteristic of the valence-fluctuation fixed point. As T drops below $-\epsilon_d$ (*roughly*), there is a transition

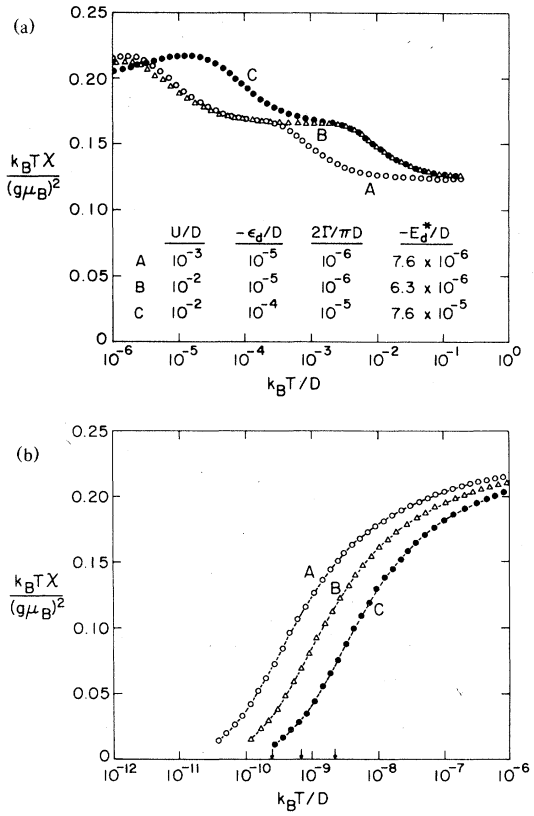

FIG. 11. Plots of $k_B T\chi(T)/(g\mu_B)^2$ vs $\ln(k_B T/D)$ which illustrate the parameter dependence of transitions between the various regimes. (a) That the transition from the free-orbital regime ($T\chi = \frac{1}{8}$) to the valence-fluctuation regime ($T\chi = \frac{1}{6}$) occurs at $T_1^* \sim \frac{1}{5}U$ is clearly illustrated by curve A compared to curves B and C. That the transition from the valence-fluctuation regime to the local-moment regime ($T\chi = \frac{1}{4}$) occurs at $T_2^* \sim \frac{1}{5}E_d^*$ is seen by comparing curve C with curves A and B. The values of E_d^* were deduced from Eq. (3.22). (b) The transition from the local-moment regime to the frozen-impurity one occurs at a temperature of order T_K. See the discussion below Eq. (3.44) and Table VIII for details, where curves A, B, and C are referred to as 7.1, 7.2, and 7.3, respectively. Note that all three curves lie along the universal Kondo-susceptibility curve indicated by the dashed curves.

to the local-moment regime, in which $T\chi$ is close to $\frac{1}{4}$ but smaller by a constant marginal coupling. As T drops further, $T\chi$ slowly decreases to zero, characteristic of the frozen-impurity fixed point. We note that the transition from the local-moment regime to the frozen-impurity regime is represented by the universal curve [dashed line in Fig. 11(b)] just as in the symmetric case [see the discussion following Eq. (3.41)].

B. Free-orbital regime

We recall that when $\tilde{\epsilon}_d$, $\tilde{\Gamma}$, and $\tilde{U}$ are zero, H_N in Eq. (1.2) reduces to $H^*_{N,\mathrm{FO}}$, the generating Hamiltonian for the free-orbital fixed point. Therefore, when $\tilde{\epsilon}_d$, $\tilde{\Gamma}$, and $\tilde{U}$ are all small, we expect to be able to write

$$H^{\mathrm{eff}}_{N,\mathrm{FO}} \cong H^*_{N,\mathrm{FO}} + 2\tilde{U}\Lambda^{(N-1)/2} n_{d\uparrow} n_{d\downarrow} + \tilde{\epsilon}_d \Lambda^{(N-1)/2}(c^\dagger_{d\mu} c_{d\mu} - 1) + \tilde{\Gamma}^{1/2}\Lambda^{(N-1)/2}(f^\dagger_{0\mu} c_{d\mu} + c^\dagger_{d\mu} f_{0\mu}) \ , \quad (3.1)$$

where the $\tilde{U}$, $\tilde{\epsilon}_d$, and $\tilde{\Gamma}$ terms are now to be *treated by perturbation theory*. We note that Eq. (3.1) is precisely of the form of the effective Hamiltonian around the free-orbital fixed point, since the last three terms in Eq. (3.1) are precisely $\delta H_{1,\mathrm{FO}}$, $\delta H_{2,\mathrm{FO}}$ and $\delta H_{3,\mathrm{FO}}$, the generators of relevant eigenoperators around H^*_{FO} [cf. Table II and Eq. (2.19)]. Furthermore, the coefficients $\tilde{K}$, ω_1, ω_2, and ω_3 are now explicitly known, to be just 0, $2\tilde{U}$, $\tilde{\epsilon}_d$, and $\tilde{\Gamma}$, respectively.

Expressing Eq. (3.1) in terms of the electron and hole operators that diagonalize $H^*_{N,\mathrm{FO}}$, we can write

$$H^{\mathrm{eff}}_{N,\mathrm{FO}} = \sum_{l=1}^{J} \eta_l^*(g^\dagger_{l\mu} g_{l\mu} + h^\dagger_{l\mu} h_{l\mu}) + 2\tilde{U}\Lambda^{(N-1)/2} n_{d\uparrow} n_{d\downarrow} + \tilde{\epsilon}_d \Lambda^{(N-1)/2}(c^\dagger_{d\mu} c_{d\mu} - 1) + \tilde{\Gamma}^{1/2}\Lambda^{(N-1)/4} \sum_l \alpha_{0l}(c^\dagger_{d\mu} g_{l\mu} + g^\dagger_{l\mu} c_{d\mu} + c^\dagger_{d\mu} h^\dagger_{l\mu} + h_{l\mu} c_{d\mu}) \ . \quad (3.2)$$

The energies of the states considered in Table I calculated using H^{eff}_N are listed in Table III. The $\tilde{U}$ term lifts the energies of the states in which $n_d = 2$ by $2\tilde{U}\Lambda^{(N-1)/2}$, the ϵ_d term contributes an impurity orbital energy of $\tilde{\epsilon}_d\Lambda^{(N-1)/2}$, and the $\tilde{\Gamma}^{1/2}$ term changes the single-particle energies η_l^* by $\tilde{\Gamma}\Lambda^{(N-1)/2}(\alpha_{0l}^2/\eta_l^*)$. It is clear that these effects account satisfactorily for the energies plotted in Fig. 10 for $N < 11$ (Note: for $U/D = 10^{-3}$ and $\Lambda = 3.0$ and $\tilde{U}\Lambda^{(N-1)/2} = 0.18$ at $N = 11$.) We note that $\tilde{U}$, $\tilde{\epsilon}_d$, and $\tilde{\Gamma}$ are all relevant variables.

One can also calculate $k_B T_N \chi(T_N)$ and $F(T_N)$ using $H^{\mathrm{eff}}_{N,\mathrm{FO}}$ in place of H_N in Eqs. (1.5) and (1.6). The calculational details are identical to those in Sec. V A of I, and one gets to the lowest nonvanishing order in each term,

$$k_B T_N \chi(T_N) = \frac{1}{8} + \frac{1}{32}\frac{U}{k_B T_N} - \frac{1}{32}\left(\frac{\epsilon_d}{k_B T_N}\right)^2 - \frac{\Gamma/\pi}{k_B T_N}\chi_{1,\mathrm{FO}}(T_N, \bar{\beta}, \Lambda) \ , \quad (3.3)$$

$$F(T_N) = -k_B T_N\left[\ln 4 - \frac{1}{4}\frac{U}{k_B T_N} + \frac{1}{4}\left(\frac{\epsilon_d}{k_B T_N}\right)^2 + \frac{2\Gamma/\pi}{k_B T_N} F_{1,\mathrm{FO}}(T_N, \bar{\beta}, \Lambda)\right] \ , \quad (3.4)$$

where $\chi_{1,\mathrm{FO}}$ and $F_{1,\mathrm{FO}}$ are the functions evaluated in Appendix C of I. An expression similar to Eq. (3.3) has independently been derived by Haldane [Ref. 9, Eq. (28)]. Thus, for $k_B T_N >> \max(U, |\epsilon_d|, \Gamma)$, we have the free-orbital regime in which $T\chi \simeq \frac{1}{8}$, $F(T) \simeq -k_B T \ln 4$. What happens as T drops below $\max(U, \epsilon_d, \Gamma)$ depends upon which of the deviation terms in Eq. (3.3) dominates. We note that the U term tends to push $T\chi$ above $\frac{1}{8}$, while the ϵ_d and Γ terms push $T\chi$ below $\frac{1}{8}$. This is consistent with the discussion in Sec. II, where we saw that $U \to \infty$ leads to the valence-fluctuation fixed point in which $T\chi = \frac{1}{6}$, while $|\epsilon_d| \to \infty$ or $\Gamma \to \infty$ leads to the frozen-impurity fixed point in which $T\chi = 0$.

We will organize the rest of our discussion in the same manner as we did in Sec. I B. That is, we first discuss the case when $\Gamma << U$, and consider what happens for various characteristic values of ϵ_d. The case $\Gamma >> U$ can be handled analytically, as is done in Appendix D.

The first typical asymmetric case to consider, therefore, is the situation when $U >> \{|\epsilon_d|, \Gamma\}$. In this case, when N gets to be large enough that $\tilde{U}\Lambda^{(N-1)/2}$ is much bigger than 1, H_N crosses over from H^*_{FO} to H^*_{VF}, as we saw in Sec. III A (cf. Fig. 10). Correspondingly, as $k_B T$ drops well below U, $T\chi$ crosses over from its value of $\frac{1}{8}$ for the free-orbital regime to its value of $\frac{1}{6}$ for the valence-fluctuation regime [cf. plot A of Fig. 11(a)]. We will let N_1^* and T_1^* denote the values of N and T around which the crossover takes place. From Figs. 10 and plot A of Fig 11(a),

$$\tilde{U}\Lambda^{(N_1^*-1)/2} \simeq \alpha, \quad T_1^* \simeq U/\alpha \quad (3.5)$$

TABLE III. States and energies of $H^{\text{eff}}_{N,\text{FO}}$ ($\tilde{K}=0$).

Charge Q	Spin S	Index r	State	Energy		
0	$\frac{1}{2}$	1	c_d	0		
		2	g_1	η_1^*	$-\tilde{\epsilon}_d\Lambda^{(N-1)/2}$	$+\tilde{\Gamma}\Lambda^{(N-1)/2}(\alpha_{01}^2/\eta_1^*)$
		3	$2c_d+h_1$	$\eta_1^*+2\tilde{U}\Lambda^{(N-1)/2}$	$+\tilde{\epsilon}_d\Lambda^{(N-1)/2}$	$+\tilde{\Gamma}\Lambda^{(N-1)/2}(\alpha_{01}^2/\eta_1^*)$
-2	$\frac{1}{2}$	1	h_1	η_1^*	$-\tilde{\epsilon}_d\Lambda^{(N-1)/2}$	$+\tilde{\Gamma}\Lambda^{(N-1)/2}(\alpha_{01}^2/\eta_1^*)$
$+2$	$\frac{1}{2}$	1	$2c_d+g_1$	$\eta_1^*+2\tilde{U}\Lambda^{(N-1)/2}$	$+\tilde{\epsilon}_d\Lambda^{(N-1)/2}$	$+\tilde{\Gamma}\Lambda^{(N-1)/2}(\alpha_{01}^2/\eta_1^*)$
-1	0	1	$\cdots$	0	$-\tilde{\epsilon}_d\Lambda^{(N-1)/2}$	
		2	c_d+h_1	η_1^*		$+\tilde{\Gamma}\Lambda^{(N-1)/2}(\alpha_{01}^2/\eta_1^*)$
	1	1	c_d+h_1	η_1^*		$+\tilde{\Gamma}\Lambda^{(N-1)/2}(\alpha_{01}^2/\eta_1^*)$
$+1$	0	1	$2c_d$	$0+2\tilde{U}\Lambda^{(N-1)/2}$	$+\tilde{\epsilon}_d\Lambda^{(N-1)/2}$	
		2	c_d+g_1	η_1^*		$+\tilde{\Gamma}\Lambda^{(N-1)/2}(\alpha_{01}^2/\eta_1^*)$
	1	1	c_d+g_1	η_1^*		$+\tilde{\Gamma}\Lambda^{(N-1)/2}(\alpha_{01}^2/\eta_1^*)$

where α is some number like 5, say. The fact that the transition from the free orbital to the valence-fluctuation regime is determined by the scale of U is amply demonstrated by plot B of Fig. 11(a), which has the same ϵ_d, values as plot A, but a U that is bigger by 10, and by plot C which has the same U as plot B, but different ϵ_d and Γ values.

C. Valence-fluctuation regime

As emphasized earlier, this regime is the one that is really characteristic of the asymmetric case, and displays many new features. The most important of these features, as we will show below, is that the flow of H_N in the vicinity of H^*_{VF} can be characterized by an effective, N-dependent, impurity-orbital energy parameter $E_d(N)$. Correspondingly, the temperature dependence of the susceptibility is characterized by an effective *temperature-dependent impurity-orbital energy* $E_d(T)$.

As we have discussed before, the valence-fluctuation fixed point is characterized by the fact that the states in which $n_d=2$ are removed from consideration, as happens when $\tilde{U}\Lambda^{(N-1)/2}$ becomes much larger than all other energies of interest. Since within the free-orbital regime, $\tilde{U}$, $\tilde{\epsilon}_d$, and $\tilde{\Gamma}$ all grow as $\Lambda^{(N-1)/2}$, we can argue as in Sec. II A that as far as the low-lying states H_N for $N > N_1^*$ are concerned, one is in effect considering the Hamiltonian (2.6). We will rewrite Eq. (2.6) as

$$H^{\text{eff}}_{N,\text{VF}} = H^*_{N,\text{VF}} + \tilde{\epsilon}_d\Lambda^{(N-1)/2}(b^\dagger_{d\mu}b_{d\mu}-1) + \tilde{\Gamma}\Lambda^{(N-1)/2}(b^\dagger_{d\mu}f_{0\mu}+f^\dagger_{0\mu}b_{d\mu}) + \tilde{J}_1\Lambda^{(N-1)/2}(b^\dagger_{d\mu}\vec{\sigma}_{\mu\nu}b_{d\nu})\cdot(f^\dagger_{0\mu'}\vec{\sigma}_{\mu'\nu'}f_{0\nu'}) + \tilde{K}_1\Lambda^{(N-1)/2}(b^\dagger_{d\mu}b_{d\mu})(f^\dagger_{0\nu}f_{0\nu}) \quad , \tag{3.6}$$

where $b_{d\mu}$ is the operator characterizing the new effective impurity degree of freedom (cf. Sec. II A), and we have let

$$J_1 \equiv \tilde{\Gamma}/(4\tilde{U}+2\tilde{\epsilon}_d), \quad K_1 \equiv -\tilde{\Gamma}/(4\tilde{U}+2\tilde{\epsilon}_d) \quad . \tag{3.7}$$

We note that Eq. (3.6) is precisely of the form of the effective Hamiltonian constructed around the valence-fluctuation fixed point. The last four terms in Eq. (3.6) are precisely (cf. Table II) $\delta H_{1,\text{VF}}$, $\delta H_{2,\text{VF}}$ (the generators of the two relevant operators), and $\delta H_{3,\text{VF}}$ and $\delta H_{4,\text{VF}}$ (the generators of the first two marginal operators). Furthermore, the coefficients of these operators are now explictly expressed in terms of $\tilde{\epsilon}_d$, $\tilde{\Gamma}$, and $\tilde{U}$. We note that $\delta H_{5,\text{VF}}$, the generator of the marginal operator that describes potential scattering, does not occur in Eq. (3.6). That is to say, the crossover from H^*_{FO} to H^*_{VF} does not generate potential scattering. This is consistent with the

discussion of Sec. III A where according to the numerical results, the effective $\bar{K}$ for $H_{HV}^{*}(\bar{K})$ was zero.

Expressing Eq. (3.6) in terms of the electron and hole operators that diagonalize $H_{N,\mathrm{VF}}^{*}$, we get

$$H_{N,\mathrm{VF}}^{\mathrm{eff}}=\sum_{l=1}^{L_1}\eta_l^{*}(g_{l\mu}^{\dagger}g_{l\mu}+h_{l\mu}^{\dagger}h_{l\mu})+\tilde{\epsilon}_d\Lambda^{(N-1)/2}(b_{d\mu}^{\dagger}b_{d\mu}-1)+\tilde{\Gamma}^{1/2}\Lambda^{(N-1)/4}\sum_{l=1}^{L_1}\alpha_{0l}(b_{d\mu}^{\dagger}g_{l\mu}+g_{l\mu}^{\dagger}b_{d\mu}+b_{d\mu}^{\dagger}h_{l\mu}^{\dagger}+h_{l\mu}b_{d\mu})$$
$$+\tilde{J}_1(b_{d\mu'}^{\dagger}\sigma_{\mu'\nu'}b_{d\nu'}\sum_{ll'}^{L_1}\alpha_{0l}\alpha_{0l'}(g_{l\mu}^{\dagger}\vec{\sigma}_{\mu\nu}g_{l'\nu}+h_{l\mu}\vec{\sigma}_{\mu\nu}h_{l'\nu}^{\dagger}+g_{l\mu}^{\dagger}\vec{\sigma}_{\mu\nu}h_{l'\nu}^{\dagger}+h_{l\mu}\vec{\sigma}_{\mu\nu}g_{l'\nu})$$
$$+\tilde{K}_1b_{d\mu}^{\dagger}b_{d\mu}\sum_{ll'}\alpha_{0l}\alpha_{0l'}(g_{l\nu}^{\dagger}g_{l'\nu}+h_{l\nu}h_{l'\nu}^{\dagger}+g_{l\nu}^{\dagger}h_{l'\nu}^{\dagger}+h_{l\nu}g_{l'\nu}) \quad . \tag{3.8}$$

This expression reconfirms that $\tilde{\epsilon}_d$ and $\tilde{\Gamma}$ are relevant variables, while $\tilde{J}_1$ is a marginal variable. $\tilde{K}_1$ looks marginal, but actually has a piece that is like the $\tilde{\epsilon}_d$ term [see discussion after Eq. (3.11)].

The question as to what value we should use for the upper limit L_1 (of l) in Eq. (3.8) turns out to be quite important for the discussion to follow. Hence we will pause to comment on it. Since the condition of validity of Eq. (3.8) is that we be interested in energies much smaller than $\tilde{U}\Lambda^{(N-1)/2}$, we can demand that the largest energy in Eq. (3.8), namely $\eta_{L_1}^{*}$, be smaller than $\tilde{U}\Lambda^{(N-1)/2}$. For example, we can set

$$\eta_{L_1}^{*}=\Lambda^{L_1-1}=\tilde{U}\Lambda^{(N-1)/2}/\alpha \quad , \tag{3.9a}$$

where α is some number like 5, say. (Such numbers are encountered at various places in our discussion. We use the same symbol α to characterize all of them, since their precise values are unimportant in view of the fact that all the transitions that occur in our discussion are fuzzy and not sharp.) Using Eq. (3.5) which connects $\tilde{U}$ to the transition iteration number N_1^{*}, we get

$$\Lambda^{L_1}\simeq\Lambda^{(N-N_1^{*})/2} \quad or \quad L_1\simeq\tfrac{1}{2}(N-N_1^{*}) \quad . \tag{3.9b}$$

[It can be shown that the condition (3.9b) arises rather naturally if one attempts to derive Eq. (3.8) formally from Eq. (3.7).]

We list in Table IV the energies of the states listed in Table I calculated using $H_{N,\mathrm{VF}}^{\mathrm{eff}}$. The $\tilde{\Gamma}^{1/2}$ term does not affect energies to first order, so we have calculated to second order in $\tilde{\Gamma}^{1/2}$, i.e., to $O(\tilde{\Gamma})$. Table IV clearly brings out the important feature that we mentioned at the beginning of this section, namely that the energy levels of H_N are describable in terms of an effective, N-dependent, impurity-orbital energy parameter $\tilde{E}_d(N)$ that plays the role of $\tilde{\epsilon}_d$. We have

$$\tilde{E}_d(N)=\tilde{\epsilon}_d+\tilde{\Gamma}\alpha_0^2\tfrac{1}{2}(N-N_1^{*})+\tilde{K}_1\Lambda^{-(N_1^{*}-1)/2} \quad , \tag{3.10}$$

where N_1^{*} corresponds to the crossover from H_{FO}^{*} to H_{VF}^{*} [cf. Eq. (3.5)].

The result (3.10) can also be proved formally. It is easy to verify that the second-order contributions from the $\tilde{\Gamma}^{1/2}$ term can be described by the Hamiltonian

$$\tilde{\Gamma}\Lambda^{(N-1)/2}\left[(b_{d\mu}^{\dagger}b_{d\mu}-1)\left(\sum_{l=1}^{L_1}\frac{\alpha_{0l}^2}{\eta_l^{*}}\right)+\tfrac{1}{2}b_{d\mu'}^{\dagger}\vec{\sigma}_{\mu'\nu'}b_{d\nu'}\left(\sum_{l=1}^{L_1}\frac{\alpha_{0l}^2}{\eta_l^{*}}(g_{l\mu}^{\dagger}\vec{\sigma}_{\mu\nu}g_{l\nu}-h_{l\mu}\vec{\sigma}_{\mu\nu}h_{l\nu}^{\dagger})\right)\right.$$
$$\left.+(1-\tfrac{1}{2}b_{d\mu}^{\dagger}b_{d\mu})\left(\sum_{l=1}^{L_1}\frac{\alpha_{0l}{}^2}{\eta_l^{*}}(g_{l\mu}^{\dagger}g_{l\mu}+h_{l\mu}^{\dagger}h_{l\mu})\right)\right] \quad . \tag{3.11}$$

The first term in Eq. (3.11) gives rise to the $\tilde{\Gamma}$ term in $\tilde{E}_d(N)$. The rest of the term affect conduction-electron states and scale, in a simple fashion, as $\tilde{\Gamma}\Lambda^{(N-1)/2}$. The $\tilde{K}_1$ term in Eq. (3.8) can be rearranged (by normal ordering the $h_{l\nu}h_{l'\nu}^{\dagger}$ term) as

$$\left(2\tilde{K}_1\sum_{l=1}^{L_1}\alpha_{0l}^2\right)b_{d\mu}^{\dagger}b_{d\mu}+\tilde{K}_1b_{d\mu}^{\dagger}b_{d\mu}\sum_{ll'}^{L_1}\alpha_{0l}\alpha_{0l'}(g_{l\mu}^{\dagger}g_{l'\mu}-h_{l\mu}^{\dagger}h_{l'\mu}+g_{l\nu}^{\dagger}h_{l'\nu}^{\dagger}+h_{l\nu}g_{l'\nu}) \quad . \tag{3.12}$$

TABLE IV. States and energies of $H^{\rm eff}_{N,\rm VF}$ ($\tilde{K}=0$). Here $\Delta_1(N)=\sum_{l=1}^{L_1}(\alpha_{0l}^2/\eta_l^*)\simeq\alpha_0^2 L_1\simeq\alpha_0^2[\frac{1}{2}(N-N_1^*)]$ and $\Delta_2(N)=\Lambda^{-(N-1)/2}2\sum_{l=1}^{L_1}\alpha_{0l}^2\simeq\Lambda^{-((N-1)/2)+L_1}\simeq\Lambda^{-(N_1^*-1)/2}$.

Charge Q	Spin S	Index r	State	Energy			
0	$\frac{1}{2}$	1	b_d	0			
		2	g_1	$\eta_1^*-(\tilde{\epsilon}_d+\tilde{\Gamma}\Delta_1+\tilde{K}_1\Delta_2)\Lambda^{(N-1)/2}$	$+\tilde{\Gamma}\Lambda^{(N-1)/2}\alpha_{01}^2/\eta_1^*$		
		3	$b_d+g_1+h_1$	$2\eta_1^*$	$+(\ )$	$+(\ )$	
-2	$\frac{1}{2}$	1	h_1	$\eta_1^*-(\tilde{\epsilon}_d+\tilde{\Gamma}\Delta_1+\tilde{K}_1\Delta_2)\Lambda^{(N-1)/2}$	$+\tilde{\Gamma}\Lambda^{(N-1)/2}\alpha_{01}^2/\eta_1^*$		
$+2$	$\frac{1}{2}$	1	b_d+2g_1	$2\eta_1^*$	$+\tilde{\Gamma}\Lambda^{(N-1)/2}\alpha_{01}^2/\eta_1^*$		$+2\tilde{K}_1\alpha_{01}^2$
-1	0	1	$\cdots$	$0-(\tilde{\epsilon}_d+\tilde{\Gamma}\Delta_1+\tilde{K}_1\Delta_2)\Lambda^{(N-1)/2}$			
		2	b_d+h_1	η_1^*	$+2\tilde{\Gamma}\Lambda^{(N-1)/2}\alpha_{01}^2/\eta_1^*$	$-3\tilde{J}_1\alpha_{01}^2$	$-\tilde{K}_1\alpha_{01}^2$
	1	1	b_d+h_1	η_1^*		$+\tilde{J}_1\alpha_{01}^2$	$-\tilde{K}_1\alpha_{01}^2$
$+1$	0	1	b_d+g_1	η_1^*	$-\tilde{\Gamma}\Lambda^{(N-1)/2}\alpha_{01}^2/\eta_1^*$	$-3\tilde{J}_1\alpha_{01}^2$	$+\tilde{K}_1\alpha_{01}^2$
		2	$2g_1$	$2\eta_1^*-(\tilde{\epsilon}_d+\tilde{\Gamma}\Delta_1+\tilde{K}_1\Delta_2)\Lambda^{(N-1)/2}$	$+2\tilde{\Gamma}\Lambda^{(N-1)/2}\alpha_{01}^2/\eta_1^*$		$+2\tilde{K}_1\alpha_{01}^2$
	1	1	b_d+g_1	η_1^*	$+\tilde{\Gamma}\Lambda^{(N-1)/2}\alpha_{01}^2/\eta_1^*$	$+\tilde{J}_1\alpha_{01}^2$	$+\tilde{K}_1\alpha_{01}^2$

The first term in Eq. (3.12) gives rise to the $\tilde{K}_1$ term in Eq. (3.10). The second term in Eq. (3.12) describes potential scattering of the conduction electrons off the impurity, but this scattering is present only for those states in which $n_d=1$. We note that the $\tilde{J}_1$ term in Eq. (3.8) describes spin-spin scattering of the conduction electron off the impurity spin within the subspace of states where $n_d=1$.

The above features of the energy levels of $H^{\rm eff}_{N,\rm VF}$ (which features can be seen to correctly describe the energy levels in Fig. 10 for N between 13 and 17) are also reflected in the susceptibility results, as we show below.

Substituting $H^{\rm eff}_{N,\rm VF}$ in place of H_N in Eqs. (1.5) and (1.6) and carrying out the perturbation expansion, we can verify that to leading orders in the parameters $\tilde{\epsilon}_d$, $\tilde{\Gamma}^{1/2}$, $\tilde{J}_1$, and $\tilde{K}_1$, $T_N\chi(T_N)$, and $F(T_N)$ are given by

$$k_B T_N\chi(T_N)=\tfrac{1}{6}-\tfrac{1}{18}\bar{\beta}\tilde{\epsilon}_d\Lambda^{(N-1)/2}-\tfrac{4}{3}\bar{\beta}\tilde{J}_1\sum_{l=1}^{L_1}\frac{\alpha_{0l}^2 e^{\bar{\beta}\eta_l^*}}{(1+e^{\bar{\beta}\eta_l^*})^2}-\tfrac{1}{18}\bar{\beta}\tilde{K}_1\left[2\sum_{l=1}^{L_1}\alpha_{0l}^2\right]$$
$$-\tfrac{1}{18}\bar{\beta}\tilde{\Gamma}\Lambda^{(N-1)/2}\sum_{l=1}^{L_1}\left[\frac{\alpha_{01}^2}{\eta_l^*}\frac{1-e^{-\bar{\beta}\eta_l^*}}{(1+e^{-\bar{\beta}\eta_l^*})^3}(1+14e^{-\bar{\beta}\eta_l^*}+e^{-2\bar{\beta}\eta_l^*})\right], \tag{3.13}$$

$$F(T_N)=-k_B T_N\left[\ln 3+\tfrac{1}{3}\bar{\beta}\tilde{\epsilon}_d\Lambda^{(N-1)/2}+\tfrac{1}{3}\bar{\beta}\tilde{K}_1\left[2\sum_{l=1}^{L_1}\alpha_{0l}^2\right]+\tfrac{4}{3}\bar{\beta}\tilde{\Gamma}\Lambda^{(N-1)/2}\sum_{l=1}^{L_1}\frac{\alpha_{0l}^2}{\eta_l^*}\frac{(1-e^{-\bar{\beta}\eta_l^*})}{(1+e^{-\bar{\beta}\eta_l^*})}\right]. \tag{3.14}$$

Since

$$2\sum_{l=1}^{L_1}\alpha_{0l}^2\simeq\Lambda^{L_1}\cong\Lambda^{(N-N_1^*)/2},$$

the $\tilde{K}_1$ term looks like the $\tilde{\epsilon}_d$ term with $\tilde{\epsilon}_d$ replaced by $\tilde{K}_1\Lambda^{-(N_1^*-1)/2}$, which is the same result as in Eq. (3.10).

As to the $\tilde{\Gamma}$ term, it is clear that for large l the summand goes as α_{0l}^2/η_l^*; hence we get a contribution which looks like the $\tilde{\epsilon}_d$ term with $\tilde{\epsilon}_d$ replaced by

$$\tilde{\Gamma}\sum_{l=1}^{L_1}\frac{\alpha_{0l}^2}{\eta_l^*}\simeq\tilde{\Gamma}\alpha_0^2 L_1\cong\tilde{\Gamma}\alpha_0^2\tfrac{1}{2}(N-N_1^*)\ ,$$

which is also the same result as in Eq. (3.10). Finally, making use of the result shown in Appendix A that

$$\bar{\beta}\sum_l\alpha_{0l}^2\frac{e^{-\bar{\beta}\eta_l^*}}{(1+e^{-\bar{\beta}\eta_l^*})^2}\equiv\chi_2^{\pm}(\tilde{K}=0)=\frac{\alpha_0^2}{2\ln\Lambda}\ , \tag{3.15}$$

we see that the $\tilde{J}_1$ term produces a constant shift in $T\chi$.

To sum up our discussion above, we have shown that in the valence-fluctuation regime, the deviation of H_N from the fixed point $H_{\rm VF}^*$ calculated to $O(\tilde{\Gamma})$ can be understood in a simple manner in terms of an effective, N-dependent, impurity-oribtal energy $\tilde{E}_d(N)$ given by Eq. (3.10). To $O(\tilde{\Gamma})$, $\tilde{E}_d(N)$ effectively replaces $\tilde{\epsilon}_d$ as the coefficient of the $(b_{d\mu}^\dagger b_{d\mu}-1)$ term in Eq. (3.8).

Before moving on to a discussion of the temperature dependence of the susceptibility, we pause to remark that such effective N-dependent coefficients of eigenoperators as $\tilde{E}_d(N)$ *can* arise quite generally in high-order (here second order in $\Gamma^{1/2}$) renormalization-group calculations whenever there are simple relationships between the eigenvalues of the transformation such as one eigenvalue being equal to the square of another, or to the product of two others, etc. (Here Λ, the eigenvalue associated with $\tilde{\epsilon}_d$ is the square of $\Lambda^{1/2}$, the eigenvalue associated with $\tilde{\Gamma}^{1/2}$.) For details see Wegner.[6]

The rest of our discussion of the valence-fluctuation regime will concentrate on the temperature dependence of the susceptibility. Analogously to $\tilde{E}_d(N)$, such a discussion leads in a natural way to an effective, temperature-dependent, impurity-orbital energy, to be denoted by $E_d(T)$. We show below that $E_d(T)$ is given by

$$E_d(T)=\epsilon_d+\frac{\Gamma}{\pi}\ln\left[\frac{U}{\alpha T}\right]\ , \tag{3.16}$$

where α is some number like 5, say [cf. discussion following Eq. (3.9a)].

In order to identify $E_d(T)$, we proceed as follows. We make use of Eqs. (1.4), (3.9a), and (3.15) in Eq. (3.13) and (3.14) to get

$$\begin{aligned}k_B T_N\chi(T_N)=&\frac{1}{6}-\frac{\epsilon_d}{18k_BT_N}-\frac{2}{3}\frac{\alpha_0^2\tilde{J}_1}{\ln\Lambda}-\frac{\tilde{K}_1}{18k_BT_N}\frac{U}{2\Lambda\alpha}\\&-\frac{\Gamma/\pi}{18k_BT_N}\left[\frac{4}{1+\Lambda^{-1}}\sum_{l=1}^{L_1}\frac{\alpha_{0l}^2}{\eta_l^*}\frac{1-e^{-\bar{\beta}\eta_l^*}}{(1+e^{-\bar{\beta}\eta_l^*})^3}(1+14e^{-\bar{\beta}\eta_l^*}+e^{-2\bar{\beta}\eta_l^*})\right]\ ,\end{aligned} \tag{3.17}$$

$$F(T_N)=-k_BT_N\left[\ln 3+\frac{\epsilon_d}{3k_BT_N}+\frac{\tilde{K}_1}{3k_BT_N}\frac{U}{2\Lambda\alpha}+\frac{4}{3}\frac{\Gamma/\pi}{k_BT_N}\left[\frac{4}{1+\Lambda^{-1}}\sum_{l=1}^{L_1}\frac{\alpha_{0l}^2}{\eta_l^*}\frac{1-e^{-\bar{\beta}\eta_l^*}}{1+e^{-\bar{\beta}\eta_l^*}}\right]\right]\ . \tag{3.18}$$

Next we take the continuum limit by letting $\bar{\beta}\to 0$ and $N\to\infty$ at fixed T_N, and then letting $\Lambda\to 1$. Then the sums over l above can be converted to integrals (exactly as in the evaluation of $\chi_{1,\rm FO}$ and $F_{1,\rm FO}$ in Appendix C of I) and we can show that

$$k_BT\chi(T)\cong\frac{1}{6}-\frac{\epsilon_d}{18k_BT}-\frac{1}{3}\frac{\Gamma/\pi}{U+\epsilon_d}+\frac{\Gamma/\pi}{2\alpha}\frac{1}{18k_BT_N}-\frac{\Gamma/\pi}{18k_BT}\int_0^{U/2\alpha}\frac{d\epsilon}{\epsilon}\frac{1-e^{-\beta\epsilon}}{(1+e^{-\beta\epsilon})^2}(1+14e^{-\beta\epsilon}+e^{-2\beta\epsilon})\ , \tag{3.19}$$

$$F(T)=-k_BT\left[\ln 3+\frac{\epsilon_d}{3k_BT}+\frac{\Gamma/(2\pi\alpha)}{3k_BT}+\frac{4}{3}\frac{\Gamma/\pi}{k_BT}\int_0^{U/2\alpha}\frac{d\epsilon}{\epsilon}\frac{1-e^{-\beta\epsilon}}{1+e^{-\beta\epsilon}}\right]\ . \tag{3.20}$$

It is easy to verify that the dominant contribution to the integral in Eq. (3.19) is given by $\ln(U/2\alpha T)$. Hence we can write

$$k_B T\chi(T) \cong \frac{1}{6} - \frac{E_d(T)}{18k_B T} - \frac{A\Gamma}{18k_B T} - \frac{1}{3}\frac{\Gamma/\pi}{U+\epsilon_d} + \cdots , \tag{3.21}$$

where $\epsilon_d(T)$ is given by Eq. (3.16) and ... indicate smaller terms. The constant A can be obtained by a careful evaluation of the integrals in Eq. (3.19). A result similar to Eq. (3.21) was first derived by Haldane [Ref. 9, Eq. (29)].

Next we discuss the temperature dependence of $T\chi$ as T decreases within the valence-fluctuation regime. This clearly depends upon which term dominates in Eq. (3.21). We note that Γ always reduces $T\chi$ below $\frac{1}{6}$; i.e., tends to drive $T\chi$ towards the frozen-impurity regime in which $T\chi$ is zero; whereas $E_d(T)$ can increase $T\chi$ above $\frac{1}{6}$, towards the local-moment regime where $T\chi = \frac{1}{4}$, if it is negative, or decrease $T\chi$ below $\frac{1}{6}$ towards the frozen-impurity regime if it is positive. From Eq. (3.16) we see that as T decreases, $E_d(T)$ increases slowly (logarithmically). Therefore, $T\chi$ will make a transition to the local-moment regime only if ϵ_d is negative and $-\epsilon_d$ is sufficiently large compared to Γ that $E_d(T)$ is negative and $-E_d(T)$ remains large compared to Γ as T decreases. We will discuss such a case first.

The condition for the transition from the valence-fluctation to the local-moment regime may be formulated more precisely as follows. The point is that from Eq. (3.21) it is clear that the valence-fluctuation regime breaks down when T gets smaller than $-E_d(T)$ or Γ, whichever occurs first. Let T_2^* be a temperature such that [cf. Eq. (3.16)]

$$\alpha T_2^* = -E_d(T_2^*) \cong -E_d^* = -\epsilon_d - \frac{\Gamma}{\pi}\ln\left(\frac{U}{-E_d^*}\right) , \tag{3.22}$$

where α is a number like 5, as before. If the solution $-E_d^*$ to Eq. (3.22) is much larger than Γ, then T can become small compared to $-E_d(T)$ while it is still much larger than Γ, and we get a crossover to the local-moment regime at a transition temperature roughly equal to T_2^*. We can rewrite Eq. (3.22) as

$$-\frac{E_d^*}{\Gamma} = -\frac{\epsilon_d}{\Gamma} - \frac{1}{\pi}\ln\left(\frac{U}{\Gamma}\right) + \frac{1}{\pi}\ln\left(-\frac{E_d^*}{\Gamma}\right) = \frac{\alpha T_2^*}{\Gamma} \tag{3.23}$$

The solution to this equation is sketched in Fig. 12. We note that $-E_d^*$ is monotonic decreasing as $-\epsilon_d$ decreases; $-E_d^* = \Gamma$ when $-\epsilon_d = \Gamma + (\Gamma/\pi)\ln(U/\Gamma)$; there is no solution for $-E_d^*$ when $-\epsilon_d$ is less than $0.6827\Gamma + \Gamma/\pi \ln(U/\Gamma)$. Thus we see that $T\chi$ can make a transition from the valence-fluctuation to the local-moment regime at a transition temperature T_2^* determined by Eq. (3.22) if ϵ_d is negative and $-\epsilon_d >> \Gamma/\pi \ln(U/\Gamma)$. We note that this condition is much more stringent than the condition $-\epsilon_d >> \Gamma$ which one might have naturally written down.

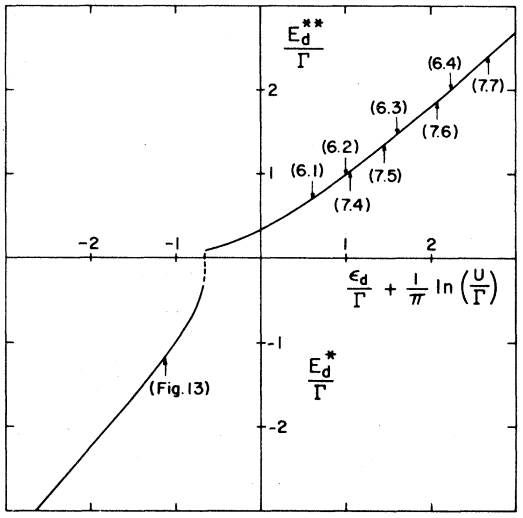

FIG. 12. Solutions of Eqs. (3.22) and (3.52). Both equations can be written as $y = x - (\ln|y|)/\pi$ where $x = \epsilon_d/\Gamma + (1/\pi)\ln(U/\Gamma)$ and $y = E_d^{**}/\Gamma$ for $y > 0$ and E_d^*/Γ for $y < 0$. Note that the solution pops from negative to positive y at $x = -(1+\ln\pi)/\pi = -0.68$. The values of (x,y) indicated by arrows are appropriate for the susceptibility curves shown in Figs. 13, 14 (7.4–7.7), and 15 (6.1–6.4). The curves shown in Fig. 11 correspond to points off the left-hand lower quadrant. See Table VIII for a complete listing of relevant numbers.

The validity of the above discussion is demonstrated by the plots A, B, and C of Fig. 11(a), in all of which $T\chi$ displays a transition from the valence-fluctuation to the local-moment regime. The $-E_d^*$ values for these three plots are (in units of D) 7.557×10^{-6}, 6.315×10^{-6}, and 7.557×10^{-5}, respectively. Using an α of 4 we get for the values of the transition temperature T_2^* the numbers 1.9×10^{-6}, 1.6×10^{-6}, and 1.9×10^{-5}, which are roughly right. At any rate the trends are clearly correct.

We next discuss the local-moment regime.

D. Local-moment regime

In this section we discuss the local-moment regime, in which $T\chi \simeq \frac{1}{4}$. The main point that will emerge from our discussion is that the basic way in which the local-moment regime for the asymmetric case differs from that for the symmetric case is it has potential scattering of the conduction electrons, but that this potential scattering has little effect on the

temperature dependence of $T\chi$. We also show the correspondence between the asymmetric Anderson model and the spin-$\frac{1}{2}$ Kondo Hamiltonian with potential scattering.

As discussed in Sec. III C, when the values of U, $-\epsilon_d$, and Γ are such that $-E_d^*$ determined by Eq. (3.22) is much bigger than Γ, we get a crossover from the valence fluctuation to the local-moment regime. In terms of $T\chi$, the transition temperature is T_2^* [cf. Eq. (3.23)]. In terms of H_N, the transition iteration number N_2^* can be determined by setting

$$\Lambda^{-(N_2^*-1)/2} \simeq (T_2^*/D)$$

or

$$N_2^* \simeq \frac{2\ln(D/T_2^*)}{\ln\Lambda} \tag{3.24}$$

so that for $N > N_2^*$, H_N arrives close to the local-moment fixed point. This is seen from Fig. 10, for which case N_2^* given by Eq. (3.24) is $\simeq 24$.

In accordance with the discussion in Sec. IV C, in the vicinity of the local-moment fixed point H_N can be described by the effective Hamiltonian

$$H^{\rm eff}_{N,\rm LM}(\tilde{K}) = H^*_{N,\rm LM}(\tilde{K}) + \tilde{J}\Lambda^{(N-1)/2}\vec{\tau}\cdot(f^\dagger_{0\mu}\vec{\sigma}_{\mu\nu}f_{0\nu}) \ , \tag{3.25}$$

where only the generator of the marginal operator $\delta H_{1,\rm LM}$ (cf. Table II) is explicitly shown. The other marginal operator is a potential-scattering term, and can be included in $H^*_{N,\rm LM}(\tilde{K})$.

We note that Eq. (3.25) can be rewritten

$$H^{\rm eff}_{N,\rm LM}(\tilde{K}) = \Lambda^{(N-1)/2}\left[\sum_{n=0}^{N-1}\Lambda^{-n/2}\xi_n(f^\dagger_{n\mu}f_{n+1\mu} + f^\dagger_{n+1\mu}f_{n\mu}) + \tilde{J}\vec{\tau}\cdot f^\dagger_{0\mu}\sigma_{\mu\nu}f_{0\nu} + \tilde{K}(f^\dagger_{0\mu}f_{0\mu} - 1)\right] \ . \tag{3.26}$$

But this is precisely the sequence of Hamiltonians one would use in a numerical renormalization-group treatment of the spin-$\frac{1}{2}$ Kondo problem[4,5] when potential scattering is present in addition to the usual spin-spin scattering off the impurity.[10] Within the framework of the same approximations as in Sec. II A of I, such a problem corresponds to the model Hamiltonian [compare Eq. (1.1)]:

$$\mathcal{H}_K = D_K\left[\int_{-1}^{1} k\,dk\,a^\dagger_{k\mu}a_{k\mu} - \rho J\int_{-1}^{1}dk\int_{-1}^{1}dk' a^\dagger_{k\mu}\tfrac{1}{2}\vec{\sigma}_{\mu\nu}a_{k'\nu}\cdot\tfrac{1}{2}\vec{\tau} + \rho K\int_{-1}^{1}dk\int_{-1}^{1}dk' a^\dagger_{k\mu}a_{k'\mu}\right] \ , \tag{3.27}$$

where D_K is the appropriate bandwidth. $\mathcal{H}_K$, when subject to discretization, etc., leads to precisely the sequence of Hamiltonians (3.26), if we identify $\tilde{J}$ and $\tilde{K}$ as

$$\tilde{J} = -\left(\frac{2}{1+\Lambda^{-1}}\right)\tfrac{1}{2}\rho J, \quad \tilde{K} = \left(\frac{2}{1+\Lambda^{-1}}\right)2\rho K \tag{3.28}$$

This reconfirms the well-known equivalence[11] between the asymmetric Anderson Hamiltonian and the spin-$\frac{1}{2}$ Kondo Hamiltonian with potential scattering. We note that in the light of our analysis, this equivalence is valid only for temperatures below the transition temperature T_2^*, so that T_2^* plays the role of the bandwidth D_K in the equivalent Kondo problem.

Next we discuss the properties of $H^{\rm eff}_{N,\rm LM}(\tilde{K})$. In terms of the electron and hole operators that diagonalize $H^*_{N,\rm LM}(\tilde{K})$ (cf. Sec. II A), we can write, using Eq. (2.16)

$$H^{\rm eff}_{N,\rm LM}(K) = \sum_{l=1}^{L_2}(\eta_l^+ g^\dagger_{l\mu}g_{l\mu} + \eta_l^- h^\dagger_{l\mu}h_{l\mu}) + \tilde{J}\vec{\tau}\cdot\sum_{ll'}^{L_2}\{\alpha^+_{0l}\alpha^+_{0l'}g^\dagger_{l\mu}\vec{\sigma}_{\mu\nu}g_{l'\nu} + \alpha^-_{0l}\alpha^-_{0l'}h_{l\mu}\vec{\sigma}_{\mu\nu}h^\dagger_{l'\nu}$$
$$+ \alpha^+_{0l}\alpha^-_{0l'}(g^\dagger_{l\mu}\vec{\sigma}_{\mu\nu}h^\dagger_{l'\nu} + h_{l'\mu}\vec{\sigma}_{\mu\nu}g_{l\nu})\} \ . \tag{3.29}$$

[By analogy with the discussion following Eq. (3.8), the upper limit L_2 is given by $\frac{1}{2}(N - N_2^*)$.] The energy levels of the states considered in Table I, calculated using $H^{\rm eff}_{N,\rm LM}(\tilde{K})$ to $O(\tilde{J})$, are listed in Table V. Comparison with the levels plotted in Fig. 10 shows that in this case (unlike the two previous regimes) $\eta_l^+ \neq \eta_l^-$ so $\tilde{K} \neq 0$, and in fact, since $\eta_1^- < \eta_1^+$, $\tilde{K} > 0$. Also, we see that $\tilde{J} > 0$.

One can also calculate the susceptibility and the free energy to $O(J)$, using $H^{\rm eff}_{N,\rm LM}$ in place of H_N in Eqs. (1.5) and (1.6). The results are

$$k_B T_B \chi(T_N) = \tfrac{1}{4} + k_B T_N \chi_0(\tilde{K}) - \tilde{J}\chi_{1,\rm LM}(\tilde{K}) \ , \tag{3.30}$$

$$F(T_N) = -k_B T_N \ln 2 + F_0(\tilde{K}) \ . \tag{3.31}$$

Here χ_0 and F_0 are the contributions from the fixed

TABLE V. States and energies of $H^{\rm eff}_{N,\rm LM}(\tilde{K})$.

Charge Q	Spin S	Index r	State	Energy
0	$\frac{1}{2}$	1	τ	0
		2	$\tau+g_1+h_1$	$\eta_1^+ + \eta_1^- + (\ )$
		3	$\tau+g_1+h_1$	$\eta_1^+ + \eta_1^- + (\ )$
-2	$\frac{1}{2}$	1	$\tau+2h_1$	$2\eta_1^-$
$+2$	$\frac{1}{2}$	1	$\tau+2g_1$	$2\eta_1^+$
-1	0	1	$\tau+h_1$	$\eta_1^- - 3\tilde{J}\alpha_{01}^{-2}$
		2	$\tau+g_1+2h_1$	$\eta_1^+ + 2\eta_1^- - 3\tilde{J}\alpha_{01}^{+2}$
	1	1	$\tau+h_1$	$\eta_1^- + \tilde{J}\alpha_{01}^{-2}$
$+1$	0	1	$\tau+g_1$	$\eta_1^+ - 3\tilde{J}\alpha_{01}^{+2}$
		2	$\tau+2g_1+h_1$	$2\eta_1^+ + \eta_1^- - 3\tilde{J}\alpha_{01}^{-2}$
	1	1	$\tau+g_1$	$\eta_1^+ + \tilde{J}\alpha_{01}^{+2}$

point, due to potential scattering alone. χ_0 was written down earlier [cf. Eq. (2.14)], and F_0 is given by

$$F_0 = -2k_B T_N \sum_{l=1}^{L_2} \ln\left[\frac{(1+e^{-\bar{\beta}\eta_l^+})(1+e^{-\bar{\beta}\eta_l^-})}{(1+e^{-\bar{\beta}\eta_l^*})^2}\right] . \quad (3.32)$$

The function $\chi_{1,\rm LM}$ is given by

$$\chi_{1,\rm LM}(\tilde{K}) \equiv \bar{\beta}\sum_{l=1}^{L_2}\left[\frac{(\alpha_{0l}^+)^2 e^{-\bar{\beta}\eta_l^+}}{(1+e^{-\bar{\beta}\eta_l^+})^2} + \frac{(\alpha_{0l}^-)^2 e^{-\bar{\beta}\eta_l^-}}{(1+e^{-\bar{\beta}\eta_l^-})^2}\right] . \quad (3.33)$$

Note that there is no $O(J)$ term in $F(T_N)$. The functions F_0, χ_0, and χ_1 are evaluated in Appendix A, where F_0 and χ_0 are shown to be zero (see also the discussion of χ_0 in Sec. II B), and $\chi_{1,\rm LM}$ to be given by [cf. Eqs. (A34), (A50), and (A30)]

$$\chi_{1,\rm LM}(\tilde{K}) = \chi_2^+ + \chi_2^- = \frac{\alpha_0^2(\tilde{K})}{\ln\Lambda} = \frac{\alpha_0^2}{\ln\Lambda}\left[1+\frac{\pi^2\alpha_0^4}{(\ln\Lambda)^2}\tilde{K}^2\right]^{-1/2} . \quad (3.34)$$

Substituting these results into Eq. (3.30), and making use of Eq. (3.28), we get, to $O(\rho J)$

$$k_B T_N \chi(T_N) = \tfrac{1}{4}\left\{1+\frac{\rho J}{A_\Lambda}\left[1+\left(\frac{\pi\rho K}{A_\Lambda}\right)^2\right]^{-1}\right\} , \quad (3.35)$$

where A_Λ is the function of Λ introduced in Eq. (5.21) of I,

$$A_\Lambda \equiv \tfrac{1}{2}(1+\Lambda^{-1})\frac{\ln\Lambda}{2\alpha_0^2} = \frac{1+\Lambda^{-1}}{1-\Lambda^{-1}}\tfrac{1}{2}\ln\Lambda = 1+\tfrac{1}{12}(\ln\Lambda)^2 - \tfrac{1}{720}(\ln\Lambda)^4 + \cdots \quad (3.36)$$

As $\Lambda \to 1$, A_Λ goes to 1 quite rapidly, and Eq. (3.35) tends to the expected continuum limit.[10] We note that $\tilde{J}$ produces a constant shift in $T\chi$. Since we saw from the energy levels that $\tilde{J} > 0$, Eq. (3.28) yields $\rho J < 0$, so that $T\chi$ is reduced below $\frac{1}{4}$, in agreement with the plots in Fig. 11. The expression (3.35) for $T\chi$ is valid only for T just less than the transition temperature T_2^*, as discussed later.

Next we discuss the relation between the effective values of ρJ and ρK in the equivalent Kondo Hamiltonian (3.27), and the parameters U, ϵ_d, and Γ of the asymmetric Anderson model. For general values of U, ϵ_d, and Γ, this relation can be established numerically, first by calculating $\tilde{J}$ and $\tilde{K}$ from the numerically determined energy levels, and then evaluating ρJ and ρK using Eq. (3.28). For limiting cases, however, the relation can be established in analytical form, as shown below.

In Sec. II A, while discussing the local-moment fixed point, we showed that when $\tilde{U}$ and $-\tilde{\epsilon}_d$ are themselves much larger than the energies of interest (i.e., U and $-\epsilon_d$ are much larger than D in addition to being much greater than Γ), then one is in effect considering the Hamiltonian (2.9), which is precisely the same as Eq. (3.25), with $\tilde{J}$ and $\tilde{K}$ being given by (2.8). Making use of Eq. (3.28), and substituting for $\tilde{U}$, $\tilde{\epsilon}_d$, and $\tilde{\Gamma}$ from Eq. (1.3), it is easy to verify that for such a case we get

$$\rho J = -\frac{2\Gamma}{\pi|\epsilon_d|} - \frac{2\Gamma}{\pi(U+\epsilon_d)} , \qquad K = \frac{\Gamma}{2\pi|\epsilon_d|} - \frac{\Gamma}{2\pi(U+\epsilon_d)} , \quad (3.37)$$

which are identical to the Schrieffer-Wolff results.[11] As we showed in I (cf. Sec. V B), for the symmetric Anderson model these results continue to be valid even when $U/D \ll 1$. However, in the typical asymmetric case that we have been considering where $\Gamma \ll -\epsilon_d \ll U$, and there is an appreciable range of temperatures for which we have a valence-fluctuation regime, the above results are no longer valid. In this case, we rather expect

$$\rho J \simeq -\frac{2\Gamma}{\pi|E_d^*|} - \frac{2\Gamma}{\pi(U+\epsilon_d)} , \qquad \rho K \cong \frac{\Gamma}{2\pi|E_d^*|} - \frac{\Gamma}{2\pi(U+\epsilon_d)} . \quad (3.38)$$

The reasons for this expectation are as follows. First,

the reason that Eq. (3.38) is different from Eq. (3.37) is that within the valence-fluctuation regime, there is an effective orbital energy $\tilde{E}_d(N)$ which does not scale in a simple fashion (as $\Lambda^{(N-1)/2}$). Now consider the Hamiltonian H_N just at $N \simeq N_2^*$, the transition point from the valence-fluctuation to the local-moment regime. From the discussion in Sec. III C, we know that it is basically given by Eq. (3.6) but with $\tilde{\epsilon}_d$ replaced by $\tilde{E}_d^*$ (related to E_d^* the same way as $\tilde{\epsilon}_d$ is related to ϵ_d), which, in the case we are considering, is negative and much larger in magnitude than Γ. Furthermore, the $\tilde{E}_d^* \Lambda^{(N-1)/2}$ is much larger than the energies of interest. Hence we can argue as in Sec. III A to claim that Eq. (3.6) can be replaced by Eq. (3.26) with $\tilde{J}$ and $\tilde{K}$ being given by [compare Eq. (2.8) for $U=\infty$]

$$\tilde{J} = -\frac{\tilde{\Gamma}}{2\tilde{E}_d^*} + \tilde{J}_1 , \quad \tilde{K} = -\frac{\tilde{\Gamma}}{2\tilde{E}_d^*} + \tilde{K}_1 . \tag{3.39}$$

The reason for the appearance of $\tilde{J}_1$ and $\tilde{K}_1$ above is that these terms are identical to the $\tilde{J}$ and $\tilde{K}$ terms in Eq. (3.26) within the supspace in which $n_d = 1$, and hence get carried through the crossover from the valence-fluctuation to the local-moment regime.[12] Equation (3.39) together with Eq. (3.28) leads to Eq. (3.38).

The next thing for us to discuss is the temperature dependence of $T\chi$ as T decreases within the local-moment regime.

Consider the flow of $H_{N,\mathrm{LM}}^{\mathrm{eff}}(\tilde{K})$ as N increases within the local-moment regime. Since J in Eq. (3.39) is the dominant variable in addition to being marginal, higher-order terms in $\tilde{J}$ become quite important as N increases. This is because when one calculates various quantities that characterize $H_{N,\mathrm{LM}}^{\mathrm{eff}}(\tilde{K})$, such as its first few energy levels, $k_B T_N \chi(T_N)$, etc., as expansions in powers of J, one gets "bad" expansions, in the sense that the expansion coefficients are polynomials in N and become large when N gets large.

We recall[1,2] that in the symmetric case, i.e., in the case where the effective Kondo Hamiltonian has no potential scattering, the bad expansions (in powers of J) for the various properties of $H_{N,\mathrm{LM}}^{\mathrm{eff}}(\tilde{K}=0)$ can be taken care by introducing one effective, N-dependent, running-coupling constant J_N (represented by Z_N in Ref. 2). The precise definition of J_N is somewhat arbitrary, but the central point is that, although J_N has a bad expansion in powers of J, all the quantities that characterize $H_{L,\mathrm{LM}}^{\mathrm{eff}}(K=0)$ have "good" expansions (free of powers of N) in powers of J_N. In particular J_{N+2} and $k_B T_N \chi(T_N)$ have good expansions in powers of J_N and this is what leads to the scaling law for the susceptibility, given by

$$\Phi(4k_B T\chi(T) - 1) = \ln(T/T_K) , \tag{3.40}$$

where $\Phi(y)$ is a universal function independent of J with an expansion for small y of the form

$$\Phi(y) = -\frac{1}{y} - \tfrac{1}{2}\ln|y| + O(y) . \tag{3.41}$$

The coupling constant J, band-edge effects, etc., enter Eq. (3.40) only via the scaling temperature T_K, called the Kondo temperature. The argument that leads to this result is briefly recalled in Appendix B. The details have been discussed extensively in Refs. 1 and 2.

In the asymmetric case, however, higher-order terms in J can be shown to generate additional potential scattering about $H_{N,\mathrm{LM}}^{*}(\tilde{K})$, and it appears *not* to be the case that *all* the quantities characterizing $H_{N,\mathrm{LM}}^{\mathrm{eff}}(\tilde{K})$ can be described in terms of *one* running-coupling constant J_N. The details about this complication are being investigated.

Nevertheless, we note that our numerical calculations for the asymmetric Anderson model seem to indicate the following remarkable result. Namely, that the susceptibility for the asymmetric local-moment case still obeys a scaling law of the form (3.40), with the same universal function $\Phi(y)$ as for the symmetric case. This result is demonstrated numerically by the fact that the $T\chi$ vs $\ln T$ plots of Fig. 11(b) can actually be mapped on to the universal Kondo susceptibility curve as indicated by the dashed curves in Fig. 11(b) (compare Fig. 3).

Assuming the validity of the scaling law (3.40) for the susceptibility for the asymmetric local-moment case, consider applying it to the susceptibility at a temperature less than, but close to T_2^*, the transition temperature, Eq. (3.35) is a good approximation to the susceptibility, since the $O(J^2)$ corrections will not have had a change to build up yet. Therefore we have, for $T = T_2^*/\alpha$, say,

$$4k_B T\chi(T) - 1 \simeq \frac{\rho J}{A_\Lambda}\left[1 + \left[\frac{\pi\rho K}{A_\Lambda}\right]^2\right]^{-1} \equiv \rho J_{\mathrm{eff}}(\Lambda) . \tag{3.42a}$$

In the continuum limit ($\Lambda \to 1$) $A_\Lambda \to 1$, and $J_{\mathrm{eff}}(\Lambda)$ reduces to

$$\rho J_{\mathrm{eff}} = \rho J[1 + (\pi\rho K)^2]^{-1} . \tag{3.42b}$$

Substituting Eq. (3.42) into Eq. (3.40), we get the result that the Kondo temperature T_K in the asymmetric case is given by

$$T_K = \frac{T_2^*}{\alpha}\exp[-\Phi(\rho J_{\mathrm{eff}})] . \tag{3.43}$$

Thus the presence of (particle-hole) asymmetry in the Anderson model, or of potential scattering in the Kondo problem, seems to make itself felt in the susceptibility only via the effective Kondo temperature, i.e., via the renormalization of ρJ as in Eqs. (3.42) and via the effective bandwidth T_2^*. These features had been suggested earlier, on the basis of perturbative treatments[4,5,11] of the Kondo problem with po-

tential scattering. An argument which lends plausibility to these results and which depends on the present renormalization-group approach is presented in Appendix C.

Finally, we discuss the dependence of the Kondo temperature T_K on the parameters of the Anderson model. Using Eqs. (3.43), (3.41), and (3.22) we get

$$T_K(\Gamma, \epsilon_d, U) \propto |E_d^*||\rho J_{\text{eff}}|^{1/2} \left[\exp -\frac{1}{|\rho J_{\text{eff}}|}\right] , \quad (3.44)$$

where ρJ is given by Eq. (3.38) and the proportionality factor is a regular power series in $\Gamma/|E_d^*|$ and $\Gamma/(U+\epsilon_d)$. In the extreme asymmetric case, when Γ/U can be neglected in comparison to $\Gamma/|E_d^*|$ in the expression for ρJ, we can use Eq. (3.40) to exprss T_K in terms of the original parameters Γ, ϵ_d, and U. We get

$$T_K \sim (\Gamma U)^{1/2} \exp\left[-\frac{\pi|\epsilon_d|}{2\Gamma}\right] , \quad (3.45)$$

a result which Haldane derived earlier[7] using perturbation theory in Γ from the asymmetric Anderson model.

In order to compare the T_K resulting from the renormalization calculations of $T\chi$ with those from analytic formulas, we must, as in I (see the end of Sec. V B), discuss the effects of perturbation theory, of renormalization by ρJ, and of finite Λ on Eq. (3.44). In fact, the only change from the arguments presented in I is that Eq. (3.44) must be multiplied by 0.364 instead of 0.182 (the factor of 2 results from the fact that the orbital energy is $\frac{1}{2}U$ in the symmetric Anderson model while it is just E_d^* in the asymmetric one). Hence we calculate T_K from

$$T_K(\Gamma, \epsilon_d, U) = 0.182|E_d^*|[\rho J_{\text{eff}}(\Lambda)]^{1/2} \times \exp -\frac{1}{|\rho J_{\text{eff}}(\Lambda)|} . \quad (3.46)$$

In Table VI we compare the values of the expression (3.46) for each of the three cases in Fig. 11(b) with the corresponding numerically determined values of T_K. The latter can be obtained from the plots via the mapping with the universal curve, or more accurately from the numerical results for $T\chi$, by looking for the temperature at which $T\chi = 0.0701$ (cf. Fig. 3). The agreement between the last two columns seems a little too good.

The next regime of behavior that we must discuss is the low-temperature, frozen-impurity regime, in which $T\chi$ is zero. For the case we have been discussing above, this regime is reached for temperatures much smaller than the Kondo temperature [cf. Fig. 11(b)]. But before discussing the frozen-impurity regime, it is convenient for us to discuss the

TABLE VI. Numerical results associated with Figs. 11 and 13. In the last two columns we compare the Kondo temperature calculated from Eq. (3.46) at the value $\Lambda = 3$ with that deduced from the numerical calculation also done at $\Lambda = 3$ – namely, the temperature where $T\chi = 0.07$. The close agreement of the two entries suggests that Eq. (3.46) is a good guide to the Kondo temperature even for ρJ as large as −0.4 as in the case of Fig. 13.

Plot	$\frac{U}{D}$	$\frac{2\Gamma}{\pi D}$	$\frac{\epsilon_d}{D}$	$\frac{E_d^*}{D}$	$\frac{2\Gamma}{\pi E_d}$	$\frac{2\Gamma}{\pi(U+E_d)}$	ρJ	ρK	$\rho J_{\text{eff}}(\Lambda)$	$\frac{T_K}{D}$ (3.46)	$\frac{T_K}{D}$ numerical
Fig 11(a)	10^{-3}	10^{-6}	-10^{-5}	-7.557×10^{-6}	−0.1323	10^{-3}	−0.133	0.033	−0.120	2.3×10^{-10}	2.7×10^{-10}
Fig. 11(b)	10^{-2}	10^{-6}	-10^{-5}	-6.315×10^{-6}	−0.1584	10^{-4}	−0.158	0.040	−0.142	7.6×10^{-9}	7.5×10^{-10}
Fig. 11(c)	10^{-2}	10^{-5}	-10^{-4}	-7.557×10^{-5}	−0.1323	10^{-3}	−0.133	0.033	−0.120	2.3×10^{-9}	2.2×10^{-9}
Fig. 13	10^{-2}	10^{-5}	-0.5×10^{-4}	-1.855×10^{-5}	−0.5391	10^{-3}	−0.540	0.135	−0.427	4.2×10^{-7}	4.8×10^{-7}

transitional cases, by which term we mean cases where the parameter values are such that one or the other of the three regimes we have discussed so far is absent. (The frozen-impurity regime is always present as long as $\Gamma \neq 0$.)

E. Transitional cases

The most interesting transitional situation to discuss is the case where, as $-\epsilon_d$ decreases, $-E_d^*$ [given by Eq. (3.22)] decreases to become comparable to Γ. Then the states in which $n_d = 1$ get strongly admixed with the states in which $n_d = 0$, and we no longer expect a transition from the valence-fluctuation regime to the local-moment regime. Another way to think about this situation is to note that, as $-E_d^*$ grows to become of order Γ, ρJ, the coupling constant that governs the local-moment regime and is given by Eq. (3.38), grows to become of order unity. Whence, from Eq. (3.45) we see that the Kondo temperature T_K rises to become of order T_2^*, so that the transition from the valence-fluctuation to the local-moment regime merges with the transition from the local-moment to the frozen-impurity regime. The result is that $T\chi$ makes a direct transition from the valence-fluctuation to the frozen-impurity regime, at a transition temperature of the order of Γ (which is the same as $-E_d^*$). We note that this situation can arise even for $-\epsilon_d >> \Gamma$, once $-\epsilon_d \lesssim \Gamma/\pi \ln U/\Gamma$. In this case the significant quantity is $E_d(T = \Gamma/\alpha)$ given by [cf. Eq. (3.16)]

$$E_d(\Gamma/\alpha) = \epsilon_d + \frac{\Gamma}{\pi} \ln\left(\frac{U}{\Gamma}\right) . \tag{3.47}$$

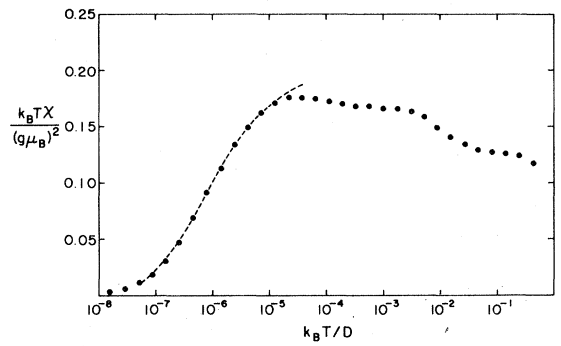

FIG. 13. Plot of $k_B T\chi(T)/(g\mu_B)^2$ vs $\ln(k_B T/D)$ for a choice of parameters ϵ_d, U, and Γ such that $-E_d^* \simeq \Gamma$ [see Eq. (3.22)]. There is considerable hybridization between the $n_d = 0$ and $n_d = 1$ impurity configurations, resulting in a relatively small value of $T\chi$ in the local-moment regime. It is difficult to see the deviations (which are a consequence of this hybridization) from the universal Kondo susceptibility (dashed curve) as the system evolves toward the frozen-impurity fixed point.

As $-\epsilon_d$ decreases through the value $(\Gamma/\pi)\ln U/\Gamma$, $\epsilon_d(\Gamma/\alpha)$ goes from a negative value through zero to a positive value. But as long as $|E_d(\Gamma/\alpha)| \lesssim \Gamma$, the transition from the valence-fluctuation to the frozen-impurity regime is basically controlled by Γ, and is very hard to treat analytically. One can only rely on the numerical results, such as plotted in Fig. 14(a).

Eventually, as $-\epsilon_d$ gets small enough or becomes positive, $E_d(\Gamma/\alpha)$ becomes much larger than Γ. In this case, as the temperature decreases within the valence-fluctuation regime $E_d(T)$ can be positive and increasing, so that the breakdown from the valence-fluctuation regime can occur because T becomes smaller than $E_d(T)$ [cf. Eq. (3.21)]. In this case we can identify a temperature T_3^* such that

$$\alpha T_3^* = E_d(T_3^*) \equiv E_d^{**} , \tag{3.48}$$

i.e.,

$$\frac{E_d^{**}}{\Gamma} = \frac{\epsilon_d}{\Gamma} + \frac{1}{\pi} \ln\left(\frac{U}{\Gamma}\right) - \frac{1}{\pi} \ln\left(\frac{E_d^{**}}{\Gamma}\right)$$

$$= E_d(\Gamma/\alpha) - \frac{1}{\pi} \ln\left(\frac{E_d^{**}}{\Gamma}\right) . \tag{3.49}$$

And as T drops below T_3^*, $T\chi$ makes a transition from the valence-fluctuation to the frozen-impurity regime. Numerical results for $T\chi$ for the case when $E_d(\Gamma/\alpha) > \Gamma$ are plotted in Fig. 14(b). We note that these plots show sharp drops in $T\chi$ reminiscent of the sharp drops in $T\chi$ for the case when $\Gamma = 0$ and $\epsilon_d > 0$ (cf. Fig. 5). These sharp drops are nonuniversal, i.e., can not be mapped on to the universal Kondo-susceptibility curve, and correspond to broad maxima when we plot χ vs T, as shown in Fig. 14(b).

As ϵ_d becomes positive and increases, so does E_d^{**}. When ϵ_d is driven to be of order U. E_d^{**} also becomes of order U, when the transition from the free-orbital to the valence-fluctuation regime merges with that from the valence-fluctuation to the frozen-impurity regime, and we get a direct transition from the free-orbital to the frozen-impurity regime at a temperature T_3^* set by ϵ_d.

That basically covers all the ranges of ϵ_d when $\Gamma << U << D$. Next we consider what happens when Γ is made comparable to or bigger than U. Then we once again get a direct transition from the free-orbital to the frozen-impurity regime. Since ϵ_d is restricted to be $\geq -\frac{1}{2}U$, this transition will be controlled by Γ if $|\epsilon_d| << \Gamma$, and by ϵ_d if $\epsilon_d >> \Gamma$.

Finally consider the case when U itself is made comparable to the bandwidth D. Since we are interested in $k_B T < D$, in this case there will be no free-orbital regime. The rest of the regimes depend on the values of ϵ_d and Γ. If $\{|\epsilon_d|, \Gamma\} << D$, we start

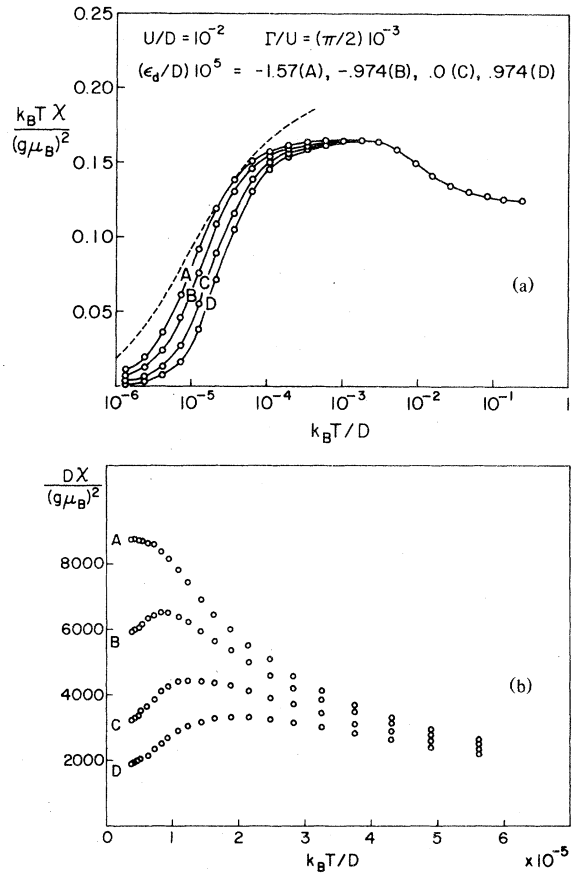

FIG. 14. Plots of $k_B T\chi/(g\mu_B)^2$ vs $\ln(k_B T/D)$ for a choice of the parameters U, ϵ_d, and Γ such that $E_d^{**} \gtrsim \Gamma$ [see Eq. (3.52)]. The transition between the valence-fluctuation fixed point and the frozen-impurity fixed point resembles the situation in which $\Gamma = 0$ and $\epsilon_d > 0$; i.e., the ground state of the impurity has zero occupancy. Deviations from the universal shape indicated by the dashed line reveal the nonmagnetic character of the impurity. (b) Plots of $D\chi/(g\mu_B)^2$ vs $k_B T/D$ for the same parameters as in (a). The deviations from universality in (a) correspond to the broad maxima in this more conventional plot. The curves labeled A, B, C, and D correspond to run numbers 7.4, 7.5, 7.6, and 7.7, respectively, in Table VIII.

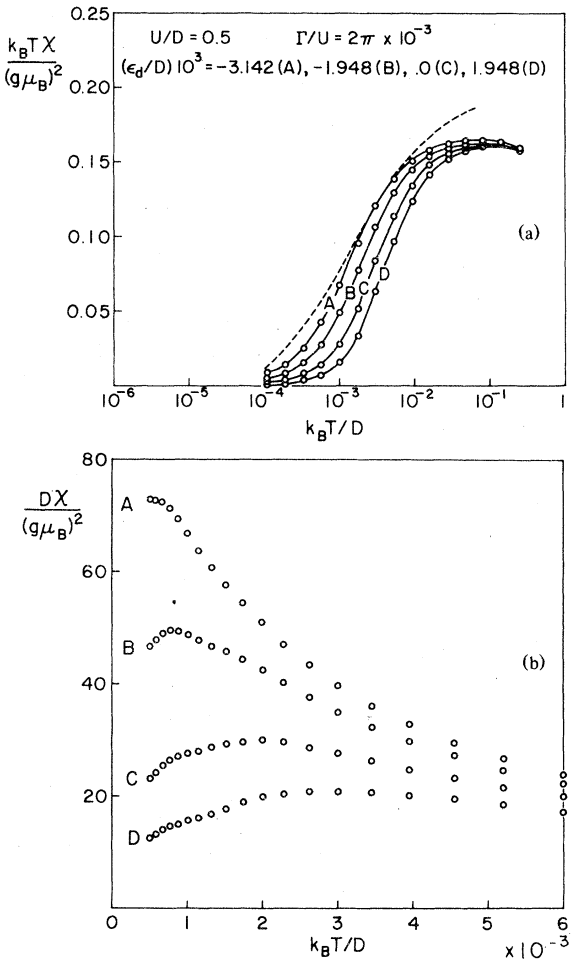

FIG. 15. Plots of $k_B T/(g\mu_B)^2$ vs $\ln(k_B T/D)$ for parameters U, ϵ_d, and Γ chosen so that $E_d^{**} \gtrsim \Gamma$ [see Eq. (3.52)]. Curves A, B, C, and D are characterized by the condition $U \sim D$, resulting in the absence of the free-impurity fixed point [cf. with Fig. 14(a)]. The nonmagnetic character of the impurity is indicated by the sharper drop of the full-line curves than of the universal (dashed) curve. (b) Plots of $D\chi/(g\mu_B)^2$ vs $(k_B T/D)$ for the same parameters as in (a). The broad maxima correspond to the deviations from universality depicted in that figure. The curves A, B, C, and D correspond to run numbers 6.1, 6.2, 6.3, and 6.4, respectively, in Table VIII.

with the valence-fluctuation regime for $k_B T \lesssim D$, and the discussion of Secs. III A–III C can be applied to this case merely by replacing U by D everywhere. Plots of $T\chi$ vs $\ln T$ for the case when $U \approx D$ are shown in Fig. 15.

F. Frozen-impurity regime

The frozen-impurity regime is the regime in which, effectively, the impurity degree of freedom is frozen out, and corresponds to a characteristic $T\chi$ value of 0. From the discussions in Secs. III B–III E, it is clear that the frozen-impurity regime is the stable low-temperature regime (i.e., there are no further transitions away from this regime). (This is true as long as $\Gamma \neq 0$. When $\Gamma = 0$, the valence-fluctuation regime is stable if $\epsilon_d = 0$, the local-moment regime is stable if $\epsilon_d < 0$, and the free-orbital regime is stable if $\epsilon_d = U = 0$.) The threshold temperature below which $T\chi$ can be considered to be in the frozen-impurity regime is given by T_K, Γ, or T_3^* depending on the parameter values that we are considering.

As we discussed in Secs. II A and II B, the frozen-impurity regime is associated with the frozen-

impurity fixed point, $H^*_{\rm FI}(K)$. The low-temperature region in which T is close to zero corresponds to a large N region in which H_N is close to $H^*_{\rm FI}(K)$. Hence we can calculate the properties of the frozen-impurity regime using an effective Hamiltonian constructed around $H^*_{N,\rm FI}(K)$, as discussed in Sec. II C. In this paper we will include in this effective Hamiltonian only the generators of the two leading irrelevant operators of eigenvalue Λ^{-1}, namely $H_{1,\rm FI}$ and $H_{2\rm FI}$ (cf. Table II). That is to say, we will use

$$H^{\rm eff}_{N,\rm FI}(\tilde{K}) = H^*_{N,\rm FI}(\tilde{K}) + \omega_1 \Lambda^{(N-1)/2}(f^\dagger_{0\mu} A_{1\mu} + A^\dagger_{1\mu} f_{0\mu}) + \omega_2 \Lambda^{(N-1)/2}(f^\dagger_{0\mu} f_{0\mu} - 1)^2 \ , \tag{3.50}$$

where the parameters ω_1 and ω_2 will be determined in terms of U, ϵ_d, and Γ, and A_1 is the operator defined in Eq. (2.17).

The central aspect of our discussion of the frozen-impurity regime will be the result that the dominant contribution to the susceptibility is a constant term proportional to ω_1 and ω_2, and the dominant contribution to the specific heat is a term linear in T and proportional to ω_1. We will also discuss the dependence of the parameters ω_1 and ω_2 on the parameters of the Anderson model, namely U, ϵ_d, and Γ. Expressing Eq. (3.50) in terms of the electron and hole operators that diagonalize $H^*_{N,\rm FI}(\tilde{K})$, we get using Eqs. (2.16) and (2.17),

$$\begin{aligned} H^{\rm eff}_{N,\rm FI}(\tilde{K}) = & \sum_l (\eta_l^+ g^\dagger_{l\mu} g_{l\mu} + \eta_l^- h^\dagger_{l\mu} h_{l\mu}) \\ & + \omega_1 \Lambda^{-(N-1)/2} \left[\sum_{ll'} (\alpha^+_{0l} \alpha^+_{0l'} \eta_l^+ g^\dagger_{l\mu} g_{l'\mu} - \alpha^-_{0l} \alpha^-_{0l'} \eta_l^- h_{l\mu} h^\dagger_{l'\mu} - \alpha^+_{0l} \alpha^-_{0l'} \eta_{l'}^- g^\dagger_{l\mu} h^\dagger_{l'\nu} + \alpha^-_{0l} \alpha^+_{0l'} \eta_l^+ h_{l\mu} g_{l'\mu}) + \text{H.c.} \right] \\ & + \omega_2 \Lambda^{-(N-1)/2} \left[\sum_{ll'} (\alpha^+_{0l} \alpha^+_{0l'} g^\dagger_{l\mu} g_{l'\mu} + \alpha^-_{0l} \alpha^-_{0l'} h_{l\mu} h^\dagger_{l'\mu} + \alpha^+_{0l} \alpha^-_{0l'} g^\dagger_{l\mu} h^\dagger_{l'\mu} + \alpha^-_{0l} \alpha^+_{0l'} h_{l\mu} g_{l'\mu}) - \Lambda^{(N-1)/2} \right]^2 \ . \end{aligned} \tag{3.51}$$

There are some technical restrictions associated with the use of Eq. (3.51): (i) Out of the eigenoperator terms, we must drop any pieces that look like a ground-state energy term (since, although this fact was not stressed earlier, the Hamiltonians H_N are actually defined with their ground-state energies subtracted), or like potential-scattering terms (since all such effects are assumed to be included in the fixed-point energies η_l^+ and η_l^-). (ii) Only first-order calculations in ω_1 and ω_2 are permitted (since other operators which can be effectively of the same strength as the second-order contributions have not been included). Furthermore, since we are only considering energies and static properties in this paper, we need only the diagonal part of Eq. (3.50). It is straightforward to verify that the diagonal part of the ω_1 term is given by

$$2\omega_1 \Lambda^{-(N-1)/2} \sum_l (\alpha^{+2}_{0l} \eta_l^+ g^\dagger_{l\mu} g_{l\mu} + \alpha^{-2}_{0l} \eta_l^- h^\dagger_{l\mu} h_{l\mu}) \ . \tag{3.52}$$

This term shifts every electron energy η_l^+ by an amount equal to $2\omega_1 \Lambda^{-(N-1)/2} \alpha^{+2}_{0l} \eta_l^+$ and every hole energy η_l^- by $2\omega_1 \Lambda^{-(N-1)/2} \alpha^{-2}_{0l} \eta_l^-$. The diagonal part of the ω_2 term can be shown to be[13]

$$\begin{aligned} & \omega_2 \Lambda^{-(N-1)/2} \sum_{ll'} \{ (\alpha^+_{0l})^2 (\alpha^+_{0l'})^2 [g^\dagger_{l\mu} g^\dagger_{l'\nu} g_{l'\nu} g_{l\mu} + g^\dagger_{l\mu} g^\dagger_{l'\nu} g_{l\nu} g_{l'\mu} (l \neq l')] + \alpha^{-2}_{0l} \alpha^{-2}_{0l'} [h^\dagger_{l\mu} h^\dagger_{l'\nu} h_{l'\nu} h_{l\mu} + h^\dagger_{l\mu} h^\dagger_{l'\nu} h_{l\nu} h_{l'\mu} (l \neq l')] \\ & \quad + 2\alpha^{-2}_{0l} \alpha^{-2}_{0l'} [g^\dagger_{l\mu} h^\dagger_{l'\mu} h_{l'\nu} g_{l\nu} - g^\dagger_{l\mu} h^\dagger_{l'\nu} h_{l'\nu} g_{l\mu}] + 2\alpha^+_{0l} \alpha^-_{0l'} \alpha^-_{0l} \alpha^+_{0l'} [g^\dagger_{l\mu} h^\dagger_{l'\mu} h_{l\nu} g_{l'\nu} - g^\dagger_{l\mu} h^\dagger_{l'\nu} h_{l\nu} g_{l'\mu}]_{l \neq l'} \} \ . \end{aligned} \tag{3.53}$$

We note that this term only affects two-particle states.

In Table VII we list the energies of the states considered in Table I calculated using the above effective Hamiltonian. By fitting the numerically calculated energy levels to these results we can determine $\tilde{K}$, ω_1, and ω_2. Note that all the low-lying energy levels of H_N are being described in terms of just three parameters.

The susceptibility and the free energy can be calculated by substituting $H^{\rm eff}_{N,\rm FI}(K)$ in place of H_N in Eqs. (1.5) and (1.6). To order ω_1 and ω_2, we get

$$k_B T_N \chi(T_N) = k_B T_N \chi_0(\tilde{K}) - \frac{\omega_1 \Lambda^{-(N-1)/2}}{\bar{\beta}} \chi_{1,\rm FI} - \frac{\omega_2 \Lambda^{-(N-1)/2}}{\bar{\beta}} [-\chi^2_{2,\rm FI} + \chi_{3,\rm FI} F_{2,\rm FI}] \ , \tag{3.54}$$

TABLE VII. States and energies of $H^{\text{eff}}_{N,\text{FI}}$ ($\tilde{K} < 0$).

Charge Q	Spin S	Index r	State	Energy
0	$\frac{1}{2}$	1	g_1	$\eta_1^+ + 2\omega_1 \Lambda^{-(N-1)/2}(\alpha_{01}^{+2}\eta_1^+)$
		2	g_2	$\eta_2^+ + 2\omega_1 \Lambda^{-(N-1)/2}(\alpha_{02}^{+2}\eta_2^+)$
		3	$2g_1 + h$	$2\eta_1^+ + \eta_1^- + 2\omega_1 \Lambda^{-(N-1)/2}(2\alpha_{01}^{+2}\eta_1^+ + \alpha_{01}^{-2}\eta_1^-)$ $+2\omega_2 \Lambda^{-(N-1)/2}(\alpha_{01}^{+4} - \alpha_{01}^{+2}\alpha_{01}^{-2})$[a]
-2	$\frac{1}{2}$	1	h_1	$\eta_1^- + 2\omega_1 \Lambda^{-(N-1)/2}(\alpha_{01}^{-2}\eta_1^-)$
+2	$\frac{1}{2}$	1	$2g_1 + g_2$	$2\eta_1^+ + \eta_2^+ + 2\omega_1 \Lambda^{-(N-1)/2}(2\alpha_{01}^{+2}\eta_1^+ + \alpha_{02}^{+2}\eta_2^+$
−1	0	1	...	0
		2	$g_1 + h_1$	$\eta_1^+ + \eta_1^- + 2\omega_1 \Lambda^{-(N-1)/2}(\alpha_{01}^{+2}\eta_1^+ + \alpha_{01}^{-2}\eta_1^-)$ $+2\omega_2 \Lambda^{-(N-1)/2}\alpha_{01}^{+2}\alpha_{01}^{-2}$
	1	1	$g_1 + h_1$	$\eta_1^+ + \eta_1^- + 2\omega_1 \Lambda^{-(N-1)/2}(\alpha_{01}^{+2}\eta_1^+ + \alpha_{01}^{-2}\eta_1^-)$ $-2\omega_2 \Lambda^{-(N-1)/2}\alpha_{01}^{+2}\alpha_{01}^{-2}$
+1	0	1	$2g_1$	$2\eta_1^+ + 2\omega_1 \Lambda^{-(N-1)/2}(2\alpha_{01}^{+2}\eta_1^+) + 2\omega_2 \Lambda^{-(N-1)/2}(\alpha_{01}^{+})^4$
		2	$g_1 + g_2$	$\eta_1^+ + \eta_2^+ + 2\omega_1 \Lambda^{-(N-1)/2}(\alpha_{01}^{+2}\eta_1^+ + \alpha_{01}^{-2}\eta_1^-)$ $+4\omega_2 \Lambda^{-(N-1)/2}\alpha_{01}^{+2}\alpha_{02}^{+2}$
	1	1	$g_1 + g_2$	$\eta_1^+ + \eta_2^+ + 2\omega_1 \Lambda^{-(N-1)/2}(\alpha_{01}^{+2}\eta_1^+ + \alpha_{01}^{-2}\eta_1^-)$

[a]Neglecting possibility of degeneracy, i.e, $\eta_1^+(\tilde{K}) \simeq 0$.

$$F(T_N) = F_0(\tilde{K}) + K_B T_N \left(\frac{4\omega_1 \Lambda^{-(N-1)/2}}{\bar{\beta}} F_{1,\text{FI}} + \frac{2\omega_2 \Lambda^{-(N-1)/2}}{\bar{\beta}} F_{2,\text{FI}}^2 \right) . \tag{3.55}$$

Here χ_0 and F_0 are the contributions from the fixed point, i.e., due to potential scattering, and have been written down earlier [cf. Eq. (2.14) for χ_0 and Eq. (3.32) for F_0]. The other functions, $\chi_{1,\text{FI}}$, $\chi_{2,\text{FI}}$, etc., are defined as follows:.

$$\chi_{1,\text{FI}}(\tilde{K}) \equiv \bar{\beta}^2 \sum_l \left(\alpha_{0l}^{+2}\eta_l^+ \frac{e^{-\bar{\beta}\eta_l^+}(1 - e^{-\bar{\beta}\eta_l^+})}{(1 + e^{-\bar{\beta}\eta_l^+})^3} + \alpha_{0l}^{-2}\eta_l^- \frac{e^{-\bar{\beta}\eta_l^-}(1 - e^{-\bar{\beta}\eta_l^-})}{(1 + e^{-\bar{\beta}\eta_l^-})^3} \right) , \tag{3.56}$$

$$\chi_{2,\text{FI}}(\tilde{K}) \equiv \bar{\beta} \sum_l \left(\alpha_{0l}^{+2} \frac{e^{-\bar{\beta}\eta_l^+}}{(1 + e^{-\bar{\beta}\eta_l^+})^2} + \alpha_{0l}^{-2} \frac{e^{-\bar{\beta}\eta_l^-}}{(1 + e^{-\bar{\beta}\eta_l^-})^2} \right) , \tag{3.57}$$

$$\chi_{3,\text{FI}}(\tilde{K}) \equiv \bar{\beta} \sum_l \left(\alpha_{0l}^{+2} \frac{e^{-\bar{\beta}\eta_l^+}(1 - e^{-\bar{\beta}\eta_l^+})}{(1 + e^{-\bar{\beta}\eta_l^+})^3} - \alpha_{0l}^{-2} \frac{e^{-\bar{\beta}\eta_l^-}(1 - e^{-\bar{\beta}\eta_l^-})}{(1 + e^{-\bar{\beta}\eta_l^-})^3} \right) , \tag{3.58}$$

$$F_{1,\text{FI}}(\tilde{K}) \equiv \bar{\beta}^2 \sum_l \left(\alpha_{0l}^{+2}\eta_l^+ \frac{e^{-\bar{\beta}\eta_l^+}}{(1 + e^{-\bar{\beta}\eta_l^+})} + \alpha_{0l}^{-2}\eta_l^- \frac{e^{-\bar{\beta}\eta_l^-}}{(1 + e^{-\bar{\beta}\eta_l^-})} \right) , \tag{3.59}$$

$$F_{2,\mathrm{FI}}(\tilde{K}) \equiv \bar{\beta} \sum_l \left[\alpha_{0l}^{+2} \frac{e^{-\bar{\beta}\eta_l^+}}{1+e^{-\bar{\beta}\eta_l^+}} - \alpha_{0l}^{-2} \frac{e^{-\bar{\beta}\eta_l^-}}{1+e^{-\bar{\beta}\eta_l^-}} \right] . \tag{3.60}$$

All these functions are to be evaluated in the limit $\bar{\beta} \to 0$ and $N \to \infty$ keeping T_N fixed. (N determines the upper limit on l in the sums.)

The thermodynamic functions above are evaluated in Appendix A. There we show that, neglecting corrections of order $\exp(-\pi^2/\ln\Lambda)$, the functions are given by [cf. Eqs. (A54)–(A57)]

$$k_B T_N \chi_0 = F_0 = \chi_{3,\mathrm{FI}} = F_{2,\mathrm{FI}} = 0 , \tag{3.61}$$

$$\chi_{1,\mathrm{FI}} = \chi_{2,\mathrm{FI}} = F_{1,\mathrm{FI}}(\tfrac{1}{6}\pi^2)^{-1} = \frac{\alpha_0^2(\tilde{K})}{\ln\Lambda} , \tag{3.62}$$

where [cf. Eq. (A30)],

$$\alpha_0^2(\tilde{K}) = \alpha_0^2 \left[1 + \frac{\pi^2 \alpha_0^4}{(\ln\Lambda)^2} \tilde{K}^2 \right]^{-1} \equiv \alpha_0^2 \phi(\tilde{K}) . \tag{3.63}$$

Substituting these results into Eqs. (3.54) and (3.55) and making use of the connection Eq. (1.4) between $\bar{\beta}$ N, and T_N, and putting back all the factors we have been suppressing, we obtain

$$\chi(T) = \frac{(g\mu_B)^2}{D} \left[-\frac{\omega_1 \phi(\tilde{K})}{2A_\Lambda} + \tfrac{1}{2}(1+\Lambda^{-1}) \frac{\omega_2 \phi^2(\tilde{K})}{4A_\Lambda^2} \right] , \tag{3.64}$$

$$F(T) = \frac{(-k_B T)^2}{D} (\tfrac{1}{3}\pi^2) \frac{\omega_1 \phi(\tilde{K})}{A_\Lambda} , \tag{3.65}$$

where A_Λ is the same quantity as defined earlier in Eq. (3.36). From Eq. (3.65) we get, for the specific heat,

$$C(T_T) = -T_T \frac{\partial^2}{\partial T^2} F(T) = \tfrac{4}{3}\pi^2 \frac{k_B^2 T}{D} \left[\frac{-\omega_1 \phi(\tilde{K})}{2A_\Lambda} \right] . \tag{3.66}$$

Thus we have the results promised earlier, namely that the susceptibility is a constant and the specific heat is linear in T. The results for C and χ can be combined to get the ratio

$$R \equiv \tfrac{4}{3}\pi^2 \frac{k_B^2}{(g\mu_B)^2} \frac{T\chi}{C} = 1 - \tfrac{1}{2}(1+\Lambda^{-1}) \frac{\omega_2}{\omega_1} \frac{\phi(\tilde{K})}{2A_\Lambda} . \tag{3.67}$$

As mentioned earlier, ω_1, ω_2, and $\tilde{K}$ can be calculated by fitting to the numerically determined energy levels. Using these we can calculate $\chi D/(g\mu_B)^2$ and R from Eqs. (3.64) and (3.67). The results for the various parameter values that we have considered so far are listed in Table VIII.

The next thing for us to discuss is the dependence of ω_1 and ω_2, or rather, of $\chi D/(g\mu_B)^2$ and R, on the parameters U, ϵ_d, and Γ. There are basically three cases for which such a discussion is in order.

(i) The first case is when U can be treated as a small parameter. This case can be handled analytically, as has been done in Appendix D where we show that

$$\frac{\chi}{(g\mu_B)^2} = \frac{A_\Lambda}{2\pi\Delta} \left[1 + A_\Lambda \left(\frac{U}{\pi\Delta} \right) + O\left(\frac{U}{\pi\Delta} \right)^2 \right] , \tag{3.68}$$

$$R = 1 + A_\Lambda \left(\frac{U}{\pi\Delta} \right) + O\left(\frac{U}{\pi\Delta} \right)^2 , \tag{3.69}$$

where

$$\Delta \equiv \frac{\Gamma^2 + [A_\Lambda(\epsilon_d + \frac{1}{2}U)]^2}{\Gamma} , \tag{3.70}$$

and A_Λ is the Λ-dependent quantity defined earlier in Eq. (3.36) ($A_\Lambda \to 1$ as $\Lambda \to 1$). The above results agree with the known continuum-theory results[15] in the limit $\Lambda \to 1$.

(ii) The second case is the asymmetric-local-moment case when U and $-\epsilon_d$ are both large enough compared to Γ that there is a substantial temperature range for which $T\chi$ is in the local-moment regime.

From the discussion of Sec. III D, we know that in this case χ seems to obey the scaling law (3.40), which can be reexpressed in the form

$$k_B T_K \chi(T) = \tfrac{1}{4}(T_K/T)\,[1 + \Phi^{-1}(\ln(T/T_K))] , \tag{3.71}$$

where Φ^{-1} denotes the function which is the inverse of Φ. The right-hand side of Eq. (3.71) is clearly another universal function of (T/T_K), and as $T \to 0$, we expect it to go to some universal constant χ_u. Since Φ for the asymmetric case seems to be the same as Φ for the symmetric case, we expect that χ_u for the asymmetric case has the same value as for the symmetric case, i.e., for the Kondo problem without potential scattering, namely,[1,2] $\chi_u = 0.1$. Hence we expect, for $T \ll T_K$,

$$\frac{\chi(T)}{(g\mu_B)^2} \cong \frac{0.1}{k_B T_K} . \tag{3.72}$$

The validity of this result for the cases plotted in Fig. 11(b) can be gathered from Table VIII, where the values of the two sides of Eq. (3.72) are compared.

In the symmetric case, one could argue[2] that R should be independent of ρJ for small enough ρJ,

TABLE VIII. Appropriate numerical values for all the numerical computations in this paper, all done for $\Lambda=3$. Runs 7.1 to 7.3 are curves A to C in Fig. 10; 7.4 to 7.7 are in Fig. 14, and 6.1 to 6.4 in Fig. 15. The values of E_d^*/Γ or E_d^{**}/Γ have been deduced from Eq. (3.22) or (3.49) and are also indicated on Fig. 12. T_K/D is the temperature where $T\chi=0.07$. The susceptibility and the coefficients ω_1' and ω_2' (of the two irrelevant operators about the frozen-impurity fixed point) are shown in units of T_K/D so that deviations from universality can be appreciated. The primes on ω_1', ω_2', and K' denote that the analysis for the frozen-impurity regime was done for even N, while the discussion in the text has been for odd N.

Run	$\frac{U}{D}$	$\frac{\Gamma}{D}$	$\frac{\epsilon_d}{D}$	$\frac{E_d^{**}}{\Gamma}$ (or E_d^*)	$\frac{T_K}{D}$	$-\omega_1'$ (in units of T_K/D)	ω_2'	χ	K'	R
7.1	10^{-3}	$\frac{1}{2}\pi\times10^{-6}$	-10^{-5}	−4.81	2.67×10^{-10}	0.114	0.405	0.106	0.108	2.07
7.2	10^{-2}	$\frac{1}{2}\pi\times10^{-6}$	-10^{-5}	−4.02	7.46×10^{-10}	0.111	0.400	0.103	0.130	2.08
7.3	10^{-2}	$\frac{1}{2}\pi\times10^{-5}$	-10^{-4}	−4.81	2.20×10^{-9}	0.112	0.395	0.104	0.105	2.06
7.4	10^{-2}	$\frac{1}{2}\pi\times10^{-5}$	-1.57×10^{-5}	1.04	0.824×10^{-5}	0.242	1.71	0.057	1.56	1.67
7.5	10^{-2}	$\frac{1}{2}\pi\times10^{-5}$	-0.974×10^{-5}	1.34	1.10×10^{-5}	0.302	2.26	0.050	1.88	1.53
7.6	10^{-2}	$\frac{1}{2}\pi\times10^{-5}$	0	1.85	1.67×10^{-5}	0.443	3.60	0.043	2.44	1.39
7.7	10^{-2}	$\frac{1}{2}\pi\times10^{-5}$	-0.974×10^{-5}	2.40	2.08×10^{-5}	0.527	4.91	0.033	3.04	1.30
6.1	0.5	$\pi\times10^{-3}$	$-\pi\times10^{-3}$	0.72	1.06×10^{-3}	0.182	1.18	0.069	1.17	1.88
6.2	0.5	$\pi\times10^{-3}$	-1.948×10^{-3}	1.00	1.52×10^{-3}	0.227	1.55	0.044	1.45	1.71
6.3	0.5	$\pi\times10^{-3}$	0	1.48	2.20×10^{-3}	0.293	2.19	0.045	1.96	1.51
6.4	0.5	$\pi\times10^{-3}$	1.948×10^{-3}	2.01	3.54×10^{-3}	0.452	3.74	0.042	2.52	1.37
Fig. 13	10^{-2}	$\frac{1}{2}\pi\times10^{-5}$	-5×10^{-5}	−1.18	4.78×10^{-7}					

and the numerical results showed this value to be $R=2$. In the asymmetric case there seems to be no simple argument which makes clear whether or not R is independent of the parameters of the Anderson model. The numerical results in Table VIII show that R in the universal range (runs 7.1–7.3) is only slightly affected by potential scattering. In the nonuniversal range (runs 7.4–7.7 and 6.1–6.4) R drops below 2, the amount of drop being a rough indication of the magnitude of the departure from universality.

(iii) The final case for which we can discuss the dependence of $\chi/(g\mu_B)^2$ and R on U, ϵ_d, and Γ is the case considered in Sec. III E where $-\epsilon_d$ is small enough compared to Γ or ϵ_d is positive such that there is a direct transition from the valence-fluctuation to the frozen-impurity regime due to a positive $E_d(T)$.

In this case, in view of our discussions in Sec. III E [cf. discussion around Eq. (3.48) and (3.49)], the situation for temperatures much less than the transition temperature T_3^* can be likened to that for an Anderson model with an effective ϵ_d equal to E_d^{**} and an effectiv U equal to ∞. Hence we can use the expression (D27) derived in Appendix D and replace ϵ_d by E_d^{**} to claim that in this case

$$\frac{\chi}{(g\mu_B)^2}=\frac{1}{A_\Lambda}\frac{\Gamma}{2\pi(E_d^{**})^2}\ . \tag{3.73}$$

The condition for the validity of this result is that E_d^{**} be much greater than Γ.

We note that the dependence of E_d^{**} on ϵ_d, U, and Γ is obtainable by solving the transcendental equation (3.48). For the case when ϵ_d is positive and comparable to U, th solution for E_d^{**} is approximately

$$E_d^{**}\cong\epsilon_d+\frac{\Gamma}{\pi}\ln\left(\frac{U}{\epsilon_d}\right)+\cdots\ . \tag{3.74}$$

Substituting this result into Eq. (3.73) we get (setting $A_\Lambda=1$)

$$\frac{\chi}{(g\mu_B)^2}=\frac{\Gamma}{2\pi\epsilon_d^2}\left(1-\frac{2\Gamma}{\pi\epsilon_d}\ln\frac{U}{\epsilon_d}+\cdots\right)\ . \tag{3.75}$$

Of course, such a series for χ can be obtained directly from the asymmetric Anderson model (for the case when $\epsilon_d \gg \Gamma$) using perturbation theory in Γ, as has been done by Haldane.[9] The expression (3.73) can be looked upon as the result of summing up of the logarithmic terms of such a perturbation series. (Of course, such a summing up is hard to perform without using renormalization-group techniques, either as above, or in the scaling-theory form used by Haldane.[7])

ACKNOWLEDGMENTS

The hospitality of NORDITA, Copenhagen, during a summer visit provided the opportunity for this project to be started. One of the authors (H.R.K.) is grateful for a summer month at IBM Yorktown Heights where some of these computations were performed. We are indebted to Luiz Oliveira for the continuous assistance he supplied in preparing this manuscript. One of us (H.R.K.) was supported in part under NSF Grants NO. DMR 75-22241 and No. DMR 78-21069. One of us (J.W.W.) was supported in part by the NSF Grant No. DMR 77-18329. One of us (K.G.W.) was supported in part by the NSF Grant No. PHY 77-22336.

APPENDIX A: DISCUSSION OF THE FREE-ELECTRON HAMILTONIAN WITH POTENTIAL SCATTERING

In this appendix we discuss the properties of the free-electron Hamiltonian with potential scattering, described by the Hamiltonian (2.11)

$$H_N^0(K) = \Lambda^{(N-1)/2}\left[\sum_{n=0}^{N-1}\Lambda^{-n/2}\xi_n(f_n^\dagger f_{n+1}+f_{n+1}^\dagger f_n)+\tilde{K}f_0^\dagger f_0\right]$$

$$= H_N^0+\tilde{K}\Lambda^{(N-1)/2}f_0^\dagger f_0 \quad . \tag{A1}$$

Spin indices are unimportant for this discussion and are suppressed.

1. *Exact results*

Since $H_N^0(\tilde{K})$ is a quadratic Hamiltonian it can be diagonalized into a set of single particle levels, to find which we express Eq. (A1) in terms of the operators that diagonalize H_N^0. We will write

$$H_N^0=\sum_l \epsilon_l a_l^\dagger a_l \quad ,$$
$$f_0=\Lambda^{-(N-1)/4}\sum \gamma_{0l}a_l \quad . \tag{A2}$$

In view of our discussion of H_N^0 in Sec. III A of I, we know that, *for N odd*, $l=\pm1, \pm2, \ldots, \pm\frac{1}{2}(N+1)$,

$$\begin{aligned}&\epsilon_l=\eta_l^*,\quad a_l=g_l,\quad \gamma_{0l}=\alpha_{0l}\quad (l>0)\quad,\\ &\epsilon_l=-\eta_{-l}^*,\quad a_l=h_{-l}^\dagger,\quad \gamma_{0l}=\alpha_{0-l}\quad (l<0)\quad;\end{aligned} \tag{A3}$$

for N even, $l=0, \pm1, \pm2, \ldots, \pm\frac{1}{2}N$,

$$\begin{aligned}&\epsilon_l=\hat{\eta}_l^*,\quad a_l=g_l,\quad \gamma_{0l}=\hat{\alpha}_{0l}\quad (l\geq 0)\quad,\\ &\epsilon_l=-\eta_{-l}^*,\quad a_l=h_{-l}^\dagger,\quad \gamma_{0l}=\hat{\alpha}_{0-l}\quad (l<0)\quad.\end{aligned} \tag{A4}$$

Expressing $H_N^0(K)$ in terms of the operators a_l we get

$$H_N^0=\sum_l \epsilon_l a_l^\dagger a_l+\tilde{K}\sum_{ll'}\gamma_{0l}\gamma_{0l'}a_l^\dagger a_{l'} \quad . \tag{A5}$$

It is easy to show that a new set of operators c_j, defined as $c_j=\sum_l u_{lj}a_l$ where u_{lj} are the elements of an orthogonal matrix, will diagonalize $H_N^0(K)$ into a set of single-particle levels $\eta_j(N)$ provided the u_{lj} satisfy the equations

$$(\eta_j-\epsilon_l)u_{lj}=\tilde{K}\gamma_{0l}\sum_{l'}\gamma_{0l'}u_{l'j} \quad . \tag{A6}$$

The solution of Eq. (A6) is easily shown to be

$$\tilde{K}^{-1}=\sum_l\frac{\gamma_{0l}^2}{\eta_j-\epsilon_l}\equiv X(N,\eta_j) \quad , \tag{A7}$$

$$u_{lj}=\frac{\gamma_{0l}}{\eta_j-\epsilon_l}\left(\sum_{l'}\frac{\gamma_{0l'}^2}{(\eta_j-\epsilon_{l'})^2}\right)^{-1/2} \quad . \tag{A8}$$

That is, the eigenvalues η_j are determined by the roots of the equation $X(N,\eta)=\tilde{K}^{-1}$, which roots can be determined graphically by plotting $X(N,\eta)$ vs η and locating the intercepts of such a plot with the horizontal line $X=\tilde{K}^{-1}$. Once η_j are determined, u_{lj} can be computed using Eq. (A8).

We first consider the case when N is odd. Using Eq. (A3) we get

$$\tilde{K}^{-1}=X(N,\eta)\equiv 2\eta\sum_{l=1}^{(N+1)/2}\frac{\alpha_{0l}^2}{\eta^2-\eta_l^{*2}} \quad . \tag{A9}$$

The graphical determination of the roots of this equation is sketched in Fig. 16(a), which shows that there are $\frac{1}{2}(N+1)$ positive eigenvalues which grow smoothly out of η_j^* as $|\tilde{K}|$ increases, and can be denoted $\eta_j^+(\tilde{K},N)$ and $\frac{1}{2}(N+1)$ negative eigenvalues that grow smoothly out of $-\eta_j^*$ and can be denoted $-\eta_j^-(\tilde{K},N)$ $[j=1,2,\ldots,\frac{1}{2}(N+1)]$. Using the results that for $l\gg1$, $\eta_l^*=\Lambda^{l-1}$, and $\alpha_{0l}^2=\alpha_0^2\Lambda^{l-1}$, one can easily show that

$$X(N,\eta)=2\eta\sum_{l=1}^{\infty}\frac{\alpha_{0l}^2}{\eta^2-\eta^{*2}}+2\alpha_0^2\sum_{n=0}^{\infty}\frac{(\eta\Lambda^{-(N+1)/2})^{2n+1}}{1-\Lambda^{-(2n+1)}} \quad , \tag{A10}$$

which shows that, as $N\to\infty$ the eigenvalues $\eta_j^\pm(\tilde{K},N)$ rapidly approach (with deviations that vanish as $\Lambda^{-(N-1)/2}$) their fixed point values, denoted by $\eta_j^\pm(\tilde{K})$. The equation determining $\eta_j^\pm$ is, from (A10),

$$\pm\tilde{K}^{-1}=2\eta_j^\pm\sum_{l=1}^{\infty}\frac{\alpha_{0l}^2}{\eta_j^\pm-\eta_l^{*2}}\equiv X(\eta_j^\pm) \quad . \tag{A11}$$

The behavior of $\eta_j^\pm(\tilde{K})$ as a function of $\tilde{K}$ is sketched in Fig. 16(b). We note that as $\tilde{K}\to\pm\infty$,

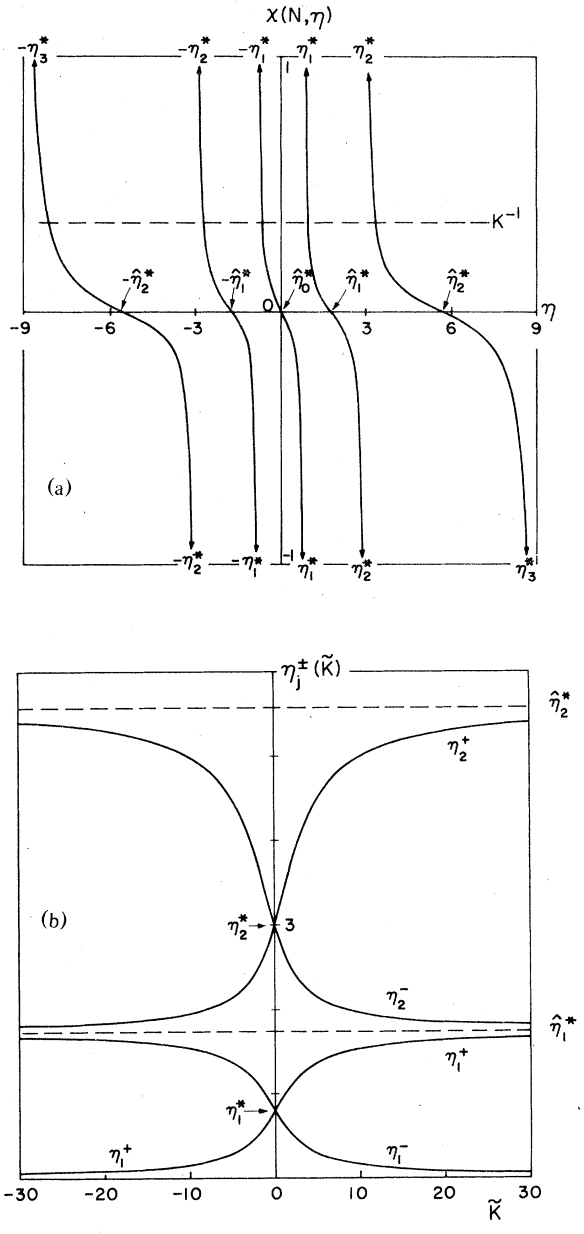

FIG. 16. Eigenvalues of the *odd-N* free-electron Hamiltonian with potential scattering $\tilde{K}$. (a) The characteristic function $X(N,\eta)$ [see Eq. (A9)] is plotted vs the energy η measured in units of $\Lambda^{-(N-1)/2}$ for the case $N=5$. Note that $X(N,\eta)$ blows up as the fixed points η_j^* of free-electron Hamiltonian for odd N and is zero at those $\hat{\eta}_j^*$ for even N. The intersection of $X(N,\eta)$ with $\tilde{K}^{-1}$ gives the roots $\eta_j^{\pm}(\tilde{K},N)$. (b) The behavior of $\eta_j^{\pm}(\tilde{K},N)$ is plotted as a function of $\tilde{K}$. Note that as $\tilde{K}\to\pm\infty$, $\eta_j^{\pm}(\tilde{K},N)$ approach the *odd* free-electron eigenvalues $\hat{\eta}_j^*$. In the limit $N\to\infty$ we denote the roots $\eta_j^{\pm}(\tilde{K})$ as the eigenvalues of the fixed-point Hamiltonian including potential scattering $H^*(\tilde{K})$.

$\{\eta_j^{\pm}\}$ go over to the odd free-electron eigenvalues $\{\hat{\eta}_l^*\}$. We will let $H^*(\tilde{K})$ denote the fixed point determined by the set of single-particle levels $\eta_j^{\pm}(\tilde{K})$.

Next we consider the case when N is even. Using Eq. (A4) in Eq. (A7), in this case we get

$$\tilde{K}^{-1}=\hat{X}(N,\eta)\equiv\frac{\hat{\alpha}_{00}^2}{\eta}+2\eta\sum_{l=1}^{N/2}\frac{\hat{\alpha}_{0l}^2}{\eta^2-\hat{\eta}_l^{*2}}\ . \tag{A12}$$

The graphical determination of the roots of this equation are sketched in Fig. 17(a). This figure shows that there are $\frac{1}{2}N$ positive eigenvalues which grow smoothly out of $\hat{\eta}_j^*$ as $|\tilde{K}|$ increases and can be denoted $\hat{\eta}_j^+(\tilde{K},N)$, and $\frac{1}{2}N$ negative eigenvalues which grow smoothly out of $-\eta_j^*$ and can be denoted $-\hat{\eta}_j^-(\tilde{K},N)$ $(j=1,2,\ldots,\frac{1}{2}N)$. The eigenvalue that grows out of $\hat{\eta}_0^*$ $(=0)$ is positive if $\tilde{K}>0$ and negative if $\tilde{K}<0$, and will be denoted $\hat{\eta}_0^+(\tilde{K},N)$ for $\tilde{K}>0$ and $-\hat{\eta}_0^-(\tilde{K},N)$ for $\tilde{K}<0$. Exactly as in the case of odd N, we can verify that as $N\to\infty$, $\hat{\eta}_{j_\pm}^{\pm}(\tilde{K},N)$ rapidly approach their fixed-point values $\hat{\eta}_j^{\pm}(\tilde{K})$. The latter are determined by the equation

$$\pm\tilde{K}^{-1}=\frac{\hat{\alpha}_{00}^2}{\hat{\eta}_j^{\pm}}+2\hat{\eta}_j^{\pm}\sum_{l=1}^{\infty}\frac{\hat{\alpha}_{0l}^2}{\hat{\eta}_j^{\pm}-\hat{\eta}_j^{*2}}\equiv\hat{X}(\hat{\eta}_j^{\pm})\ . \tag{A13}$$

The behavior of $\hat{\eta}_j^{\pm}(\tilde{K})$ as a function of $\tilde{K}$ is sketched in Fig. 17(b). We note that as $\tilde{K}\to\pm\infty$, $\{\hat{\eta}_j^{\pm}\}$ go over to the even free-electron eigenvalues $\{\eta_l^*\}$. We will let $\hat{H}^*(\tilde{K})$ denote the fixed point determined by the set of single-particle levels $\hat{\eta}_j^{\pm}(\tilde{K})$.

We make one further remark about the ground-state charge associated with $\hat{H}^*(\tilde{K})$. We recall that (cf. Sec. III A of I) our convention for assigning charge was such that for the cases when $\tilde{K}=0$ the zero of charge corresponds to having one electron in $\hat{\eta}_0^*$ (cf. Table II of I). Therefore, when $\tilde{K}>0$ and we associate an electron operator with $\hat{\eta}_0^+$, the ground state (with no electrons or holes) of $\hat{H}^*(\tilde{K})$ must be assigned charge -1; when $\tilde{K}<0$, and we associate a hole operator with $\hat{\eta}_0^-$, the ground state of $\hat{H}^*(\tilde{K})$ must be assigned charge $+1$.

Next we consider the expansion for f_0 in terms of the new operators c_j. Using Eqs. (A2), (A8), and (A7), we get

$$f_0=\Lambda^{-(N-1)/4}\sum_j\left(\sum_l\gamma_{0l}u_{lj}\right)c_j$$

$$=\Lambda^{-(N-1)/4}\sum_j K^{-1}\left(\sum_{l'}\frac{\alpha_{0l'}^2}{(\eta_j-\epsilon_{l'})^2}\right)^{-1/2}c_j\ . \tag{A14}$$

For large N, the term in large parentheses in Eq. (A14) is independent of N. By labeling c_j in terms of electron and hole operators, it is straightforward to show

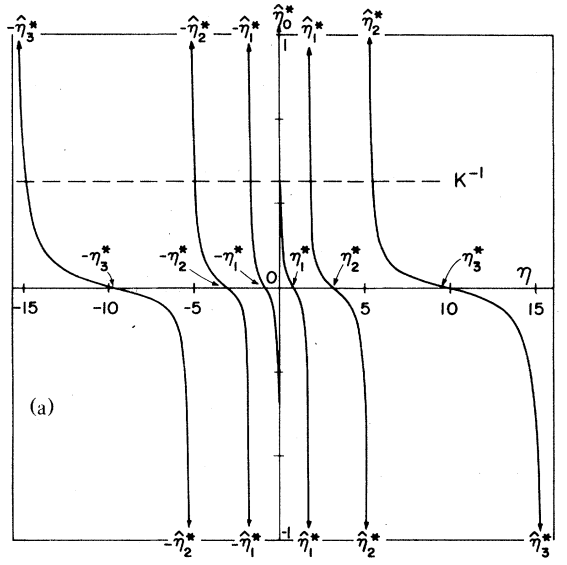

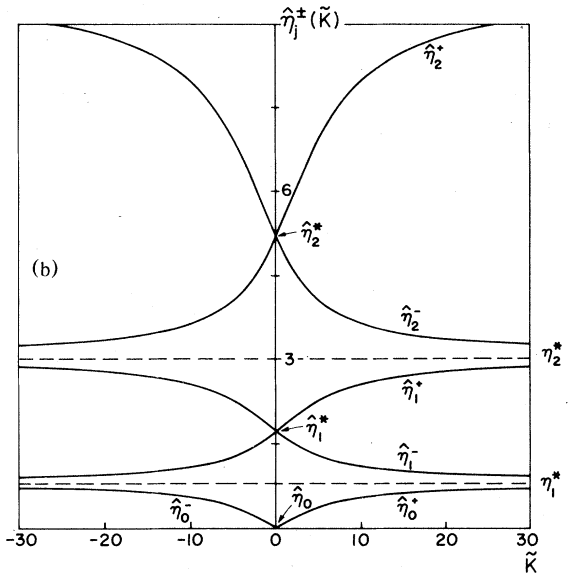

FIG. 17. Eigenvalues of the *even-N* free-electron Hamiltonian with potential scattering $\tilde{K}$. (a) The characteristic function $\hat{X}(N=6,\eta)$ is plotted vs η measured in units $\Lambda^{-5/2}$. Note the contrast with Fig. 16(a) in that $\hat{X}$ now blows up at the fixed points $\hat{\eta}_j^*$ of odd-N free-electron Hamiltonian, etc. (b) Similarly, the roots of $\eta_j^{\pm}(\tilde{K},N)$ are obtained from the graphical solution of $\hat{X}=\tilde{K}^{-1}$. In the limit $N\to\infty$, we denote the roots $\hat{\eta}_j^{\pm}(\tilde{K})$ as the eigenvalue of the fixed-point Hamiltonian including potential scattering $H^*(\tilde{K})$. Finally, we note that there is one-to-one mapping between $H^*(\tilde{K}')$ and $H^*(\tilde{K})$ where $\tilde{K}'=-(2/\pi)\times\ln\Lambda/(1-\Lambda^{-1})\tilde{K}^{-1}$ [see Eq. (A64)].

that for N odd we get

$$f_0=\Lambda^{-(N-1)/4}\sum_j(\alpha_{0j}^+g_j+\alpha_{0j}^-h_j^\dagger)\ , \tag{A15}$$

as was stated in Sec. II C [cf. Eq. (2.16)]. $\alpha_{0j}^{\pm}$ are given by

$$\alpha_{0j}^{\pm}=\tilde{K}^{-1}\left[\sum_{l=1}^{\infty}\alpha_{0l}^2\left(\frac{1}{(\eta_j^{\pm}-\eta_l^*)^2}+\frac{1}{(\eta_j^{\pm}+\eta_l^*)^2}\right)\right]^{-1/2}$$

$$=\tilde{K}^{-1}[-X'(\eta_j^{\pm})]^{-1/2}\ . \tag{A16}$$

The second result above follows from the definition (A11) of $X(\eta_j^{\pm})$. Similarly, for N even, we can write

$$f_0=\Lambda^{-(N-1)/4}\sum_j(\hat{\alpha}_{0j}^+g_j+\hat{\alpha}_{0j}^-h_j^\dagger)\ , \tag{A17}$$

with the understanding that for $\tilde{K}>0$ there is a g_0 but no h_0, whereas for $\tilde{K}<0$ there is a h_0 but no g_0 [cf. the discussion following Eq. (A12)]. Using Eqs. (A14) and (A13) we get

$$\hat{\alpha}_{0j}^{\pm}=\tilde{K}^{-1}\left[\sum_{l=1}^{\infty}\hat{\alpha}_{0l}^2\left(\frac{1}{(\eta_j^{\pm}-\hat{\eta}_l^*)^2}+\frac{1}{(\eta_j^{\pm}+\hat{\eta}_l^*)^2}\right)\right]^{-1/2}$$

$$=\tilde{K}^{-1}[\hat{-X}'(\eta_j^{\pm})]^{-1/2}\ . \tag{A18}$$

Finally, we calculate the $O(\Lambda^{-(N-1)/2})$ deviations of $\eta_j^{\pm}(\tilde{K},N)$ and $\hat{\eta}_j^{\pm}(\tilde{K},N)$ from their fixed-point values. For example, by substituting $\eta_j^{\pm}(N)=\eta_j^{\pm}+\delta_j^{\pm}\Lambda^{-(N-1)/2}$ into Eq. (A10) and collecting together the terms of $O(\Lambda^{-(N-1)/2})$, we can show that

$$\eta_j^{\pm}(N)=\eta_j^{\pm}-\frac{\eta_j^{\pm}}{\Lambda}\frac{\Lambda^{-(N-1)/2}}{X'(\eta_j^{\pm})}$$

$$=\eta_j^{\pm}+\tilde{K}(\alpha_{0j}^{\pm})^2\frac{\eta_j^{\pm}}{\Lambda}\Lambda^{-(N-1)/2}\ . \tag{A19}$$

The scond step above follows from Eq. (A16). Similarly

$$\hat{\eta}_j^{\pm}(N)=\hat{\eta}_j^{\pm}-\frac{\hat{\eta}_j^{\pm}}{\Lambda}\frac{\Lambda^{-(N-1)/2}}{\hat{X}'(\hat{\eta}_j^{\pm})}$$

$$=\hat{\eta}_j^{\pm}+\tilde{K}(\hat{\alpha}_{0j}^{\pm})^2\frac{\hat{\eta}_j^{\pm}}{\Lambda}\Lambda^{-(N-1)/2}\ . \tag{A20}$$

Of course, one can also diagonalize Eq. (A1) directly numerically, by diagonalizing the $(N+1)\times(N+1)$ matrix $\mathcal{K}_N^0(K)$ whose only nonvanishing matrix elements are

$$(\mathcal{K}_N^0)_{n,n+1}=(\mathcal{K}_N^0)_{n+1,n}$$

$$=\Lambda^{(N-1-n)/2}\xi_n,\quad n=0,1,\ldots,(N-1)$$

$$(\mathcal{K}_N^0)_{0,0}=\Lambda^{(N-1)/2}\tilde{K}\ . \tag{A21}$$

[Compare with similar discussion in Sec. III A of I.] The single-particle levels $\eta_j(N)$ are given by the eigenvalues of this matrix. If the real orthogonal matrix that diagonalizes $\mathcal{K}_N^0$ be denoted $\mathfrak{M}$, then we have the result that

$$\sum_{n'=0}^{N} (\mathcal{K}_N^0)_{nn'} \mathfrak{M}_{n'j} = \eta_j(N) \mathfrak{M}_{nj} \quad . \tag{A22}$$

The new operators c_j that diagonalize $H_N^0(K)$ are then given by

$$f_n = \sum_j \mathfrak{M}_{nj} c_j, \quad c_j = \sum_n \mathfrak{M}_{nj} f_n \quad . \tag{A23}$$

$\mathfrak{M}$ and $\eta_j(N)$ can be evaluated numerically using standard diagonalization routines on a computer. In this way all the results that we discussed earlier in this appendix have been verified to be true.

Next we consider the proofs of results (2.17) and (2.18) used in Sec. II C. Equation (2.16) has been proved earlier. To prove Eq. (2.17), consider Eq. (A22) for $n=0$. Using Eq. (A21) we get

$$\tilde{K} \mathfrak{M}_{0j} + \xi_0 \mathfrak{M}_{1j} = \eta_j \Lambda^{-(N-1)/2} \mathfrak{M}_{0j} \quad . \tag{A24}$$

But from Eq. (A23), $\mathfrak{M}_{oj}$ and $\mathfrak{M}_{1j}$ can be seen to be the expansion coefficients for expressing f_0 and f_1 (respectively) in terms of the new operators c_j. By relabeling c_j in terms of electron and hole operators and by using the result (A15), it is easy to show that for N odd

$$\tilde{K} f_0 + \xi_0 f_1 = \Lambda^{-3[(N-1)/4]} \sum_j (\alpha_{0j}^+ \eta_j^+ g_j - \alpha_{0j}^- \eta_j^- h_j^\dagger) \quad , \tag{A25a}$$

as stated in Eq. (2.17). For N even we get

$$\tilde{K} f_0 + \xi_0 f_1 = \Lambda^{-3[(N-1)/4]} \sum_j (\hat{\alpha}_{0j}^+ \hat{\eta}_j^+ g_j - \hat{\alpha}_{0j}^- \hat{\eta}_j^- h_j^\dagger) \quad . \tag{A25b}$$

Similarly, one can prove Eq. (2.18) by considering Eq. (A22) for $n=1$.

2. *Asymptotic (i.e., $j \gg 1$) results for $\eta_j^\pm$, $\alpha_{0j}^\pm$, etc.*

For $j \gg 1$, the quantities $\eta_j^\pm$ $\alpha_{0j}^\pm$, etc., can be evaluated exactly (analytically), as shown below.

First consider the case when N is odd. For $\eta_j^\pm \gg 1$ we can write [cf. Eq. (A11)]

$$X(\eta_j^\pm) \cong 2\alpha_0^2 \eta_j^\pm \sum_{l=1}^{\infty} \frac{\Lambda^{l-1}}{(\eta_j^\pm)^2 - \Lambda^{2(l-1)}}$$

$$\cong 2\alpha_0^2 \eta_j^\pm \sum_{l=-\infty}^{\infty} \frac{\Lambda^{l-1}}{(\eta_j^\pm)^2 - \Lambda^{2(l-1)}} \quad . \tag{A26}$$

The first approximation above follows from the fact that the dominant terms in the sum in Eq. (A11) are for $\eta_l^* \simeq \eta_j^\pm \gg 1$, for which $\alpha_{0l}^2 \simeq \alpha_0^2 \Lambda^{l-1}$ and $\eta_l^* = \Lambda^{l-1}$; the second approximation follows from the fact that the extra terms that are added are of order $(1/\eta_j^\pm)$. The last sum in Eq. (A26) can be evaluated exactly using a Sommerfeld-Watson transformation,[14] and we get

$$X(\eta) \cong \frac{\pi\alpha_0^2}{\ln\Lambda} \left[\cot\left(\frac{\pi \ln\eta}{\ln\Lambda}\right) + 2 \sum_{k=1}^{\infty} \frac{(-1)^k}{\cosh^2(\pi^2 k/\ln\Lambda)} \frac{\tan(\pi \ln\eta/\ln\Lambda)}{\tan^2(\pi \ln\eta/\ln\Lambda) + \tanh^2(\pi \ln\eta/\ln\Lambda)} \right]$$

$$\simeq \frac{\pi\alpha_0^2}{\ln\Lambda} \cot\left(\frac{\pi \ln\eta}{\ln\Lambda}\right) \quad , \tag{A27}$$

since the neglected terms are of order $\exp(-2\pi^2 k/\ln\Lambda)$. Substituting this result into Eq. (A11), it is straightforward to verify that the asymptotic solutions for $\eta_j^\pm$ can be written

$$\eta_j^\pm = \Lambda^{(j-1)\pm\gamma}, \quad \tilde{K}^{-1} = \frac{\pi\alpha_0^2}{\ln\Lambda} \cot\pi\gamma \quad , \tag{A28}$$

We note that in the limit $\Lambda \to 1$, $\eta_j^\pm = [(j-1) \pm \gamma] \times \ln\Lambda$, so that γ is essentially the phase shift.

Furthermore, using (A16) we can derive the asymptotic solutions for $\alpha_{0j}^\pm$. We have, using Eq. (A28),

$$\alpha_{0j}^\pm = \tilde{K}^{-1} \left[\frac{\pi^2\alpha_0^2}{(\ln\Lambda)^2 \eta_j^\pm} \operatorname{cosec}^2\left(\frac{\pi \ln\eta_j^\pm}{\ln\Lambda}\right) \right]^{-1/2} \quad . \tag{A29}$$

Substituting the results (A28) into (A29), we get

$$\alpha_{0j}^\pm = \alpha_0(\tilde{K})(\eta_j^\pm)^{1/2},$$

$$\alpha_0(\tilde{K}) \equiv \alpha_0 \left[1 + \frac{\pi^2\alpha_0^4}{(\ln\Lambda)^2} \tilde{K}^2\right]^{-1/2} \quad . \tag{A30}$$

Following exactly the same procedure as above, we can show that the asymptotic solutions for $\eta_j^\pm$ and $\hat{\alpha}_{0j}^\pm$ are

$$\hat{\eta}_j^\pm = \Lambda^{j-1/2\pm\gamma}, \quad \hat{\alpha}_{0j}^\pm = \alpha_0(\tilde{K})(\hat{\eta}_j^\pm)^{1/2} \quad , \tag{A31}$$

where γ and $\alpha_0(\tilde{K})$ are the same as before

All of the above asymptotic solutions have been checked to be correct using the exact results from the numerical diagonalization.

3. *Evaluation of thermodynamic sums*

Next we discuss the evaluation of the various thermodynamic sums involving $\eta_l^{\pm}$ and $\alpha_0^{\pm}$ that we encountered in the text. The basic sums that we need are

$$k_B T_B \chi_0^{\pm}(\tilde{K}) \equiv \sum_l \left[\frac{e^{-\bar{\beta}\eta_l^{\pm}}}{(1+e^{-\bar{\beta}\eta_l^{\pm}})^2} - \frac{e^{-\bar{\beta}\eta_l^{*}}}{(1+e^{-\bar{\beta}\eta_l^{*}})^2} \right] , \tag{A32}$$

$$\chi_1^{\pm}(\tilde{K}) \equiv \bar{\beta}^2 \sum_l (\alpha_{0l}^{\pm})^2 \eta_l^{\pm} \frac{e^{-\bar{\beta}\eta_l^{\pm}}(1-e^{-\bar{\beta}\eta_l^{\pm}})}{(1+e^{-\bar{\beta}\eta_l^{\pm}})^3} , \tag{A33}$$

$$\chi_2^{\pm}(\tilde{K}) \equiv \bar{\beta} \sum_l (\alpha_{0l}^{\pm})^2 \frac{e^{-\bar{\beta}\eta_l^{\pm}}}{(1+e^{-\bar{\beta}\eta_l^{\pm}})^2} , \tag{A34}$$

$$\chi_3^{\pm}(\tilde{K}) \equiv \pm \bar{\beta} \sum_l (\alpha_{0l}^{\pm})^2 \frac{e^{-\bar{\beta}\eta_l^{\pm}}(1-e^{-\bar{\beta}\eta_l^{\pm}})}{(1+e^{-\bar{\beta}\eta_l^{\pm}})^3} , \tag{A35}$$

$$F_0^{\pm}(\tilde{K}) \equiv -k_B T_N \sum_l 2 \ln \left[\frac{1+e^{-\bar{\beta}\eta_l^{\pm}}}{1+e^{-\bar{\beta}\eta_l^{*}}} \right] , \tag{A36}$$

$$F_1^{\pm}(\tilde{K}) \equiv \bar{\beta}^2 \sum_l (\alpha_{0l}^{\pm})^2 \eta_l^{\pm} \frac{e^{-\bar{\beta}\eta_l^{\pm}}}{1+e^{-\bar{\beta}\eta_l^{\pm}}} , \tag{A37}$$

$$F_2^{\pm}(\tilde{K}) \equiv \pm \bar{\beta} \sum_l (\alpha_{0l}^{\pm})^2 \frac{e^{-\bar{\beta}\eta_l^{\pm}}}{1+e^{-\bar{\beta}\eta_l^{\pm}}} . \tag{A38}$$

The functions defined in the text are then obtainable as $\chi_0 = \chi_0^+ + \chi_0^-$, $F_0 = F_0^+ + F_0^-$, $\chi_{1,\mathrm{FI}} = \chi_1^+ + \chi_1^-$, $\chi_{2,\mathrm{FI}} = \chi_{1,\mathrm{LM}} = \chi_2^+ + \chi_2^-$, etc. We want to evaluate these sums in the limit when $\bar{\beta} \to 0$ and $N \to \infty$ keeping T_N fixed. (N determines the upper limits on l in the sums.)

We note certain common features of the above sums. First, each of the summands is exponentially damped [as $\exp(-\bar{\beta}\eta_l)$] for large l, so that the upper limits on l can be set to ∞ in all the sums. Thus the functions are independent of T_N. Second, for $\bar{\beta} \ll 1$ the sums are dominated by the terms for which $\bar{\beta}\eta_l \simeq 1$, when we can replace $\eta_l^{\pm}$, η_l^{*}, and $\alpha_{0l}^{\pm}$ by their asymptotic values. Furthermore, the lower limits on l in each of the sums can be replaced by $-\infty$, since the contributions due to the extra terms that are thereby introduced are of order $\bar{\beta}$, and vanish as $\bar{\beta} \to 0$. Using these approximations we get

$$k_B T_N \chi_0^{\pm} = \sum_{l=-\infty}^{\infty} \left[\frac{e^{-u_l^{\pm}}}{(1+e^{-u_l^{\pm}})^2} - \frac{e^{-u_l^{*}}}{(1+e^{-u_l^{*}})^2} \right] , \tag{A39}$$

$$\chi_1^{\pm} = \alpha_0^2(\tilde{K}) \sum_{l=-\infty}^{\infty} (u_l^{\pm})^2 \frac{e^{-u_l^{\pm}}(1-e^{-u_l^{\pm}})}{(1+e^{-u_l^{\pm}})^3} , \tag{A40}$$

$$\chi_2^{\pm} = \alpha_0^2(\tilde{K}) \sum_{l=-\infty}^{\infty} u_l^{\pm} \frac{e^{-u_l^{\pm}}}{(1+e^{-u_l^{\pm}})^2} , \tag{A41}$$

$$\chi_3^{\pm} = \pm \alpha_0^2(\tilde{K}) \sum_{l=-\infty}^{\infty} u_l^{\pm} \frac{e^{-u_l^{\pm}}(1-e^{-u_l^{\pm}})}{(1+e^{-u_l^{\pm}})^3} , \tag{A42}$$

$$F_0^{\pm} = -2k_B T_N \sum_{l=-\infty}^{\infty} \ln \left[\frac{1+e^{-u_l^{\pm}}}{1+e^{-u_l^{*}}} \right] , \tag{A43}$$

$$F_1^{\pm} = \alpha_0^2(\tilde{K}) \sum_{l=-\infty}^{\infty} (u_l^{\pm})^2 \frac{e^{-u_l^{\pm}}}{1+e^{-u_l^{\pm}}} , \tag{A44}$$

$$F_2^{\pm} = \pm \alpha_0^2(\tilde{K}) \sum_{l=-\infty}^{\infty} u_l^{\pm} \frac{e^{-u_l^{\pm}}}{1+e^{-u_l^{\pm}}} , \tag{A45}$$

where we have introduced the variables

$$u_l^{\pm} \equiv \bar{\beta}\eta_l^{\pm} = \bar{\beta}\Lambda^{l-1+\gamma}, \quad u_l^{*} \equiv \bar{\beta}\eta_l^{*} = \bar{\beta}\Lambda^{l-1} . \tag{A46}$$

We note that if we let $\bar{\beta} \to \bar{\beta}\Lambda$, $(u_l^{\pm}, u_l^{*}) \to (u_{l+1}^{\pm}, u_{l+1}^{*})$, which means that the sums (A39)–(A45) are periodic in $\ln\bar{\beta}$ with period $\ln\Lambda$, and can be evaluated quite easily using a computer. In the limit $\Lambda \to 1$, the sums become independent of $\bar{\beta}$.

Next, we consider the limit as $\Lambda \to 1$. In this case the variables $u_l^{\pm}$ and u_l^{*} vary slowly with l, and the sums can be replaced by integrals. For $\chi_1^{\pm}$, $\chi_2^{\pm}$, $\chi_3^{\pm}$, $F_1^{\pm}$, and $F_2^{\pm}$, we choose $u \equiv u_l^{\pm}$ to be the integration variable. For $\chi_0^{\pm}$ and $F_0^{\pm}$ it is convenient to choose $u \equiv u_l^{*}\Lambda^{\pm\gamma/2}$ as the integration variable. In either case we have $\Delta l = \Delta u/(u \ln\Lambda)$. Hence we get, in the limit as $\Lambda \to 1$,

$$k_B T_N \chi_0^{\pm} = \pm \frac{1}{\ln\Lambda} \int_0^{\infty} \frac{du}{u} \left[\frac{e^{-u\Lambda^{\gamma/2}}}{(1+e^{-u\Lambda^{\gamma/2}})^2} - \frac{e^{-u\Lambda^{-\gamma/2}}}{(1+e^{-u\Lambda^{-\gamma/2}})^2} \right] , \tag{A47}$$

$$F_0^{\pm} = \mp \frac{2k_B T_N}{\ln\Lambda} \int_0^{\infty} \frac{du}{u} \ln \left[\frac{1+e^{-u\Lambda^{\gamma/2}}}{1+e^{-u\Lambda^{-\gamma/2}}} \right] , \tag{A48}$$

$$\chi_1^{\pm}=\frac{\alpha_0^2(\tilde{K})}{\ln\Lambda}\int_0^{\infty}u\,du\,\frac{e^{-u}(1-e^{-u})}{(1+e^{-u})^3}=\frac{\alpha_0^2(\tilde{K})}{\ln\Lambda}\frac{1}{2}\ , \tag{A49}$$

$$\chi_2^{\pm}=\frac{\alpha_0^2(\tilde{K})}{\ln\Lambda}\int_0^{\infty}du\,\frac{e^{-u}}{(1+e^{-u})^2}=\frac{\alpha_0^2(\tilde{K})}{\ln\Lambda}\frac{1}{2}\ , \tag{A50}$$

$$\chi_3^{\pm}=\pm\frac{\alpha_0^2(\tilde{K})}{\ln\Lambda}\int_0^{\infty}du\,\frac{e^{-u}(1-e^{-u})}{(1+e^{-u})^3}=\pm\frac{\alpha_0^2(\tilde{K})}{\ln\Lambda}\frac{1}{4}\ , \tag{A51}$$

$$F_1^{\pm}\frac{\alpha_0^2(\tilde{K})}{\ln\Lambda}\int_0^{\infty}u\,du\,\frac{e^{-u}}{(1+e^{-u})}=\frac{\alpha_0^2(\tilde{K})}{\ln\Lambda}\frac{1}{12}\pi^2\ , \tag{A52}$$

$$F_2^{\pm}=\pm\frac{\alpha_0^2(\tilde{K})}{\ln\Lambda}\int_0^{\infty}du\,\frac{e^{-u}}{1+e^{-u}}=\pm\frac{\alpha_0^2(\tilde{K})}{\ln\Lambda}\ln 2\ . \tag{A53}$$

Thus, we have, in the limit as $\Lambda\to 1$,

$$k_B T_N\chi_0=F_0=\chi_{3,\mathrm{FI}}=F_{2,\mathrm{FI}}=0\ , \tag{A54}$$

$$\chi_{1,\mathrm{FI}}=\frac{\alpha_0^2(\tilde{K})}{\ln\Lambda}\ , \tag{A55}$$

$$\chi_{2,\mathrm{FI}}=\chi_{1,\mathrm{LM}}=\frac{\alpha_0^2(\tilde{K})}{\ln\Lambda}\ , \tag{A56}$$

$$F_{1,\mathrm{FI}}=\frac{\alpha_0^2(\tilde{K})}{\ln\Lambda}\frac{1}{6}\pi^2\ . \tag{A57}$$

When $\Lambda>1$, the integrals (A47)–(A53) can be considered as approximations to the sums (A39)–(A45). However, there is a theorem (see Ref. 2, p. 832 for the proof) according to which the error due to replacing the sums by the integrals is only of order $\exp(-\pi^2/\ln\Lambda)$. Therefore, to a very good approximation, we can regard the results (A54)– (A57) as valid even for $\Lambda>1$ [as long as $\exp(-\pi^2/\ln\Lambda)\ll 1$] with $\alpha_0(\tilde{K})$ being given by Eq. (A30).

Finally, we note that functions $\chi_0^{\pm}$, $\chi_1^{\pm}$, etc., can be evaluated exactly for any given Λ, $\bar{\beta}$, and $\tilde{K}$ using the exact, numerically determined values for $\eta_l^{\pm}$, η_l^*, and $\alpha_{0l}^{\pm}$. In this way, all the above conclusions have been verified to be correct.

4. *Mapping between $H^*(\tilde{K}')$ and $\hat{H}^*(\tilde{K})$*

Finally, we demonstrate one-to-one mapping between $H^*(\tilde{K}')$ and $\hat{H}^*(\tilde{K})$, which in the language of Sec. II B, are two lines of fixed points of $\mathcal{T}^2$. This mapping was invoked in Sec. II B to show that the strong-coupling and the frozen-impurity lines of fixed points are the same.

In order to prove this mapping, we consider the Hamiltonian

$$H_N=H_N^0+\tilde{K}_0\Lambda^{+(N-1)/2}f_0^{\dagger}f_0+\tilde{K}_1\Lambda^{(N-1)/2}f_1^{\dagger}f_1\ . \tag{A58}$$

for *even* N, in the limit $\tilde{K}_0\to\infty$. We can solve H_N in two ways.

The first way is to first solve (for even N)

$$H_N^0(K_0)=H_N^0+\tilde{K}_0\Lambda^{(N-1)/2}f_0^{\dagger}f_0 \tag{A59}$$

in the limit as $\tilde{K}_0\to\infty$. This has already been discussed, and we know that this leads to the even fixed point H^* as even $N\to\infty$. Furthermore, we note that $\tilde{K}_0\to\infty$ freezes the states in which $f_0^{\dagger}f_0=0$, giving rise to a ground-state charge of -1. One can also verify that the expansion for f_1 in terms of the operators that diagonalize $H_N^0(\tilde{K}_0)$ for $\tilde{K}_0\to\infty$ is given by

$$f_1=-\Lambda^{-(N-1)/4}\left(\frac{\ln\Lambda}{\pi\alpha_0^2}\right)\sum_l\alpha_{0l}c_l\ . \tag{A60}$$

Hence the $f_1^{\dagger}f_1$ term generates potential scattering about the even fixed point. We conclude that for $\tilde{K}_0=\infty$, H_N leads to $H^*(\tilde{K}')$ plus a ground-state charge of -1 as even $N\to\infty$, where $\tilde{K}'$ is given by

$$\tilde{K}'-\tilde{K}_1\left(\frac{\ln\Lambda}{\pi\alpha_0^2}\right)^2\ . \tag{A61}$$

The second way to solve H_N is to diagonalize it directly. By using exactly the same methods as we used in diagonalizing $H_N^0(K)$, one can show that in the limit as $K_0\to\infty$, the eigenvalues of H_N for even N are given by the roots of the equation

$$\frac{\hat{\alpha}_{00}^2}{\eta}+2\eta\sum_{l=1}^{N/2}\frac{\hat{\alpha}_0^2}{\eta^2-\hat{\eta}_l^{*2}}=-\tilde{K}_1\ . \tag{A62}$$

In view of our earlier discussions, one would conclude from Eq. (A62) that as even $N\to\infty$, H_N leads to the fixed point $\hat{H}^*(\tilde{K})$ where

$$\tilde{K}^{-1}=-\tilde{K}_1\ . \tag{A63}$$

Hence we have proved the result that $\hat{H}^*(\tilde{K})$ is the same as $H^*(\tilde{K}')$ plus a ground state of charge -1, with $\tilde{K}$ and $\tilde{K}'$ being related as

$$\tilde{K}'=-\frac{\ln\Lambda}{\pi\alpha_0^2}\tilde{K}^{-1}=-\frac{2}{\pi}\frac{\ln\Lambda}{1-\Lambda^{-1}}\tilde{K}^{-1}\ . \tag{A64}$$

The details of the above proof are not given here.

APPENDIX B: DISCUSSION OF THE SCALING LAW FOR THE SUSCEPTIBILITY OF THE KONDO HAMILTONIAN WITH POTENTIAL SCATTERING

The perturbation expansion for the running-coupling constant J_N has the general form (the tilde

over all J's has been suppressed)

$$J_N = J + a_{2,N}J^2 + a_{3,N}J^3 + \cdots \quad . \tag{B1}$$

The coefficient of the $O(J)$ term is 1 because J is a marginal variable. The coefficients $a_{2,N}$ and $a_{3,N}$ are polynomials in N, and can become large as N increases. This is why Eq. (B1) is a bad expansion.

We can invert Eq. (B1) to get

$$J = J_N - a_{2,N}J_N^2 + (2a_{2,N}^2 - a_{3,N})J_N^3 + \cdots \quad . \tag{B2}$$

If we substitute Eq. (B2) into Eq. (B1) written for J_{N+2}, we get a recursion relation between J_{N+2} and J_N

$$J_{N+2} = J_N + A_2J_N^2 + A_3J_N^3 + \cdots \quad , \tag{B3}$$

where

$$A_2 = a_{2,N+2} - a_{2,N} \quad , \tag{B4a}$$

$$A_3 = a_{3,N+2} - 2a_{2,N+2}a_{2,N} + (2a_{2,N}^2 - a_{3,N}) \quad . \tag{B4b}$$

Equation (B3) is a good expansion because A_2, A_3, etc., are expected to be independent of N.

The solution for the recursion relation (B3) is

$$\Psi(J_N) + \tfrac{1}{2}(N-1) = \psi(J_{N_0}) + \tfrac{1}{2}(N_0 - 1) \quad , \tag{B5}$$

where

$$\Psi(J) \equiv \frac{1}{A_2 J} + \left(\frac{A_3}{A_2^2} - 1\right)\ln|A_2 J| + O(J) \quad . \tag{B6}$$

Now consider the expansion for the susceptibility. We expect an xpansion of the form

$$k_B T_N \chi(T_N) = \tfrac{1}{4} + Y_1(\bar{\beta})J + Y_2(\bar{\beta},N)J^2 + \cdots \quad . \tag{B7}$$

In terms of J_N,

$$k_B T_N \chi(T_N) = \tfrac{1}{4} + J_N Y_1(\bar{\beta}) + J_N^2[Y_2(\bar{\beta},N) - Y_1(\bar{\beta})a_{2N}] + \cdots \tag{B8}$$

which can be rewritten

$$y(T_N) \equiv [4k_B T_N \chi(T_N) - 1] = B_1(\bar{\beta})J_N + B_2(\bar{\beta})J_N^2 + \cdots \quad . \tag{B9}$$

The coefficients B_1, B_2, etc., are expected to be independent of N, but can, in general, depend on $\bar{\beta}$.

Equation (B9) can be inverted to get

$$J_N = \frac{1}{B_1}y(T_N) - \left(\frac{B_2}{B_1^3}\right)[y(T_N)]^2 + \cdots \quad . \tag{B10}$$

By substituting this equation and the result [cf. Eq. (1.4)]

$$\tfrac{1}{2}(N-1)\ln\Lambda = -\ln\left(\frac{k_B T_N}{D}\right) + \ln\left(\frac{1+\Lambda^{-1}}{2\bar{\beta}}\right) \quad , \tag{B11}$$

into Eq. (B5), we get the result

$$\Phi(y(T)) - \ln(k_B T) = \Phi(y(T_0)) - \ln(k_B T_0) \quad , \tag{B12}$$

where we have written T for T_N and T_0 for T_{N_0}. Φ is given by [cf. (B10) and (B6)]

$$\Phi(y) \equiv (\ln\Lambda)\Psi(J_N) = \left(\frac{B_1 \ln\Lambda}{A_2}\right)\frac{1}{y} + \left(\frac{A_3}{A_2^2} - 1\right)\ln\Lambda \ln|y| + O(y) \, . \tag{B13}$$

If we now take the limit as $\bar{\beta} \to 0$ and $\Lambda \to 1$ keeping T and T_0 fixed, we get the scaling law (3.41), where T_K is related to T_0 by

$$\ln(T_0/T_K) = \Phi[y(T_0)] \tag{B14}$$

and can be computed by choosing T_0 to be high enough that $y(T_0)$ can be calculated perturbatively.

APPENDIX C: DISCUSSION OF THE KONDO PROBLEM WITH POTENTIAL SCATTERING

Starting from the model Hamiltonian (3.27), we diagonalize exactly the piece of (3.27) that excludes the ρJ term, namely

$$\mathcal{H}_K^0 \equiv D_K\left(\int_{-1}^{1} dk\, k a_k^\dagger a_k + \rho K \int_{-1}^{1} dk \int_{-1}^{1} dk'\, a_k^\dagger a_{k'}\right) \quad . \tag{C1}$$

This can be done by means of the transformation

$$a_k = \int_{-1}^{1} dq\, u(kq) c_q \quad , \tag{C2}$$

$$u(k,q) = [\cos\delta(q)]\delta(q-k) + \frac{\sin\delta(q)}{\pi} P\left(\frac{1}{q-k}\right) \quad , \tag{C3}$$

where $\delta(q)$ is the phase shift determined by the equation

$$\pi\cot\delta(q) + P\int \frac{dk}{q-k} = (\rho K)^{-1} \quad . \tag{C4}$$

In the above equations, P denotes the principal part. In terms of c_q, $\mathcal{H}_K^0$ is diagonal:

$$\mathcal{H}_K^0 = D_K \int_{-1}^{1} dq q c_q^\dagger c_q \quad . \tag{C5}$$

These results can be verified, for example, by linearly discretizing $\mathcal{H}_K^0$, solving the resulting Hamiltonian, and then taking the continuum limit, or directly [if enough care is taken in handling the generalized functions $u(k,q)$] by substituting Eqs. (C2)–(C4) in Eq. (C1). We note that

$$\int_{-1}^{1} a_k\, dk = \int_{-1}^{1} dq \frac{\sin\delta(q)}{\pi\rho K} c_q \quad , \tag{C6}$$

this follows from Eqs. (C2)–(C4).

Substituting these results into the model Hamiltonian (3.27), we get

$$\mathcal{H}_K = D_K\left(\int_{-1}^{1} q c_q^\dagger c_q dq - \rho J \int_{-1}^{1} dq \int_{-1}^{1} dq' \frac{\sin\delta(q)}{\pi\rho K}\frac{\sin\delta(q')}{\pi\rho K} c_q^\dagger \tfrac{1}{2}\vec{\sigma} c_{q'} \cdot \tfrac{1}{2}\vec{\tau}\right) . \tag{C7}$$

We note that $\sin\delta(q)$ is a smooth function of q, and can be expanded in powers of q. In accordance with our discussion of Sec. V D of I, the dominant term is the term independent of q, as the terms involving powers of q produce irrelevant operators about the local-moment fixed point. Hence we get

$$\mathcal{H}_K \simeq D_K\left(\int_{-1}^{1} q c_q^\dagger c_q dq - \rho J_{\text{eff}} \int_{-1}^{1} dq \int_{-1}^{1} dq' \, c_q^\dagger \tfrac{1}{2}\vec{\sigma} c_{q'} \cdot \tfrac{1}{2}\vec{\tau}\right) , \tag{C8}$$

where

$$\rho J_{\text{eff}} = \rho J\left(\frac{\sin\delta(0)}{\pi\rho K}\right)^2 = \rho J \cos^2\delta(0) = \frac{\rho J}{[1+(\pi\rho K)^2]} , \tag{C9}$$

where the last two results follow from Eq. (C4) for $q=0$. As far as the susceptibility is concerned, the difference between c_q and a_k is irrelevant. Hence we get the result that for small $-\rho J$, the low-temperature susceptibility for the Kondo problem with potential scattering can still be written

$$\Phi(4k_B T\chi - 1) = \ln[T/T_K(J_{\text{eff}})] , \tag{C10}$$

$$T_K(J_{\text{eff}}) = D(J_{\text{eff}})|\rho J_{\text{eff}}|^{1/2}\exp\left(-\frac{1}{\rho|J_{\text{eff}}|}\right) , \tag{C11}$$

where Φ is the same universal function as for the Kondo problem without potential scattering. Note that the effective bandwidth $D(J)$ *is* affected by the irrelevant operators about the local-moment fixed point and will in general depend on the higher-order terms in Eq. (B7) when we expand $\sin\delta(q)$ and hence on ρK.

APPENDIX D: ANALYTICAL TREATMENT OF THE SMALL-U CASE

The procedure we follow in order to treat the small U case of the asymmetric Anderson model analytically is basically the same as for the symmetric $\Gamma >> U$ case treated in Appendix E of I. We break up H_N as [cf. Eq. (2.18) of I]

$$H_N = H_{N0} + \tilde{U}\Lambda^{(N-1)/2}(c_{d\mu}^\dagger c_{d\mu} - 1)^2 , \tag{D1}$$

$$H_{N0} \equiv H_N^0 + \tilde{\delta}_d \Lambda^{(N-1)/2} c_d^\dagger c_d + \tilde{\Gamma}^{1/2}\Lambda^{(N-1)/4}(c_d^\dagger f_0 + f_0^\dagger c_d) , \tag{D2}$$

diagonalize H_{N0} exactly, and treat the U term as a perturbation. The conditions for the validity of this procedure will arise out of the analysis. Spin indices have been suppressed in H_{N0} for convenience.

The diagonalization of H_{N0} can be carried out exactly as in Appendix E of I. Using the same notation [refer to Eqs. (B4)–(B6) of I], we can write H_{N0} for odd N as

$$H_{N0} = \sum_{l=-J}^{J} \eta_l^* a_l^\dagger a_l + \tilde{\Gamma}^{1/2}\Lambda^{(N-1)/4}\sum_{l=-J}^{J}\alpha_{0l}(a_0^\dagger a_l + a_l^\dagger a_0) , \tag{D3}$$

where, in contrast to the symmetric case where η_0 was exactly zero [cf. Eq. (E6) of I], η_0 now has the value

$$\eta_0 \equiv \tilde{\delta}_d \Lambda^{(N-1)/2} = (\tilde{\epsilon}_d + \tilde{U})\Lambda^{(N-1)/2} . \tag{D4}$$

In this case, a set of oprators $\hat{a}_j = \sum_l U_{lj} a_l$ where U_{lj} are the elements of an orthogonal matrix will diagonalize H_{N0} into a set of single-particle levels $\hat{\eta}_j(N)$ provided that the U_{lj} satisfy the equations [compare Eqs. (E7) and (E8) of I]

$$(\hat{\eta}_j - \eta_l^*) U_{lj} = \tilde{\Gamma}^{1/2}\Lambda^{(N-1)/4}\alpha_{0l} U_{0j} \quad (l \neq 0) , \tag{D5}$$

$$(\hat{\eta}_j - \delta_d \Lambda^{(N-1)/2}) U_{0j} = \tilde{\Gamma}^{1/2}\Lambda^{(N-1)/4}\sum_{l\neq 0}\alpha_{0l} U_{lj} . \tag{D6}$$

The solutions to the above equations are that the eigenvalues $\hat{\eta}_j(N)$ are determined by the roots of the equation

$$\frac{\hat{\eta}_j - \tilde{\delta}_d\Lambda^{(N-1)/2}}{\tilde{\Gamma}\Lambda^{(N-1)/2}} = 2\hat{\eta}_j \sum_{l=1}^{J}\frac{\alpha_{0l}^2}{\hat{\eta}_j^2 - \eta_l^{*2}} \equiv X(\hat{\eta}_j, N) ; \tag{D7}$$

U_{0j} is given by

$$U_{0j} = \left(1 + \tilde{\Gamma}\Lambda^{(N-1)/2}\sum_{l=-J}^{J}\frac{\alpha_{0l}^2}{(\hat{\eta}_j - \eta_l^*)^2}\right)^{-1/2} , \tag{D8}$$

and U_{lj} for $l \neq 0$ are determined by Eq. (D5). The function X defined in Eq. (D7) is the same as what appeared in our discussion of $H_N^0(\tilde{K})$ in Appendix A [cf. Eq. (A9)].

For the purposes of this appendix we will assume that $\tilde{\delta}_d << 1$ and $\tilde{\Gamma} << 1$. In Figure 18 is sketched the graphical determination of the roots of Eq. (D7) for the two characteristic cases $\tilde{\delta}_d << \tilde{\Gamma}$ and $\tilde{\delta}_d >> \tilde{\Gamma}$:

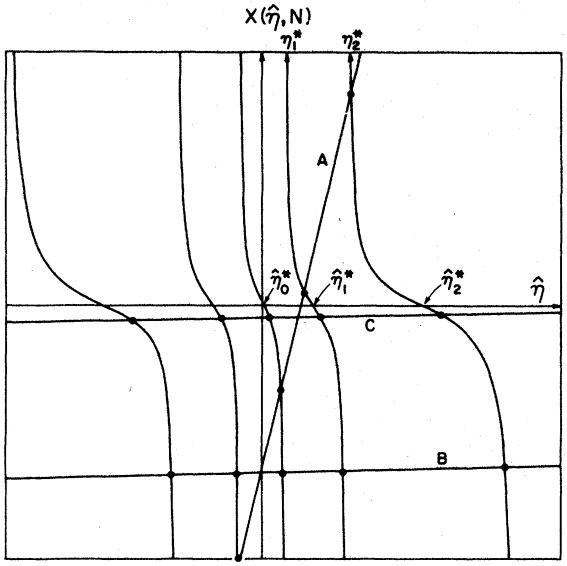

FIG. 18. Eigenvalues of H_{N0}. The characteristic function $X(\hat{\eta},N)$ is plotted vs η measured in units of $\Lambda^{-(N-1)/2}$, and for the case of odd N, blows up at η_j^*. The eigenvalues are given by the graphical solution of $X=(\hat{\eta}-\tilde{\delta}_d\Lambda^{(N-1)/2})\times\tilde{\Gamma}\Lambda^{(N-1)/2}=y(\hat{\eta})$. For the *free-orbital regime* we set N small enough that $\tilde{\delta}_d$, $\tilde{\Gamma}\ll\Lambda^{-(N-1)/2}$. Accordingly $y(\hat{\eta})$, curve A, is a very steeply inclined straight line intersecting the η axis at $\tilde{\delta}_d\Lambda^{(N-1)/2}$, and yields the solution (D10). For the *frozen-impurity* regime (i.e., $N\to\infty$), $y(\eta)$ is just the constant $-\tilde{\delta}_d/\tilde{\Gamma}$. We have shown two extreme cases: $\tilde{\delta}_d\ll\tilde{\Gamma}$ with curve C and $\tilde{\delta}\gg\tilde{\Gamma}$ with curve B.

1. Free-orbital regime

When N is small enough that $\Gamma\Lambda^{(N-1)/2}\ll 1$ and $\delta_d\Lambda^{(N-1)/2}\ll 1$, to zero order in the small quantities the roots of Eq. (D7) are given by (see Fig. 18)

$$\hat{\eta}_0=0,\quad \hat{\eta}_j=\eta_j^*\quad (j\neq 0)\ . \tag{D9}$$

This is just the free-orbital fixed point $H_{\rm FO}^*$ ($\tilde{K}=0$). The leading deviations are easily shown to be

$$\hat{\eta}_0\cong\tilde{\delta}_d\Lambda^{(N-1)/2}\ ,$$

$$\hat{\eta}_j-\eta_j^*\cong\tilde{\Gamma}\Lambda^{(N-1)/2}\alpha_{0j}^2/\eta_j^*\quad (j\neq 0)\ . \tag{D10}$$

Furthermore, one can verify that

$$U_{00}\cong 1+\tilde{\Gamma}\Lambda^{(N-1)/2}\sum_{l=1}^{J}\frac{\alpha_{0l}^2}{\eta_l^*}\ ,$$

$$U_{0j}\cong\tilde{\Gamma}^{1/2}\Lambda^{(N-1)/4}\frac{\alpha_{0j}^2}{\eta_j^*}\quad (j\neq 0) \tag{D11}$$

so that the U term in Eq. (D1) is just $\tilde{U}\Lambda^{(N-1)/2}(\hat{a}_0^\dagger\hat{a}_0-1)^2$ to leading order. All this is characteristic of the free-orbital regime.

2. Frozen-impurity regime

Clearly, as $N\to\infty$, $\hat{\eta}_j(N)$ tend to the fixed-point values given by the roots of the equation

$$-\frac{\tilde{\delta}_d}{\tilde{\Gamma}}=\pm 2\eta_j^{\pm}\sum_{l=1}^{\infty}\frac{\alpha_0^2}{(\eta_j^{\pm})^2-\eta_l^{*2}}\equiv\pm X(\eta_j^{\pm})\ , \tag{D12}$$

where we have denoted the positive eigenvalues by η_j^+ and the negative eigenvalues by $-\eta_j^-$. From the discussion of Appendix A, it is clear that $\eta_j^{\pm}$ correspond to a potential scattering $\tilde{K}$ given by [compare Eq. (A11)]

$$\tilde{K}=-\tilde{\Gamma}/\tilde{\delta}_d\ . \tag{D13}$$

Furthermore, the limit $\tilde{\delta}_d\Lambda^{(N-1)/2}\to\infty$ gets rid of the $n_d\neq 0$ states of the impurity, whence the ground state acquires a charge of -1. Thus for $N\to\infty$ we have the frozen-impurity fixed point $H_{\rm FI}^*(\tilde{K})$. We note that $\tilde{K}$ is negative, and in the symmetric limit ($\tilde{\delta}_d\to 0$), $\tilde{K}\to-\infty$. All of this is in agreement with earlier discussions.

Next we consider the $O(\Lambda^{-(N-1)/2})$ deviations from the fixed point for a large but finite N. This will enable us to obtain the coefficients ω_1 and ω_2 (discussed in Sec. III F) explicitly. Making use of Eqs. (D7), (A10), and (D12), it is easy to verify that to $O(\Lambda^{-(N-1)/2})$

$$\eta_j^{\pm}(N)-\eta_j^{\pm}=\eta_j^{\pm}\frac{(\tilde{\Gamma}^{-1}-\tilde{\Lambda}^{-1})}{X'(\eta_j^{\pm})}\Lambda^{-(N-1)/2}\ . \tag{D14}$$

Neglecting Λ^{-1} in comparison to $\tilde{\Gamma}^{-1}$, and making use of Eq. (A16), we can rewrite this as

$$\eta_j^{\pm}(N)-\eta_j^{\pm}=-(\tilde{K}^2\tilde{\Gamma}^{-1})\Lambda^{-(N-1)/2}\alpha_{0j}^{\pm 2}\eta_j^{\pm}\ . \tag{D15}$$

This deviation is precisely of the form of the ω_1 term discussed in Sec. III F [see discussion following (3.52)], and we can explicitly identify that

$$\omega_1=-\tfrac{1}{2}\tilde{K}^2\tilde{\Gamma}^{-1}=-\tilde{\Gamma}/(2\tilde{\delta}_d^2)\ , \tag{D16}$$

where the second result follows from Eq. (D13).

The U term in Eq. (D1) gives rise to an $O(\Lambda^{-(N-1)/2})$ deviation about $H_{\rm FI}^*(\tilde{K})$ that looks like the ω_2 term discussed in Sec. III F. To see this, note that in terms of the electron hole operators that characterize the fixed point,

$$c_d\equiv a_0=\sum_j U_{0j}\hat{a}_j=\sum_j(U_{0j}^+g_j+U_{0j}^-h_j^\dagger)\ . \tag{D17}$$

From Eq. (D8) we see that for large N,

$$U_{0j}^{\pm}\cong\left[\tilde{\Gamma}\Lambda^{(N-1)/2}\sum_l\frac{\alpha_{0l}^2}{(\eta_j^{\pm}-\eta_l^*)^2}\right]^{-1/2}$$

$$=[-\tilde{\Gamma}\Lambda^{(N-1)/2}X'(\eta_j^{\pm})]^{-1/2}\ . \tag{D18}$$

Once again making use of Eq. (A16), we can rewrite this as

$$U_{0\tilde{l}}^{\pm} = \tilde{K}\tilde{\Gamma}^{-1/2}\Lambda^{-(N-1)/4}\alpha_{0\tilde{j}}^{\pm} \quad . \tag{D19}$$

Substituting Eqs. (D17) and (D19) into Eq. (D1), one can easily verify that the $\tilde{U}$ term generates a deviation about $H_{\rm FI}^{*}(\tilde{K})$ precisely of the form of the ω_2 term discussed in Sec. III F, where ω_2 is now explicitly given by

$$\omega_2 = \tilde{U}(\tilde{K}\tilde{\Gamma}^{-1/2})^4 = \tilde{U}\tilde{\Gamma}^2/\tilde{\delta}_d^4 \quad . \tag{D20}$$

(We note that the U term also generates additional potential scattering. Since we are only interested in the lowest-order calculations we will neglect this effect.)

Substituting the results for ω_1 and ω_2 into the expressions for χ and R [cf. Eqs. (3.64) and (3.67)], we get

$$\chi = \frac{(g\mu_B)^2}{D}\frac{K^2\phi(\tilde{K})}{4A_\Lambda\Gamma}\left[1+\tfrac{1}{2}(1+\Lambda^{-1})U\frac{\tilde{K}^2\phi(\tilde{K})}{A_\Lambda\Gamma}\right] , \tag{D21}$$

$$R = 1+\tfrac{1}{2}(1+\Lambda^{-1})U\frac{\tilde{K}^2\phi(\tilde{K})}{A_\Lambda\tilde{\Gamma}} \quad , \tag{D22}$$

where $\phi(\tilde{K})$ is defined by Eq. (3.63) and A_Λ by Eq. (3.62). Substituting these results as well as the definitions Eq. (1.3) for $\tilde{U}$, $\tilde{\Gamma}$, and $\tilde{\delta}_d$, and making use of Eq. (D13), we finally get the results

$$\frac{\chi}{(g\mu_B)^2} = \frac{A_\Lambda}{2\pi\Delta}\left[1+A_\Lambda\frac{U}{\pi\Delta}+O\left(\frac{U}{\pi\Delta}\right)^2\right] , \tag{D23}$$

$$R = 1+A_\Lambda\frac{U}{\pi\Delta}+O\left(\frac{U}{\pi\Delta}\right)^2 , \tag{D24}$$

where

$$\Delta \equiv \frac{\Gamma^2+A_\Lambda^2(\epsilon_d+\frac{1}{2}U)^2}{\Gamma} \tag{D25}$$

We note that in the symmetric case, $\epsilon_d = -\frac{1}{2}U$ when $\Delta = \Gamma$, and the above results reduce to those obtained in I [cf. Eqs. (5.40) and (5.41) of I]. In the limit $U=0$, $\Lambda\to 1$ ($A_\Lambda\to 1$), the above results agree with the calculations by Salomaa.[15] The condition for the validity of Eqs. (D23) and (D24) is that Γ/D and $U/\pi\Delta$ be small compared to unity.

Finally we note that in the limit when ϵ_d is positive and $\epsilon_d >> \Gamma$, U

$$\Delta \cong A_\Lambda^2\epsilon_d^2/\Gamma \quad , \tag{D26}$$

in which case to leading order in the small quantities

$$\frac{\chi}{(g\mu_B)^2} \cong \frac{1}{A_\Lambda}\frac{\Gamma}{2\pi\epsilon_d^2} \quad . \tag{D27}$$

According to the discussion above, this result is valid provided $U\Gamma/\epsilon_d^2$ is small. Actually Eq. (D27) is the dominant term in the zero-temperature susceptibility even if this condition is not satisfied, as long as ϵ_d is positive and $\epsilon_d >> \Gamma$. This result follows from the fact that in this case the ground-state subspace essentially has $n_d = 0$ (see Fig. 7 corresponding to the manifold of states), which therefore makes no contribution to the susceptibility. The dominant [$O(\Gamma)$] contribution comes from virtual transitions to the $n_d = 1$ subspace, and is given precisely by Eq. (D27). U enters only when we calculate $O(\Gamma^2)$ contributions. For further discussion see Sec. III F, where we make use of Eq. (D27) to calculate these contributions.

---

*Permanent address: Dept. of Phys., Indian Institute of Science, Bangalore 560012, India.

[1]H. R. Krishna-murthy, J. W. Wilkins, and K. G. Wilson, Phys. Rev. B 21, 1003 (1980) (preceding paper).

[2]K. G. Wilson, Rev. Mod. Phys. 47, 773 (1975).

[3]P. W. Anderson, Phys. Rev. 124, 41 (1961).

[4]For a review of this subject, and for references to previous work see *Magnetism, Vol. V*, edited by G. T. Rado and H. Suhl, (Academic, New York, 1973).

[5]Other review articles include C. Rizzutto, Rep. Prog. Phys. 37, 147 (1974); G. Gruner, Adv. Phys. 23, 941 (1974); and G. Gruner and A. Zawadowski, Rep. Prog. Phys. 37, 1497 (1974).

[6]For a formal theory of fixed points, linear, and nonlinear deviations from fixed points, etc., see F. Wegner, Phys. Rev. B 5, 4529 (1972); also, K. G. Wilson and J. B. Kogut, Phys. Rep. C 12, 76 (1974).

[7]F. D. M.Haldane, Phys. Rev. Lett. 40, 416, 911(E) (1978).

[8]We note that Eq. (2.9) is precisely the sequence of Hamiltonians one would use in a renormalization-group treatment of the Kondo Hamiltonian including potential scattering. See Sec. III D for details.

[9]F. D. M. Haldane, J. Phys. C 11, 5015 (1978).

[10]For previous work on the spin-$\frac{1}{2}$ Kondo problem including potential scattering, see K. K. Murata, thesis (Cornell University, 1971) (unpublished), and references therein.

[11]J. R. Schrieffer and P. A. Wolff, Phys. Rev. 149, 491 (1966).

[12]We note that this discussion neglects the changes in $\tilde{J}_1$ and $\tilde{K}_1$ within the valence-fluctuation regime, which changes

would appear if we calculated things to higher orders in $\tilde{J}_1$, and would lead to N-dependent coupling constants such as $\tilde{J}_{1N}$. Such effects can in principle be included in Eq. (3.39) by substituting $\tilde{J}_{1N_2^*}$ for $\tilde{J}_1$, but would be much smaller than what we have kept in Eq. (3.39). [For example, $\tilde{J}_{1N_2^*} - \tilde{J}_1 \sim \tilde{J}_1^2 \ln(U/-E_d^*)/\ln\Lambda$].

[13]Unless it should be the case that either η_1^+ or η_1^- is nearly zero, in which case we must add the term

$$2\sum_{l\neq 1} \alpha_{01}^{+2}\alpha_{01}^{-}\alpha_{0l}^{+}(g_{1\mu}^{\dagger}g_{1\nu}^{\dagger}h_{l\nu}^{\dagger}g_{l\mu} + g_{l\mu}^{\dagger}h_{l\nu}g_{1\nu}g_{1\mu})$$

if $\eta_1^+ \simeq 0$; or the term

$$2\sum_{l\neq 1} \alpha_{01}^{-2}\alpha_{0l}^{-}\alpha_{0l}^{+}(h_{l\mu}^{\dagger}h_{l\nu}^{\dagger}g_{l\nu}^{\dagger}h_{l\mu} + h_{l\mu}^{\dagger}g_{l\nu}h_{l\nu}h_{l\mu})$$

if $\eta_1^- \simeq 0$; since these terms can connect nearly degenerate states. This is needed only for the energies.

[14]J. Mathews and R. L. Walker, *Mathematical Methods of Physics* (Benjamin, Menlo Park, California, 1973), p. 73.

[15]M. Salomaa, Z. Phys. B 25, 49 (1976).